Università Degli Studi di Roma "La Sapienza"

Dottorato di Ricerca in ENERGETICA

XVIII ciclo

Tesi

MULTISCALE FINITE ELEMENT METHODS FOR TURBULENCE MODELING IN TURBOMACHINERY CFD

ANDREA SANTORIELLO

Docente guida
Prof. Franco Rispoli

Coordinatore del dottorato
Prof. Maurizio Cumo

Anno 2005

University of Rome “La Sapienza”

MULTISCALE FINITE ELEMENT METHODS FOR TURBULENCE MODELING IN TURBOMACHINERY CFD

Ph D Thesis

ANDREA SANTORIELLO

November 2005

to my Katia

I certify that I have read this dissertation and that, in my opinion, it is fully adequate in scope and quality as a dissertation for the degree of Doctor of Philosophy.

Tayfun E. Tezduyar, *Ph.D.*
James F. Barbour Professor
Mechanical Engineering and Materials Science
Rice University
Houston, Texas

Acknowledgements

I am profoundly grateful to some special persons who had a fundamental influence in the development of this work:

Dr Alessandro Corsini, for being a sincere friend and the guiding light in these glittering years. What You have done for me is simply unforgettable;
Professor Franco Rispoli, for his intelligence, his continuous support and the passion for research He naturally communicates;
Dr Domenico Borello, Dr Rafael Saavedra and Mr Filippo Menichini, for all the moments we shared.

I would like to thank Professor Tayfun Tezduyar, for his kindness and his helpful suggestions and explanations that improved my culture.

I am grateful to much of the under- and post-graduate students that during these years worked in the room 21 of the Department of Mechanics and Aeronautics of University "La Sapienza", with particular reference to Luca Aureli, Carlo Iossa, Paolo Orsini and Michele Ricchiuti.

Finally I would like to thank my family, and above all Katia, that has been giving me all her love, understanding and support, and has been sharing with me all the important moments of our lives.

Thank You all

Andrea Santoriello

Contents

CHAPTER 3

Turbulent Flow Computations

CHAPTER 4

Stabilized Finite Element Methods

CHAPTER 5

Scalar Test Cases

Preface

The subject of Finite Element Method (FEM) has been developing for decades, and has reached now a so widespread diffusion that lots of journals and books focus on it and introduce each day new arguments of discussion for the research community.

The high performance calculators that have been growing up since the eighties and are nowadays available at reasonable prices, significantly accelerated this spreading process of FEM, both for research investigation and for industries, being responsible for the growth of more and more different fields of application for problem discretization methods in general.

It is a matter of fact that continuous problems, which model real phenomena, could be solved with rigorous mathematics only in few cases (and in simplified conditions), which practically means intractability of realistic types of continuum problems. The researcher is thus allowed to attempt to solve discretized problems that should hopefully recast the real situation in the continuum limit. In this framework FEM found its origin and started to develop and involve several fields of application, the most important being solid and fluid mechanics.

In the last decade turbomachinery design and development has started to represent a fertile field for FEM, since one of the key features to be issued for improving their performance is a better knowledge of their fluid dynamics, with particular interest in the secondary flows and loss phenomena. In this viewpoint, a large extent of experimental work must be performed, including in this definition all the techniques that permit to obtain trustable information on the real physics of these complex flows, due to the difficulties that could arise in executing measurements on unhandy and small locations. This discussion should be enriched with some economics considerations that lead to the conclusion that the number of prototypes must be reduced, so as the market time of new devices, but on this aspect another Ph D Thesis would be needed.

FEM and CFD represent thus an inviting “strategy” for turbomachinery industries, due to the relatively low costs with respect to measurement campaigns and prototyping, and the relatively short time to obtain results, limited just by the PC clusters performance, that are growing faster and faster. The conditions under which the last statement is correct are mainly two:

1. It is possible to consider CFD as an experimental investigation?
2. FEM is the best mathematical background for CFD?

Concerning the latter question, that involves a comparison with Finite Volumes Methods (FVM), the reader could readily understand the writer’s opinion, so only few concepts will be reported, due to a large number of publications on the argument: the intrinsic ability of FEM to fulfill the prescribed boundary conditions of the problem, especially in the outflow regions, the global satisfaction of well established conservation laws, the higher precision due to a rigorous mathematical approach, are just some of the advantages

of FEM with respect to the Finite Volume approach, still widely used in commercial CFD codes.
This Ph D thesis focuses on the first question, namely it addresses the theme of CFD performance and reliability in turbomachinery flow prediction, splitting the argumentations in two main themes: turbulence modeling and numerical aspects of FEM.

Concerning turbulence modeling, it is possible to find several closure strategies within the RANS approach, that in this work is considered as the state of the art of this science branch. Amongst the several new formulations proposed in the recent years, some interesting linear and non-linear models will be considered, in order to have the big picture of the problem of modeling complex flows, and to understand how they fit in the more general framework of computational mechanics.

On a numerical point of view, the need of dealing with advanced turbulence modeling, which represents a necessary step towards more meaningful results, magnifies the main differences between solid mechanics and fluid mechanics computation, due to the lack of optimality in the Galerkin method for the typical differential operators introduced by the latter.

The previous argumentations could be seen as a simple explanation of the need for stabilized formulations to solve turbomachinery flows, which opened the way to something that could be defined as a new discipline in science, and more in particular in computer science: stabilized finite element methods.

In the recent years, stabilization techniques permitted to obtain more and more accurate results on several types of flow, and reached high level of reliability, thus justifying the idea of their influence in the process of modeling multiscale phenomena, such as turbulence.

This work, which represents the “concluding act” of a Ph D experience, presents new finite element formulations for multiscale problems, developed at the Department of Mechanics and Aeronautics of University “La Sapienza”, and addresses the study of the link between stabilization and advanced turbulence modeling.

Andrea Santoriello

List of symbols and abbreviations

The main rules followed to choose styles of characters and notations are briefly described:

- Matrices and Vectors are **bold** and *italic*, i.e. ***A, B, a, b, ….*** both of them could be written in upper or lower case, depending on the context;
- *Italic style* is used to indicate number of components, dimension of a problem, and more in general *concepts* to be highlighted or useful for the rest of the text;
- Parentheses indicate a function;
- Indicial notation will be generally used for derivatives and components, i.e. $\boldsymbol{u_i}$ is the *i-th* component of the $\boldsymbol{u}$ vector, $\boldsymbol{u_{,i}}$ is the *i-th* derivative of the $\boldsymbol{u}$ vector;
- Quotations from other publications will be presented in the following way: *"quotation"*;
- When possible, acronyms of mathematical tools, turbulence closures and test cases will be used, as well established in literature;

In the following, a (hopefully) helpful list of the most important symbols and abbreviations used in the text is presented.

Ω, Ω_e	Problem Domain, Element Domain
Γ, Γ_e	Boundary, Element Boundary
Γ_g	Dirichlet boundary
Γ_h	Neumann boundary
$\bar{\Omega}$	Closed Domain
w	weight functions
u	unknowns of the problem
h	element characteristic length
$\boldsymbol{S^h}$	set of trial solutions
$\boldsymbol{W^h}$	set of weight functions
$\boldsymbol{H^{nh}}$	Sobolev space of order n on the support of characteristic length h
K_{ji}	generic element of the stiffness matrix
F_j	generic element of right-hand side
ξ, η, ζ	coordinates in the logic element
N_i	shape functions
$\boldsymbol{J}$	Jacobian matrix
$\boldsymbol{x}, \boldsymbol{r}$	position vectors
$\frac{D}{Dt}$	material derivative
ρ	fluid density
ν	kinematic viscosity

μ	dynamic viscosity
$\nabla\cdot$	divergence operator, i.e. $\nabla\cdot\boldsymbol{u}=u_{j,j}$
∇	gradient operator, i.e. $\nabla\boldsymbol{u}=\left[u_{,x}\,u_{,y}\,u_{,z}\right]^{T}$
p	static-fluid pressure
δ_{ij}	Kronecker delta operator
e_{ij}	rate of strain tensor, i.e. $e_{ij}=\frac{1}{2}\left(u_{i,j}+u_{j,i}\right)$
ω_{ij}	vorticity tensor, i.e. $\omega_{ij}=\frac{1}{2}\left(u_{i,j}-u_{j,i}\right)$
Re	Reynolds number
Re_T	Turbulence Reynolds number
$o(..)$	"order of" operator
$\propto$	symbol of proportionality
$\overline{\phi}$	mean (in Reynolds decomposition sense)
u',v',w'	velocity components fluctuations (Reynolds decomposition sense)
l_k	Kolmogorov scale
$RANS$	Reynolds Averaged Navier-Stokes
$\boldsymbol{R}$	Reynolds stress tensor (i.e. $R_{ij}=-\rho\overline{u_i'u_j'}$)
ε	viscous rate of turbulent kinetic energy dissipation
k	turbulent kinetic energy
P_k	turbulent kinetic energy production term
d_k	turbulent kinetic energy distribution term
ν_t	turbulent eddy viscosity
S_{ij}	mean strain rate tensor
W_{ij}	mean rotation rate tensor
l_m	mixing length
$LS74$	Launder & Sharma linear k-ε turbulence closure
$\tilde{\varepsilon}$	modified dissipation rate
τ	turbulence time scale
$CLS96$	Craft, Launder & Suga non-linear k-ε turbulence closure
$\underline{\boldsymbol{U}}(\boldsymbol{x},t)$	filtered velocity field
$\dot{\boldsymbol{u}}(\boldsymbol{x},t)$	subgrid scale component
R_{res}	residual norm
R_{sol}	error norm
$\lvert\ \rvert$	absolute value
$\lVert\ \rVert_2$	norm two (also used as Euclidean norm)
$PSPG$	Pressure Stabilizing Petrov-Galerkin
$SUPG$	Streamline Upwind Petrov-Galerkin
SPG	Spotted Petrov-Galerkin

Pe	element Peclet number
$sgn()$	"sign of" function, i.e. $sgn(u)=1$ for $u>0$, $sgn(u)=-1$ for $u<0$
$\boldsymbol{s}$	unit vector in direction of the streamlines
$\boldsymbol{r}$	unit vector in direction of the solution gradient
$\boldsymbol{\pi}$	vector of weight function modifications
r	element reaction number
DRD	Diffusion for Reaction Dominated problems
$DRDJ$	Diffusion for Reaction Dominated problems with Jump factor
VMS	Variational MultiScale
$V\text{-}SGS$	Variable SubGrid Scale formulation
r_s	r-switch coefficient
$g_e(x,y)$	element Green's function
$\delta(x,y)$	Dirac's delta operator
TI	Turbulence intensity
y^+	Dimensionless wall distance
δ^*	Displacement thickness
θ^*	Momentum thickness
H	Shape factor
C_p	Static Pressure Coefficient

Chapter 1

THE FINITE ELEMENT METHOD FOR COMPUTATIONAL FLUID DYNAMICS

1.1 Introduction

As remarkably underlined in Taylor and Zienkiewicz (2000), the Finite Element Method could be seen as "*a general discretization procedure of continuum problems posed by mathematically defined statements*", based on a decomposition of the original system into individual components, or 'elements', whose behavior could be readily understood, and rebuilding the original system from such components.

This procedure involves two stages, respectively the system discretization in elements, whose behavior could be easier understood by means of a particular class of parameters, and the description of the whole system as an assembly of the elements.

The use of such a strategy is shared by most of the classical mathematical approximation procedures, thus "softening" the borderlines between Finite Element method and other formulations.

This chapter will first introduce the reader to some basic mathematical aspects of the Finite Element method and to the notation used in the rest of the work, stressing on the features proper of computational fluid dynamics (*CFD*). The analysis is made quick and synthetic, for further details the reader could refer to Chung (1978), Gresho and Sani (1998), Hughes (2000), Taylor and Zienkiewicz (2000) and Tezduyar (2001).

After that, aspects related to the weighted residual method and the Galerkin formulation will be discussed, remarking when needed all the necessary hypotheses, finalized to implement the formulation in a CFD finite element tool, such as the code *XENIOS*.

Finally, the element point of view will be presented, addressing the expression and properties of the shape functions and introducing some considerations about the fundamental issue of *convergence*.

1.2 Problem statement and weighted residual method

Many continuum problems that arise in engineering could be modeled by means of a system of partial differential equations with appropriate boundary and initial conditions on the unknowns, which could be thought as a scalar or more in general as a vector. In this work only second order differential operators are considered, with the structure typically encountered in fluid flow modeling equations.

The problem statement could be described as follows: find a function $\boldsymbol{u}$ which satisfies this matrix equation on a closed domain $\bar{\Omega}$:

$$\boldsymbol{A}\boldsymbol{u} = \boldsymbol{f} \tag{1.1}$$

where $\boldsymbol{A}$ is a $n \times n$ matrix, $\boldsymbol{u}$ is a vector of n variables (the unknowns) and $\boldsymbol{f}$ is the source vector of n components. It is worth noting that the set of differential equations could be non-linear, as often happens in real physics and that the non-diagonal terms of the $\boldsymbol{A}$ matrix represent coupling between the variables. The unknown $\boldsymbol{u}$ must also satisfy a system of boundary conditions on the domain boundary Γ, described as follows:

$$\boldsymbol{B}(\boldsymbol{u}) = \begin{Bmatrix} \boldsymbol{u} = \boldsymbol{g} & \rightarrow \Gamma_g \\ \boldsymbol{u}_{,n} = \boldsymbol{h}_n & \rightarrow \Gamma_h \end{Bmatrix} \tag{1.2}$$

where Γ has been divided in two parts, namely Γ_g and Γ_h, as follows:

$$\overline{\Gamma_g \cup \Gamma_h} = \Gamma \tag{1.3a}$$

$$\Gamma_g \cap \Gamma_h = \varnothing \tag{1.3b}$$

with *Dirichlet* boundary conditions imposed on Γ_g and *Neumann* boundary conditions imposed on Γ_h.

In an equivalent way we could write (1.1) and (1.2) in vector form as:

$$\boldsymbol{A}(\boldsymbol{u}) - \boldsymbol{f} = \begin{bmatrix} A_1(\boldsymbol{u}) - f_1 \\ A_2(\boldsymbol{u}) - f_2 \\ \cdots\cdots\cdots \\ A_n(\boldsymbol{u}) - f_n \end{bmatrix} = \boldsymbol{0} \quad \text{in } \Omega \tag{1.4a}$$

$$\boldsymbol{B}(\boldsymbol{u}) = \begin{bmatrix} B_1(\boldsymbol{u}) \\ B_2(\boldsymbol{u}) \\ \cdots\cdots\cdots \\ B_n(\boldsymbol{u}) \end{bmatrix} \qquad \text{on } \Gamma \tag{1.4b}$$

where A_i and B_i represent respectively the *i-th* row of the matrix $\boldsymbol{A}$ and the *i-th* component of the boundary conditions vector $\boldsymbol{B}$. Eqs. (1.1) and (1.2) together, or equivalently (1.4), express what is called the *strong form* of the original differential problem.

If we consider the Finite Element method as an integral approach to the problem, two ways could be followed to obtain the formulation, the first one being the *weighted residual method* and the second the determination of *variational functionals*. In this work only the first one will be considered, because variational functionals could be derived only for some simple types of problem, fluid dynamics of viscous flows being not included (Corsini (1996)).

The weighted residual method could be seen as a general approach to differential problems, since the integral equation of the problem is obtained towards the inner product of the differential equations for a basis of weight functions, integrated in all the domain.

Let now consider the form (1.4a) of the problem and let multiply it by a set of arbitrary functions $\boldsymbol{w}$, that we will call *weight functions*. Since the set of differential equations must be satisfied at each point of the domain, it is simple to conclude that:

$$\int_{\Omega} \boldsymbol{w}^T \boldsymbol{A}(\boldsymbol{u}) d\Omega - \int_{\Omega} \boldsymbol{w}^T \boldsymbol{f} d\Omega = 0 \tag{1.5}$$

where $\boldsymbol{w}$ could be written in vector form as:

$$\boldsymbol{w} = \begin{bmatrix} w_1 \\ w_2 \\ \cdots\cdots \\ w_n \end{bmatrix} \tag{1.6}$$

whose components are the weights for each different variable of the problem.

The integral statement we are dealing with is more powerful, because (1.5) must be fulfilled for all $\boldsymbol{w}$, being this the only condition that allows (1.1) to be satisfied at any point of the domain.

Before going further in details on this last statement, let note that the existence of (1.5) involves a background of hypotheses, implicitly related to the fact that each of the terms must not be infinite, that implies the necessity of having certain restrictions on the functions $\boldsymbol{w}$ and $\boldsymbol{u}$. Considering the latter, the order of derivatives must be considered in order to make a decision about these restrictions: if *n order* derivatives are involved, then the only way to obtain integrable terms is the continuity of *n-1 order* derivatives, as well stated in Taylor and Zienkiewicz (2000).

This situation could be manipulated via the continuity of the problem, which permits to apply an *integration by parts* on (1.5), that reduces the order of derivatives on $\boldsymbol{u}$, giving rise to derivatives of $\boldsymbol{w}$, with a subsequent beneficial balance between the restrictions on $\boldsymbol{u}$ and $\boldsymbol{w}$. In order to have simplified analytical developments, let consider the linearization of the original differential operator $\boldsymbol{A(u)}$. The integration by parts leads to the following formulation of the original second order differential problem:

$$\int_{\Omega} \boldsymbol{E(w)}^T \boldsymbol{F(u)} d\Omega - \int_{\Omega} \boldsymbol{w}^T \boldsymbol{f} d\Omega + \int_{\Gamma} \boldsymbol{w}^T \boldsymbol{G(u)} d\Gamma = 0 \tag{1.7}$$

where $\boldsymbol{E}$ involves derivatives of the weight functions, while $\boldsymbol{F}$ involves lower order derivatives of $\boldsymbol{u}$ with respect to $\boldsymbol{A}$. Moreover, $\boldsymbol{G(u)}$ contains derivatives normal to the boundary of the unknown. The nature of the last integral in (1.7) must be clarified, demonstrating another benefit introduced by integration by parts.

By now, retaining in mind the restrictions on the terms in the integrals, no approximations have been done, and in fact we could state an equivalence between *strong form* of the problem and formulation (1.7), subjected to some condition on its last integral that permits to fulfil the Neumann boundary conditions. If we impose that the operator $\boldsymbol{G(u)}$ is equal to $-\boldsymbol{h_n}$, then we obtain what is called the *weak form* of the original problem, that automatically satisfies its Neumann boundary conditions.

In order to demonstrate this equivalence we have to ensure that (1.5) and (1.7) are fulfilled for *all* $\boldsymbol{w}$, which should thus take their origin from a basis of infinite components.

Let now introduce a function $\tilde{\boldsymbol{u}}$ as the *trial solution* for the problem, chosen in such a way to satisfy the Dirichlet boundary conditions. Let also call $\boldsymbol{\varepsilon}$ the *residual* or *error*, which reads as:

$$\boldsymbol{A(\tilde{u})} - \boldsymbol{f} = \boldsymbol{\varepsilon} \tag{1.8}$$

In view of this notation, (1.5) could be re-written in a more meaningful way (the same procedure could be followed for (1.7)):

$$\left(\boldsymbol{w}, \boldsymbol{\varepsilon}\right) = 0 \tag{1.9}$$

Eq. (1.9) corresponds to an *inner product* and is equivalent to ask for the orthogonality between the error and the space of the weight functions, but since the latter is infinite-dimensional, the only way to satisfy (1.9) is to have null residual at each point of the domain, which means $\tilde{\boldsymbol{u}} = \boldsymbol{u}$, and thus demonstrates the equivalence between strong and weak formulation.

Actually, when dealing with discretized solution methods, it is not possible to have infinite functions at our disposal, both for weights and trial solution, which are both approximated by finite-dimensional sets of functions.

Considering the trial solution, it could be described in the form of a finite series:

$$\tilde{\boldsymbol{u}}^h = \sum_{i=1}^{n_{tot}} \boldsymbol{D_i} N_i \tag{1.10a}$$

$$\boldsymbol{D}_i = \begin{bmatrix} D_{i1} \\ D_{i2} \\ ..... \\ D_{in} \end{bmatrix} \tag{1.10b}$$

where the superscript h represents the characteristic length of the *grid* (or *mesh*) that discretizes the domain with n_{tot} *nodes*, $\boldsymbol{D_{ik}}$ is the value assumed on the *i-th* node by the *k-th* unknown vector component, and N_i are *linearly independent functions,* called *shape functions*, which take unit value on the corresponding node.

There are some constraints in the choice of the shape functions, because the trial solution must fulfil the boundary conditions, which are given data of the problem, and must guarantee the existence of the integrals to be computed, as already requested for (1.5).

The first condition is respected if the choice of $\tilde{\boldsymbol{u}}^{\boldsymbol{h}}$ leads to automatic satisfaction of the *Dirichlet boundary conditions* $\boldsymbol{g}$. The latter could be completely understood introducing the notion of *Sobolev spaces* (see Chung (1978) for further details), but it could be intuitively depicted stating that if n is the maximum order of derivatives appearing in the integrals, then the square of the n-1 order derivatives must be integrable.

All these considerations could be summarized with this synthetic definition of the set $\boldsymbol{S^h}$ of the trial functions:

$$\boldsymbol{S}^h = \left\{ \tilde{\boldsymbol{u}}^h / \tilde{\boldsymbol{u}}^h \in \boldsymbol{H}^{1h},\ \tilde{\boldsymbol{u}}^h = \boldsymbol{g} \ \ on \ \ \Gamma_g \right\} \tag{1.11}$$

where $\boldsymbol{H}^{1h}$ is the *first order Sobolev space* defined on the support of the grid with characteristic length h.

Turning the attention to the weight functions, they are chosen in such a way to fulfil same Sobolev conditions for the integration, and the homogeneous counterpart of the Dirichlet boundary conditions, which permits to discard all integrals on Γ_g form (1.7). Therefore the weight functions must belong to a finite dimensional set $\boldsymbol{W}^h$, described as follows:

$$\boldsymbol{W}^h = \left\{ \boldsymbol{w}^h / \boldsymbol{w}^h \in \boldsymbol{H}^{1h}, \boldsymbol{w}^h = \boldsymbol{0} \ \ on \ \ \Gamma_g \right\} \tag{1.12}$$

Now it is possible to write the *finite dimensional approximation of the weak formulation* (1.7), which reads as follows:

$$\int_{\Omega} \boldsymbol{E}(\boldsymbol{w}^h)^T \boldsymbol{F}(\tilde{\boldsymbol{u}}^h) d\Omega - \int_{\Omega} (\boldsymbol{w}^h)^T \boldsymbol{f} d\Omega + \int_{\Gamma_h} (\boldsymbol{w}^h)^T \boldsymbol{G}(\tilde{\boldsymbol{u}}^h) d\Gamma = 0 \qquad (1.13)$$

where $\boldsymbol{G}(\tilde{\boldsymbol{u}}^h)$ is forced to be equal to $-\boldsymbol{h_n}$.

In view of (1.13), the orthogonality condition on the residual (1.9) could be satisfied only in an *average sense*, since the finite element trial solution $\tilde{\boldsymbol{u}}^{\boldsymbol{h}}$ could approach the differential problem solution $\boldsymbol{u}$ only on the n_{tot} nodes of the grid. The condition (1.13) represents a weighted integral of the solution residual, and must be recast in a system of equations in the $\boldsymbol{D_i}$ unknowns, which are the values to be determined on the grid nodes.

In order to have a complete understanding of the weak form of the problem, some further considerations must be done about the boundary conditions. It should be noted that trial solutions are required to satisfy explicitly the Dirichlet boundary conditions, which are thus called *essential boundary conditions*, while Neumann boundary conditions are not imposed directly on the trial functions, but are implied by the satisfaction of the integral equation (1.13) with $\boldsymbol{G}(\tilde{\boldsymbol{u}}^h)$ forced to be equal to $-\boldsymbol{h_n}$, being thus called *natural boundary conditions* (Hughes (2000)), because they *naturally* appear in the residual formulation.

Starting from (1.7), or from (1.13) in approximated way, it is possible to demonstrate that the original differential equations and the natural boundary conditions are the *Euler-Lagrange equations* of the weak form of the problem.

1.3 The Galerkin weighted residual formulation

In this Section the Galerkin formulation of the weighted residual method is presented, introducing the reader to the treatment of the Finite Element Method in the XENIOS code.

There are various ways to choose the weight functions, leading to different Finite Element formulations. The most widespread one is the *Galerkin method*, that is also used in the XENIOS code. It is characterized by the choice of using weight functions with the same basis of the trial functions, namely:

$$\boldsymbol{w}^h = \sum_{j=1}^{n_{tot}} \boldsymbol{C_j} N_j \qquad (1.14a)$$

$$\boldsymbol{C_j} = c_j \begin{bmatrix} 1 \\ 1 \\ .. \\ 1 \end{bmatrix} = c_j \boldsymbol{I_n} \qquad (1.14b)$$

where $\boldsymbol{C_j}$ is a vector of n components all equal to the value *cj* assumed by the weight in the *j-th* node.

To be more precise, the conditions expressed by (1.11) and (1.12) for the Dirichlet boundary conditions enforce $\boldsymbol{W^h}$ to be a subspace of $\boldsymbol{S^h}$, since we must consider that not all n_{tot} nodes have unknown values of the variables. Thus, if we consider the last n_g nodes to be the ones on the Dirichlet boundary Γ_g we could write:

$$\tilde{\boldsymbol{u}}^h = \sum_{i=1}^{n_{tot}-n_g} \boldsymbol{D_i} N_i + \sum_{l=n_{tot}-n_g+1}^{n_{tot}} \boldsymbol{g_l} N_l \tag{1.15}$$

$$\boldsymbol{w}^h = \sum_{j=1}^{n_{tot}-n_g} \boldsymbol{C_j} N_j \tag{1.16}$$

Let now introduce the expressions (1.15) and (1.16) in the weighted residual formulation (1.13), the integral formulation could be re-written as:

$$\begin{aligned} &\int_\Omega \boldsymbol{E}\Big(\sum_{j=1}^{n_{tot}-n_g} \boldsymbol{C_j} N_j\Big)^T \boldsymbol{F}\Big(\sum_{i=1}^{n_{tot}-n_g} \boldsymbol{D_i} N_i\Big) d\Omega = \int_\Omega \Big(\sum_{j=1}^{n_{tot}-n_g} \boldsymbol{C_j} N_j\Big)^T \boldsymbol{f} d\Omega + \\ &-\int_\Omega \boldsymbol{E}\Big(\sum_{j=1}^{n_{tot}-n_g} \boldsymbol{C_j} N_j\Big)^T \boldsymbol{F}\Big(\sum_{l=n_{tot}-n_g+1}^{n_{tot}} \boldsymbol{g_l} N_l\Big) d\Omega + \int_{\Gamma_h} \Big(\sum_{j=1}^{n_{tot}-n_g} \boldsymbol{C_j} N_j\Big)^T \boldsymbol{h_n} d\Gamma \end{aligned} \tag{1.17}$$

Since (1.17) must be valid for all the $\boldsymbol{w^h}$, then it must not depend on the choice of $\boldsymbol{C_j}$. In this way we could write an equation for each *j*, thus obtaining n_{tot}-n_g equations, sufficient in number to determine the unknown values of the variable $\boldsymbol{u}$. Each of these equations reads as:

$$\begin{aligned} &\int_\Omega \boldsymbol{E}(\boldsymbol{I_n} N_j)^T \boldsymbol{F}\Big(\sum_{i=1}^{n_{tot}-n_g} \boldsymbol{D_i} N_i\Big) d\Omega = \int_\Omega (\boldsymbol{I_n} N_j)^T \boldsymbol{f} d\Omega + \\ &-\int_\Omega \boldsymbol{E}(\boldsymbol{I_n} N_j)^T \boldsymbol{F}\Big(\sum_{l=n_{tot}-n_g+1}^{n_{tot}} \boldsymbol{g_l} N_l\Big) d\Omega + \int_{\Gamma_h} (\boldsymbol{I_n} N_j)^T \boldsymbol{h_n} d\Gamma \end{aligned} \tag{1.18}$$

Since we made the hypothesis of a linear second order differential operator, or, which is the same, considering the linearized form of the original differential operator, Eq. (1.18) could be re-written as:

$$\sum_{i=1}^{n_{tot}-n_g}\left[\int_{\Omega}\boldsymbol{E}(\boldsymbol{I_n}N_j)^T F(N_i)d\Omega \quad \boldsymbol{D_i}\right]=\int_{\Omega}(\boldsymbol{I_n}N_j)^T \boldsymbol{f}d\Omega+$$
$$-\int_{\Omega}\boldsymbol{E}(\boldsymbol{I_n}N_j)^T \boldsymbol{F}(\sum_{l=n_{tot}-n_g+1}^{n_{tot}}\boldsymbol{g_l}N_l)d\Omega+\int_{\Gamma_h}(\boldsymbol{I_n}N_j)^T \boldsymbol{h_n}d\Gamma \tag{1.19}$$

If we now put

$$\int_{\Omega}\boldsymbol{E}(\boldsymbol{I_n}N_j)^T F(N_i)d\Omega=\boldsymbol{K_{ji}} \tag{1.20a}$$

and

$$\int_{\Omega}(\boldsymbol{I_n}N_j)^T \boldsymbol{f}d\Omega-\int_{\Omega}\boldsymbol{E}(\boldsymbol{I_n}N_j)^T \boldsymbol{F}(\sum_{l=n_{tot}-n_g+1}^{n_{tot}}\boldsymbol{g_l}N_l)d\Omega+$$
$$+\int_{\Gamma_h}(\boldsymbol{I_n}N_j)^T \boldsymbol{h_n}d\Gamma=F_j \tag{1.20b}$$

it is possible to write in a synthetic way the resulting linear system of equations in the $\boldsymbol{D_i}$ unknowns:

$$\sum_{i=1}^{n_{tot}-n_g}\boldsymbol{K_{ji}}\boldsymbol{D_i}=F_j \qquad j=1,....n_{tot}-n_g \tag{1.21}$$

This is the final expression of the *Galerkin weighted residual formulation*. Finally, it is worth noting that the procedure followed to obtain (1.21) is valid both if u is a scalar variable, in which case K_{ji} is a coefficient and D_i is the scalar value of the unknown on the *i-th* node, and if $\boldsymbol{u}$ is a vector of n components, in which case each $\boldsymbol{K_{ji}}$ is a vector of n *components*, and each $\boldsymbol{D_i}$ is a vector of n components, which represents the solution for the vector $\boldsymbol{u}$ on the *i-th* node.

1.4 The element point of view

In the preceding Sections a *global point of view* has been adopted, because of its usefulness in establishing the mathematical properties of the Finite Element method. Nevertheless, in order to obtain a Finite Element method from the previous analytical developments, it is necessary to start from a *local approach*.

On an engineering point of view, the formulation must be capable of reproducing the local behavior of each element, that could be readily understood without many complications, and could be interpreted as a component of the global continuous system, whose behavior could be rebuilt simply as an assembly of its components.

In addition to these considerations, it must be noted that the major difficulty arising in a global approach would be the satisfaction of global boundary conditions. This aspect could be readily understood with a glance at (1.15), in which N_i and N_l functions must be chosen in order to satisfy the Dirichlet conditions $\boldsymbol{g}$ on the nodes on Γ_g, and this must be obtained notwithstanding the geometry of the domain.

Another question that must be addressed is the ease in the implementation into a computer code. To this end, let consider the generic contribution K_{ji} to the matrix of the problem (often called stiffness matrix), as defined in (1.20a), and for the sake of simplicity let consider the situation of u representing a scalar variable. If $i \neq j$, non-diagonal coefficients are introduced in the matrix and the solution procedure is more cumbersome. The only way to overcome these difficulties is to have N_i and N_j (and also their derivatives) defined just in the neighborhood of the nodes to which they refer. In this way it is possible to have a *banded matrix*, which is a desired feature for all the numerical solution procedures adopted in computer codes.

All these considerations lead to the conclusion that a local approach must be adopted, based on an element point of view. To this end, let consider the decomposition of the original domain in a certain number *nel* of non-overlapping elements by means of a certain *grid* (or mesh), as shown in Fig. 1.1.

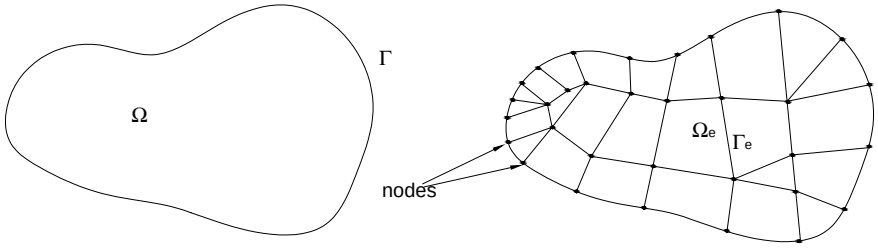

Fig. 1.1. Domain discretization.

The procedure to be followed must be equivalent to the global approach and should be the more similar as possible for each element of the grid. In order to design a local contribution of each element domain Ω_e to the global problem in Ω, a local system of coordinates is adopted, where all the terms are computed easily and with a standard procedure, then all the information are collected and assembled in the global matrix of the problem, by means of the knowledge of connections between different elements and of the position of the nodes.

The Finite Element formulation of the problems will thus read as:

$$\sum_{e=1}^{nel}\left[\sum_{i=1}^{n_{tot}-n_g} \boldsymbol{K_{ji}}^{\boldsymbol{e}} \boldsymbol{D_i}\right] = \sum_{e=1}^{nel} F_j^{\,e} \qquad j = 1,....n_{tot} - n_g \tag{1.22}$$

where on left-hand side the contribution of a certain element e is non-zero only if it is in the "neighborhood" of i and j nodes, and on right-hand side the contribution of the

element e is non-zero only if it is in the "neighborhood" of j node (for examples of the assembling procedure the reader could consult Hughes (2000), where some one-dimensional problems are addressed).
A particular attention must be given to the boundary integrals, because now the integration by parts must be applied element by element, so each element e contributes with boundary integrals on Γ_e. More in particular, each element has some sides (or surfaces in three dimensions) in common with other elements, and if it lays on the global domain boundary, it has one or more sides (or surfaces) on Γ. For the first type of sides there are two integrals, which represent the contributions of two facing elements, and give rise to what is called a *jump term* (Hughes et al. (1998), Tezduyar and Osawa (2000)). Usually this contributions are discarded from the formulation, even if they should be considered when higher order shape functions are employed. Concerning the second type of boundary integrals they contribute to right-hand side when element e has a boundary on Γ_h and it is in the "neighborhood" of j node.

1.5 Finite elements and shape functions

1.5.1 Convergence

The final scope of the Finite Element method is obviously the *convergence* to the true solution of the governing differential problem. The discussion on mathematical properties of Finite Elements, pursued in the preceding Sections, leads to two fundamental concepts:

a. The global representation of a variable is obtained towards the assembly of integrals over the local domains Ω_e of non-overlapping finite elements;
b. The Galerkin finite element formulation is obtained using shape functions that act also as weights in the Galerkin integral (Chung (1978)).

This simplified description permits to understand that the two crucial issues of a Finite Element method are the *elements* and the *shape functions*. To be more precise, the finite element interpolation is characterized by the shape of the element and the type of shape functions, and both of them must meet certain criteria such that convergence could be reached.

The concept of convergence that could be addressed is not "*how good the approximated solution is*", because this would imply the knowledge of the exact solution of the problem. The real question is "*how the approximated solution could be improved*", and the answer should be "*increasing the number of nodes (and elements)*" or equivalently "*reducing the element characteristic length* h". This criterion turns to a *sufficient* condition of convergence when the following three constraints are fulfilled by the shape functions:

1. they must be *continuous* with their first order derivatives into the element;

2. they must be continuous along the element boundary;
3. they must be *complete*.

The first two requirements are imposed for the existence of the integrals, because for second order differential operators integration by parts permits to have at the maximum first order derivatives of the shape functions in the integrals over the domains, while the terms into boundary integrals involve the Neumann boundary conditions and the shape functions directly. The third requirement actually means that if the mesh is progressively refined, the elements are so little that the exact solution would be constant in each of them. Thus the shape functions must be capable of reconstructing a constant behavior of the solution when $h \to 0$.

These conditions pose some restrictions in the choice of the analytical expression of the shape functions. In this respect some typical choices are *polynomial* expressions (typically linear or quadratic) or polynomial multiplied by *exponential* or *trigonometric* functions. It is obvious that a higher order of the shape function causes a better precision in the interpolation of the variation of the solution into each element, but it requires more nodes on the sides (or surfaces in three dimensions) and in the element interior. In this way the benefits obtained in terms of precision are paid with more complicated computations and difficulties in the implementation in computer codes. This problem is also influenced by the geometry of the elements and by the choice of the system of coordinates in which perform the calculation of the integrals. A compromise is thus needed, and usually it is given by *polynomial shape functions*, with *linear* ones being the most common choice. It is worth noting that the XENIOS code features linear and quadratic polynomial shape functions.

1.5.2 Isoparametric finite elements

In general, the geometry of the elements which discretize the global domain is *triangular* or *quadrilateral* in two-dimensional problems and *tetrahedrical* or *hexahedrical* in three-dimensional problems. The nodes of the grid are usually on the corners and on the sides (and surfaces in three dimensions), depending on the order of the shape functions. It is useful now to state that in this work only quadrilateral elements in 2D and hexahedrical in 3D will be considered.

In order to design the expression of the shape functions, the fundamental point of *geometrical mapping* must be addressed. In particular, if the real domain has a complex geometry, then it could be hard to work with shape functions defined on the Cartesian coordinates. It is easier to make a coordinate transformation and define a *non-dimensional* system of coordinates (*natural* or *normal coordinates*) and write shape functions with respect to it. Moreover the transformation could be chosen in such a way to lead to the same logic domain for all the elements of the grid, in order to have a unique expression for the shape functions.

Limiting for simplicity the attention to two-dimensional problems, the quadrilateral element imagine in the natural system of coordinates (ξ,η) is shown in Fig. 1.2.

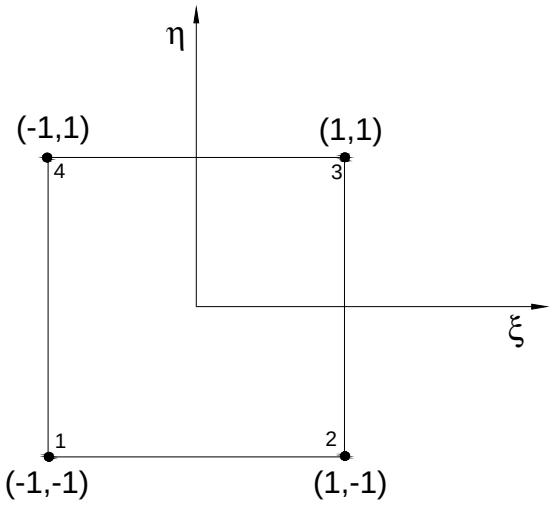

Fig. 1.2. two-dimensional quadrilateral finite element in natural coordinates.

The real geometry of the element, and the expression of the shape functions in it are obtained by means of the following coordinate transformation:

$$\begin{Bmatrix} x \\ y \end{Bmatrix} = f \begin{Bmatrix} \xi \\ \eta \end{Bmatrix} \tag{1.23}$$

More in detail, the function *f*, which is proper of the element under consideration, gives rise to a biunivocal correspondence between logic and real coordinates, which is schematically represented in Fig. 1.3.

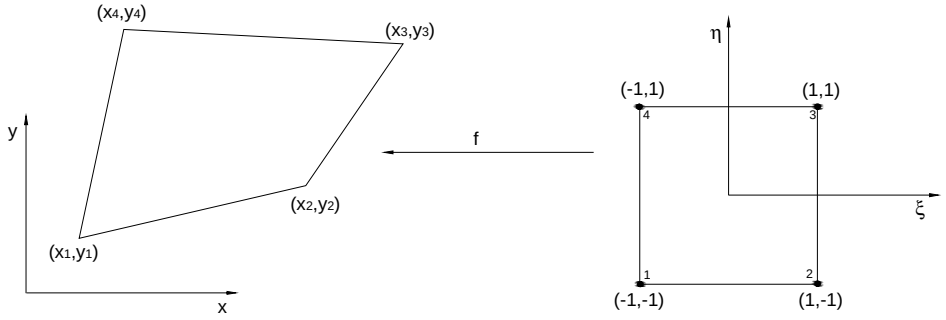

Fig. 1.3. Corresponding real and natural quadrilateral element.

A better understanding of the coordinate transformation could be attained if it is expressed with respect to the coordinates of the *nen* nodes of the real finite element. In particular x and y coordinates of a certain point must be functions of the corresponding (ξ,η) couple, with coefficients related to the *nen* coordinates of the element nodes x_i and y_i:

$$x(\xi,\eta)=\sum_{i=1}^{nen}\phi_i(\xi,\eta)x_i \qquad y(\xi,\eta)=\sum_{i=1}^{nen}\phi_i(\xi,\eta)y_i \tag{1.24}$$

Where ϕ_i are the *interpolation functions*, that permit to map in the real system of coordinates a point described by the couple (ξ,η) in the logic domain. If linear elements are considered, then ϕ_i expression is bilinear with respect to ξ and η, and reads like this:

$$\phi_i(\xi,\eta)=\alpha_{0i}+\alpha_{1i}\xi+\alpha_{2i}\eta+\alpha_{3i}\xi\eta \tag{1.25}$$

It is possible to obtain all the coefficients α_{ji} solving a linear system of equations that require information from four corner nodes, as well described in Chung (1978), where it is also possible to find details on the procedure to obtain high order polynomial interpolation functions and the extension to three-dimensional elements.

Before presenting the analytical expression the interpolation functions for two- and three-dimensional finite elements used in the XENIOS code, it is now crucial to discuss about the shape functions and their link with the interpolation functions. In this respect, Zienkiewicz (1971) introduced the extremely advantageous concept of *isoparametric elements*. The idea is that the same parametric function which maps the geometry can be used as shape function for describing the variation of the solution into the element, thus obtaining:

$$\phi_i(\xi,\eta,\zeta)=N_i(\xi,\eta,\zeta) \tag{1.26}$$

where the formulation has been considered for the more general three-dimensional context, being ζ the third logic coordinate. It is thus possible to write:

$$x(\xi,\eta,\zeta)=\sum_{i=1}^{nen}N_i(\xi,\eta,\zeta)x_i \tag{1.27}$$

$$u(\xi,\eta,\zeta)=\sum_{i=1}^{nen}N_i(\xi,\eta,\zeta)u_i \tag{1.28}$$

where u_i are the values assumed in the nodes by the unknown.

In order to perform the integration of all the terms in natural coordinates, the problem of derivation of the shape functions must be addressed, because the original problem

features derivatives with respect to Cartesian coordinates. These could be easily expressed in terms of the natural derivatives, following these simple passages:

$$\begin{Bmatrix} \frac{\partial N_i}{\partial \xi} \\ \frac{\partial N_i}{\partial \eta} \\ \frac{\partial N_i}{\partial \zeta} \end{Bmatrix} = \begin{bmatrix} \frac{\partial x}{\partial \xi} & \frac{\partial y}{\partial \xi} & \frac{\partial z}{\partial \xi} \\ \frac{\partial x}{\partial \eta} & \frac{\partial y}{\partial \eta} & \frac{\partial z}{\partial \eta} \\ \frac{\partial x}{\partial \zeta} & \frac{\partial y}{\partial \zeta} & \frac{\partial z}{\partial \zeta} \end{bmatrix} \begin{Bmatrix} \frac{\partial N_i}{\partial x} \\ \frac{\partial N_i}{\partial y} \\ \frac{\partial N_i}{\partial z} \end{Bmatrix} = \boldsymbol{J} \begin{Bmatrix} \frac{\partial N_i}{\partial x} \\ \frac{\partial N_i}{\partial y} \\ \frac{\partial N_i}{\partial z} \end{Bmatrix}$$

$$\Downarrow \tag{1.29}$$

$$\begin{Bmatrix} \frac{\partial N_i}{\partial x} \\ \frac{\partial N_i}{\partial y} \\ \frac{\partial N_i}{\partial z} \end{Bmatrix} = \boldsymbol{J^{-1}} \begin{Bmatrix} \frac{\partial N_i}{\partial \xi} \\ \frac{\partial N_i}{\partial \eta} \\ \frac{\partial N_i}{\partial \zeta} \end{Bmatrix}$$

where $\boldsymbol{J}$ is the *jacobian matrix* of the coordinate transformation.

Following this procedure, it is possible to calculate all the integrals in the logic system of coordinates thus eliminating the difficulties arising with the original geometry. The generic term K of the formulation could be integrated by using the following identity:

$$\int_V K dV = \int_{-1}^{1}\int_{-1}^{1}\int_{-1}^{1} K(\det J) d\xi d\eta d\zeta \tag{1.30}$$

Integrals are evaluated by means of a *Gauss-Legendre quadrature approach*, as simply explained in Segerlind (1984).

1.5.3 Shape functions

In the following, the analytical expression of the shape functions for all the types of elements implemented in the XENIOS code are presented. It is worth noting that the node numbering to which they refer is local and is related to the global numbering of the nodes by means of an *array* of connections.

The first element to be presented is the quadrilateral one with linear shape functions, called *Q1 element*, and characterized by four corner nodes, as shown in Fig. 1.4.

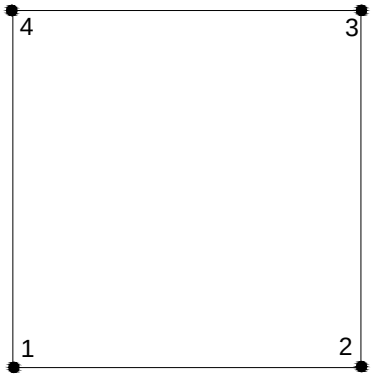

Fig. 1.4. two-dimensional element with four nodes (Q1 element).

The shape functions for the four nodes of the Q1 element read as follows:

$$\begin{bmatrix} \frac{1}{4}(1-\xi)(1-\eta) \\ \frac{1}{4}(1+\xi)(1-\eta) \\ \frac{1}{4}(1+\xi)(1+\eta) \\ \frac{1}{4}(1-\xi)(1+\eta) \end{bmatrix} \tag{1.31}$$

In two-dimensional problems it is also widely adopted the *Q2 element*, with quadratic shape functions and nine nodes, as shown in Fig. 1.5.

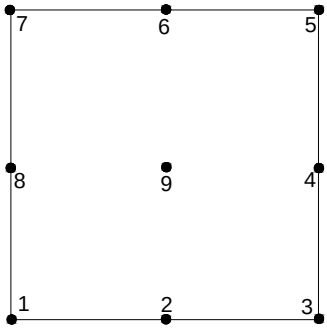

Fig. 1.5. two-dimensional element with nine nodes (Q2 element).

The shape functions for this element read as follows:

$$\begin{bmatrix} \frac{1}{4}\xi\eta(1-\xi)(1-\eta) \\ -\frac{1}{2}\eta\left(1-\xi^2\right)(1-\eta) \\ -\frac{1}{4}\xi\eta(1+\xi)(1-\eta) \\ -\frac{1}{2}\xi(1-\xi)\left(1-\eta^2\right) \\ \frac{1}{2}\xi(1+\xi)\left(1-\eta^2\right) \\ \frac{1}{4}\xi\eta(1+\xi)(1+\eta) \\ \frac{1}{2}\eta\left(1-\xi^2\right)(1+\eta) \\ -\frac{1}{4}\xi\eta(1-\xi)(1+\eta) \\ \left(1-\xi^2\right)\left(1-\eta^2\right) \end{bmatrix} \tag{1.32}$$

In three-dimensional problems, there are again Q1 and Q2 element available, with eight and twenty-seven nodes respectively. Concerning the first type, Fig. 1.6 sketches the geometry and the nodes.

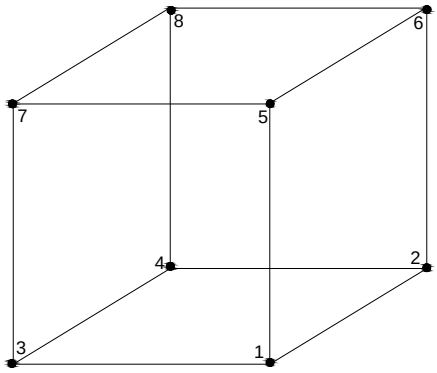

Fig. 1.6. three-dimensional element with eight nodes (Q1 element).

The related shape functions read as follows:

$$\begin{bmatrix} \frac{1}{8}(1-\xi)(1-\eta)(1-\zeta) \\ \frac{1}{8}(1+\xi)(1-\eta)(1-\zeta) \\ \frac{1}{8}(1-\xi)(1+\eta)(1-\zeta) \\ \frac{1}{8}(1+\xi)(1+\eta)(1-\zeta) \\ \frac{1}{8}(1-\xi)(1-\eta)(1+\zeta) \\ \frac{1}{8}(1+\xi)(1-\eta)(1+\zeta) \\ \frac{1}{8}(1-\xi)(1+\eta)(1+\zeta) \\ \frac{1}{8}(1+\xi)(1+\eta)(1+\zeta) \end{bmatrix} \tag{1.33}$$

For the Q2 three-dimensional element, less used for its higher computational cost, the reader could consult Corsini (1996).

References

Chung T. J., "Finite Element Analysis in Fluid Dynamics", *McGraw-Hill*, (1978).

Corsini A., "Analisi del flusso tridimensionale turbolento nei canali di una turbina idraulica. Previsione delle prestazioni con tecnica agli elementi finiti a matrice di rigidezza non assemblata" *(in italian), Ph D thesis, University of Rome "La Sapienza"*, (1996).

Gresho P. M. and Sani R. L., "Incompressibile Flow and the Finite Element Method", *John Wiley and Sons*, (1998).

Hughes T. J. R., "The Finite Element Method – Linear Static and Dynamic Finite Element Analysis", *Dover*, (2000).

Hughes T. J. R., Feijòo G. R., Mazzei L., Quincy J. B., "The variational multiscale method-a paradigm for computational mechanics", *Computer Methods in Applied Mechanics and Engineering*, v. 166, pp. 3-24, (1998).

Segerlind L. J., "Applied Finite Element Analysis", *John Wiley and Sons*, (1984).

Taylor R. L. and Zienkiewicz O. C., "The Finite Element Method", *5th edition, Butterworth-Heinemann*, (2000).

Tezduyar T. E.,"Lecture Series on Finite Elements in Fluids", *University of Tokyo, Tokyo,* (2001).

Tezduyar T. E., Osawa Y., "Finite element stabilization parameters computed from element matrices and vectors", *Computer Methods in Applied Mechanics and Engineering*, v. 190, pp. 411-430, (2000).

Zienkiewicz O. C., "The Finite Element method in Engineering Science", *McGraw-Hill*, (1971).

Chapter 2

INTRODUCTION TO FLUID DYNAMICS OF INCOMPRESSIBLE FLOWS

2.1 Introduction

The study of the evolution in time and space of a variable such as velocity components of a fluid flow requires some fundamental preliminary choices. The first decision to be made concerns the system of coordinates in which the flow has to be described. In this respect two main approaches could be considered, namely the *Lagrangian* and the *Eulerian* one. The first one is "attached" to a fluid particle (Chung (1978)) and must follow it with rotations and translations of the coordinate axes, while the second one introduces a system of coordinates fixed in space.

In general, Eulerian coordinates are preferred, because they better reproduce the scientist point of view, being based on an eye fixed at a point in space and observing particles of fluid passing, with the scope of obtaining a picture of the spatial distribution of the flow quantities (in general velocity components, pressure and turbulent variables).

All the characteristic parameters of the fluid are functions of both space and time, because their evolution is related to what happens to the particle they are moving with at a certain time. In order to describe a particular function $f(\boldsymbol{x},t)$, it is necessary to understand that it is a property of the fluid particle that at the instant t is passing in the position $\boldsymbol{x}$. The evolution of the function f is thus governed by a local rate of change due to *temporal changes* at position $\boldsymbol{x}$, and by the *convective* rate of change due to the transportation of the element to another position (Batchelor (1967)), giving rise to what is called *material derivative*, which reads as:

$$\frac{Df}{Dt} = \frac{\partial f}{\partial t} + \frac{\partial f}{\partial x_j}\frac{\partial x_j}{\partial t} = \frac{\partial f}{\partial t} + \frac{\partial f}{\partial x_j}u_j = f_{,t} + f_{,j}\,u_j \tag{2.1}$$

This chapter will introduce the reader to the fluid dynamics of *incompressible steady* flows, restricting the attention to the properties of interest for turbomachinery aerodynamics. The description of such flows needs the introduction of some conservation laws, that are discussed in the following with respect to an *inertial* frame of reference.

The *laminar* hypothesis will be first considered, in order to simplify the analytical developments, but the description will soon turn to a *turbulent* context, that is the main issue of this work.

2.2 Conservation laws for incompressible flows

2.2.1 Conservation of mass

Let consider a fixed closed surface A that encloses a volume V entirely occupied by the fluid. In the absence of any source of fluid, the mass of the fluid is conserved, so the density variation in each control volume V must be balanced by a net flux on the surface A. So we could write:

$$\frac{d}{dt}\int_V \rho dV + \int_A \rho u_j n_j dA = 0 \tag{2.2}$$

Considering that the volume V is fixed in space, then the time derivative could be put into the integral sign, and applying the transformation of the surface integral by means of the *divergence* theorem, it is possible to write (2.2) in a more meaningful way:

$$\int_V \left[\frac{\partial \rho}{\partial t} + \nabla \cdot (\rho \boldsymbol{u}) \right] dV = 0 \tag{2.3}$$

where the control volume could be selected without any restriction, so (2.3) is satisfied if the integrand is zero everywhere in the fluid:

$$\frac{\partial \rho}{\partial t} + \nabla \cdot (\rho \boldsymbol{u}) = 0 \tag{2.4a}$$

or equivalently:

$$\frac{D\rho}{Dt} + \nabla \cdot \boldsymbol{u} = 0 \tag{2.4b}$$

Eq. (2.4), in the two forms of (2.4a) and (2.4b), is the fundamental *mass conservation equation*, and could be simplified if the flow is *incompressible*, as in the rest of the work will be assumed. In this condition, fluid density is not affected by changes in pressure, but it could be approximately stated that fluid density of each element is constant (Batchelor (1967)), that implies the material derivative of density to be zero, so it is possible to write the *mass conservation equation for incompressible flows*:

$$\nabla \cdot \boldsymbol{u} = 0 \tag{2.5a}$$

or equivalently

$$u_{j,j} = 0 \tag{2.5b}$$

It could be thus inferred that an incompressible flow presents a zero rate of expansion.

2.2.2 Conservation of momentum

The momentum conservation could be analyzed considering the equilibrium between the rate of change of momentum of a certain portion of fluid and the sum of all forces acting on this portion. According to the definition (2.1) of *material derivative*, and retaining in mind the invariability of the control volume V, the rate of change of momentum is:

$$\int_V \rho \frac{D\boldsymbol{u}}{Dt} dV \tag{2.6}$$

where it must be recalled that the flow has been assumed *incompressible* (i.e. null material derivative of density).

As well explained in Batchelor (1967), the fluid experiments both *volume* and *surface* forces. The first ones could be written as:

$$\int_V \rho \boldsymbol{F} dV \tag{2.7}$$

while the latter have *i-th* component that could be obtained by means of the stress tensor σ_{ij}, that could be written both as a surface and as a volume integral:

$$\int_A \sigma_{ij} n_j dA = \int_V \sigma_{ij,j}\, dV \tag{2.8}$$

Considering again that the control volume could be chosen without any restriction, then the balance of momentum sources could be written on each point, and for the *i-th* component reads as:

$$\rho \frac{Du_i}{Dt} = \rho F_i + \sigma_{ij,j} \tag{2.9}$$

Which could be re-written expliciting the material derivative and retaining in mind that the flow is *steady*:

$$\rho u_j u_{i,j} = \rho F_i + \sigma_{ij,j} \tag{2.10}$$

Eq. (2.10), called usually *momentum conservation equation* or *equation of motion*, could be used for the determination of the distribution of fluid velocity, but could be solved only after a better knowledge of the right-hand side terms.

The first one represents body forces, and considering an *inertial* frame of reference, could be usually identified with gravity, thus being $\boldsymbol{F}=\boldsymbol{g}$.

Concerning the stress tensor σ_{ij}, it is the manifestation of short range interactions between fluid particles, thus being intimately related to internal reactions in the fluid, and requires some more considerations in order to be explicited.

If the flow is at rest, then the concept that it cannot withstand any tendency to be deformed without change of volume could be interpreted observing that in this case the stress tensor has only non-zero normal stresses, and reads as:

$$\sigma_{ij} = -p\delta_{ij} \tag{2.11}$$

where all the normal stresses are identical, which means that the stress tensor in a fluid at rest is everywhere isotropic and all axes are principal axes. Moreover the sign minus (-) is related to the fact that the usual state of fluids at rest is compression, with the variable p called *static-fluid pressure*.

When the fluid is in motion there is no reason to believe that tangential stresses will remain zero, as shown in real experiments, so the stress tensor will be no more isotropic, and could be decomposed in an *isotropic* part and a *non-isotropic* one. The first one could be obtained as the average of the invariant σ_{ii}, namely:

$$p = -\frac{1}{3}\sigma_{ii} \tag{2.12}$$

where a new definition of *pressure* has been introduced, which represents now the mean normal stress with sign reversed, and could not be related in a simple way to the *static-fluid pressure*, that refers to an equilibrium state (i.e. it is a variable of state). The stress tensor could be thus written as:

$$\sigma_{ij} = -p\delta_{ij} + \tau_{ij} \tag{2.13}$$

The deviatoric part τ_{ij} of the tensor is due entirely to the existence of motion, and is associated to the *internal friction* that permits the *transport of momentum* in the fluid, as a manifestation of a departure from equilibrium. The most relevant parameter that governs this departure is the *velocity gradient* ∇u. To be more precise, only short range interactions are important, so if we approximate the velocity filed locally as a linear function, then ∇u will be the maximum order of derivatives appearing in the expression of the deviatoric part of the stress tensor. For sufficiently small values of the magnitude of ∇u, it is possible to state that τ_{ij} depends linearly on it, reading as:

$$\tau_{ij} = A_{ijkl} u_{k,l} \tag{2.14}$$

where the fourth order tensor A_{ijkl} must be *symmetric* with respect to i and j because of the symmetry of the tangential stress tensor τ_{ij} (see Cohen and Kundu (2002)), and depends on the local properties of the material. At this point it is useful to introduce the hypothesis that the material is *homogeneous* and *isothermal*, so A_{ijkl} does not depend on the position. Moreover simple fluids are usually *isotropic*, so that A_{ijkl} does not depend on the orientation of the element, and could be written as a combination of delta tensors (i.e. see Batchelor (1967) for further details):

$$A_{ijkl} = \mu(\delta_{ik}\delta_{jl} + \delta_{il}\delta_{jk} - \frac{2}{3}\delta_{ij}\delta_{kl}) \tag{2.15}$$

where the scalar coefficient μ is the viscosity of the fluid, which must be positive, and the effects of *bulk viscosity* have been assumed to be negligible, as well explained in Cohen and Kundu (2002). With this expression, the tangential stresses read as:

$$\tau_{ij} = \mu(u_{i,j} + u_{j,i} - \frac{2}{3}\delta_{ij}u_{k,k}) \tag{2.16}$$

Fluids for which a linear relation between the tangential stresses and the *rate of strain* tensor e_{ij} (equal to $\frac{1}{2}(u_{i,j}+u_{j,i})$) holds, are called *Newtonian* fluids.

Recalling that the flow is *incompressible* and *steady*, and the frame of reference is *inertial*, it is possible to re-write the *momentum equation* (2.10) in a more meaningful way, which is :

$$\rho u_j u_{i,j} = -P_{,i} + \mu u_{i,jj} \tag{2.17}$$

where the new pressure P includes also the *potential* of the gravity field. Eq. (2.17) is the *Navier-Stokes equation of motion* for *incompressible, homogeneous, isothermal, isotropic* and *steady flows* in an *inertial* frame of reference. In view of its expression, it is now worthwhile expliciting the name of the terms appearing: the left-hand side one is called *convective (or advective) term*, since it represents the transport (or convection) of momentum into the control volume; the first term on right-hand side is the *pressure gradient term*, and the last one is the *diffusive term*.

2.3 The Reynolds number

Most of the research in fluid dynamics concerns with the development of experimental and/or numerical procedures able to reproduce the main characters of real

flows. In this respect the best procedure is to consider a similar geometrical apparatus, and try to obtain information about the real flow by means of the study of a *dynamical similar* one. Given the geometrical similarity between the real flow domain and the experimental apparatus or the numerical grid, it is possible to establish some conditions ensuring that the experimental or numerical flow pattern, in the following called *laboratory flow pattern*, will give similar dynamic behavior with respect to the real one if corresponding geometrical positions are considered (Tritton (1998)).

Let consider the laboratory flow pattern, and let normalize all the lengths with respect to a characteristic length L of the apparatus (i.e. the diameter of the duct, the chord of a blade etc.). Let do the same for the velocities, that must be referred to a characteristic velocity U (i.e. the bulk velocity in the duct, the free stream velocity on a blade etc.). In this way it is possible to define non-dimensional values of all parameters and variables to be calculated, as described in the following, where some basic criteria of dimensional analysis have been employed:

$$\tilde{x}_i = x_i / L \tag{2.18a}$$

$$\tilde{t} = t / \left(L / U \right) \tag{2.18b}$$

$$\tilde{u}_i \left(\tilde{\boldsymbol{x}}, \tilde{t} \right) = u_i \left(\boldsymbol{x}, t \right) / U \tag{2.18c}$$

$$\tilde{P} \left(\tilde{\boldsymbol{x}}, \tilde{t} \right) = P \left(\boldsymbol{x}, t \right) / \rho U^2 \tag{2.18d}$$

If the conservation equations (2.5) and (2.17) are expressed with this new notation, it is possible to obtain their non-dimensional (or normalized) counterparts:

$$\frac{U}{L} \tilde{u}_{j,j} = 0 \tag{2.19a}$$

$$\rho \frac{U^2}{L} \tilde{u}_j \tilde{u}_{i,j} = -\rho \frac{U^2}{L} \tilde{P}_{,i} + \mu \frac{U}{L^2} \tilde{u}_{i,jj} \tag{2.19b}$$

which, after some simple passages, read as:

$$\tilde{u}_{j,j} = 0 \tag{2.20a}$$

$$\tilde{u}_j \tilde{u}_{i,j} = -\tilde{P}_{,i} + \frac{1}{Re} \tilde{u}_{i,jj} \tag{2.20b}$$

where

$$Re = \frac{\rho UL}{\mu} \tag{2.20c}$$

The non-dimensional Navier-Stokes equation contains a parameter *Re*, called *Reynolds number*, which permits to identify dynamical similar flows: if two different flow patterns with similar geometrical features are characterized by the same Reynolds number, then their non-dimensional (or normalized) solution will be the same under the same normalized set of boundary conditions (Pope (2000)). This conclusion has a relevant importance in all the fluid dynamics research, since it permits to forecast the main characteristics of a certain real flow that could be not accessible to experiments, by means of a laboratory flow pattern which has similar geometrical domain and same Reynolds number. Moreover it is possible to repeat the same considerations for the dependent quantities, useful for the analysis of the properties of the flow: it is possible to infer these properties for a certain flow if the same properties are known for a dynamical similar one.

Focusing on the expression of *Re*, it is possible to understand that it indicates the relative importance of two dynamical processes, the *convective* on the *diffusive*, and in the following we will understand that when convection dominates (i.e. *Re* is high), the numerical solution of the problem is cumbersome.

The Reynolds number is the only non-dimensional parameter which characterize incompressible and steady flows without body forces. If other terms appear in the governing equations due to the physics of the flow (i.e. free surfaces, waves etc.), the procedure of finding non-dimensional parameters is applicable, but now there is the need for more non-dimensional parameters which added to the geometrical similarity permit to obtain same normalized solutions.

2.4 The CFD approach to fluid dynamics

In the previous Section we dealt with the *laboratory flow pattern*, as the flow field that, being dynamically similar with the real one, has a normalized solution equal to it. More in particular this work focus on *CFD*, which implies that the laboratory flow pattern is a *numerical solution field* obtained with a computer code.

As already explained in the Preface, a variety of reasons could be cited for the increased importance of simulation techniques (i.e. see Löhner (2001), Tezduyar et al. (1993), (1994) and (1996)), with arguments that could be used also in other science branches. To mention but a few:

- The need to *forecast performance* of a new product before its commercial spreading is of fundamental importance for companies, and in this process the major cost is related to the realization of prototypes. In this respect a

preliminary numerical assessment of different solutions is useful to reduce the variety of prototypes;

- The *cost of experiments* is often unsustainable and sometimes it is actually impossible to conduct experiments, i.e. because of the difficulty of reaching the point where probing data. The numerical investigation can give an answer where is needed, with the only limit of the grid resolution.
- The *computer speed and memory capacity* continue to improve year after year.

Nonetheless, it is important to understand that CFD is a *discrete* approach to the flow pattern and, even if it would be possible to demonstrate the correctness of all the governing equations, as if the mathematical model of the real problem would be exact, still the quality of the results would be dependent on the grid resolution, that should be able to describe the smallest *scale of motion* of the flow field (Corsini (1996), Lentini (1996)). This argumentations give rise to the following question: how to deal with turbulent flows?

2.4.1 Turbulent flows and their computation

Laminar flows are characterized by large scale physics, easy to be captured with relatively *coarse* (or rough) grids. The *mass conservation* and the *equation of motion* represent thus a complete system of equations able to reconstruct the flow pattern.

Turning to *turbulent flows*, the physics involves very small scales, increasing too much the quantity of grid nodes, and even if modern calculators are able to manage with lots of data, still it is not worthwhile proceeding in a direct integration of Navier-Stokes equations (*DNS* – Direct Numerical Simulation), except for very simple flow configurations (i.e. for further details see Hoffman and Johnson (2004)).

As underlined in Cohen and Kundu (2002), turbulence could be characterized by some key words, which in the following will be shortly explained: *diffusion*, *non-linearity*, *vorticity*, *dissipation*, *randomness*.

An empirical approach to turbulent flows permits to quickly understand their high rate of *diffusion* of both momentum and heat. This phenomenon is related to the relevant *non-linearity* of turbulent flows, which grows up with the *Reynolds number* and is related to the importance of convective effects. Moreover the non-linearity of these flows gives rise to disturbances which are represented by small flow structures, called *vortices,* that give *three-dimensional* character to turbulent flows.

On a computational point of view, the more interesting concepts are *dissipation* and *randomness*. Each vortex undergoes a *stretching* process, which extracts kinetic energy from the average motion and transfers it to smaller and smaller structures, until it is balanced by the heat production due to viscosity, which is represented by the *viscous rate of turbulent kinetic energy dissipation*, from now on called ε. The equilibrium between these opposite processes is reached when vortices have a critical dimension, to which the grid discretization should refer. In order to have an order of magnitude of this scale, let

present some results based on dimensional analysis. If l is the scale of largest vortices, it defines the rate of subtraction of energy from the mean flow, as follows:

$$\varepsilon = o\left[\frac{u'^2}{t}\right] = o\left[\frac{u'^2}{l/u'}\right] = o\left[\frac{u'^3}{l}\right] \tag{2.21}$$

where *u'* is used to represent the order of magnitude of velocity fluctuations, and t is the characteristic time of the largest vortices, related to their scale and to the velocity fluctuations too. As already said, this rate must be equal to the *viscous rate of turbulent kinetic energy dissipation.* On the other hand, the scale of the smallest vortices could depend only on ε and viscosity, being not related to what happens on larger scales, and according to the *Kolmogorov* criterium, it reads as:

$$l_k = \left[\frac{\nu^3}{\varepsilon}\right]^{1/4} \tag{2.22}$$

It could be demonstrated (see Corsini (1996) or Lentini (1996)) that the ratio between l and l_k is related to the *turbulence Reynolds number* Re_T:

$$\frac{l}{l_k} = o\left(Re_T^{3/4}\right) \tag{2.23a}$$

where

$$Re_T = o\left(Re\right) \tag{2.23b}$$

Thus it could be readily concluded that the grid nodes should be proportional to the cube of the ratio (2.23a), which means that the number of nodes *ntot* increases in the following way:

$$ntot \propto Re^{2.25} \tag{2.24}$$

It is obvious that when *Re* becomes relevant, the computing load becomes unsustainable, and DNS calculations require too much computing resources, even for nowadays computers. More loading is the situation of unsteady turbulent flows, for which *ntot* should be almost proportional to the *cube* of *Re*. In Hoffman and Johnson (2004) it is claimed that for a flow at $Re=10^6$, 10^{18} mesh points are needed to perform an accurate DNS, but these are numbers out of the possibilities of any foreseeable supercomputer.

As a final argumentation in this synthetic analysis of the turbulence computation issue, it should be clear that turbulent flows contain a certain amount of *randomness*, which introduces two consequences:

- The superposition of non-linear and randomic effects, which makes the fluid response to perturbations unstable, that means that a small change in the fluid properties, i.e. due to a little inhomogeneity or impurity, could cause a totally different flow pattern (Pope (2000)). This consideration reduces DNS reliability, because more than a calculation should be done under different sets of parameters in order to have some idea about the real flow behavior.
- A *statistical approach* is more appropriate for the study of turbulent flows, because the flow details contain randomic dependencies, whereas the average quantities are repeatable from experiment to experiment (Tritton (1998)).
- The DNS approach must not be discarded by researchers, because of three fundamental reasons: first, for moderate Reynolds number it permits to provide data for the development of better RANS and LES approaches; second, it could be applied to niche areas also at relevant Reynolds number; third, the current rate of performance improvement of supercomputers suggests a potential doubling of Reynolds number of DNS calculations every six years, and Sandham (2002) forecasts that with timescales upwards of 20 years, the application of DNS will start to be reliable also for aerodynamics purpose, which is the most extreme.

2.4.2 The RANS approach

Let now consider the statistical behavior of a certain variable $\phi(t)$, which could represent a particular velocity component. If several experiments are conducted with the same conditions, it is possible to obtain an *ensemble* of evaluations of ϕ at a certain time t, and it is possible to calculate the *ensemble average* of the experiments $\overline{\phi}(t)$ as:

$$\overline{\phi}(t) = \frac{1}{N}\sum_{i=1}^{N}\phi_i(t) \tag{2.25}$$

where N is the number of samples.

Let also consider the simplified situation in which the ensemble average does not depend on time, which means that the flow is *statistically steady*, then we could write:

$$\overline{\phi}(t) = \lim_{\Delta t\to\infty}\frac{1}{\Delta t}\int_{t_0}^{t_0+\Delta t}\phi(t) = \overline{\phi} \tag{2.26}$$

which practically means that for a *(statistically) steady flow* the ensemble averages could be commuted with the time averages taken over a sufficient relevant time interval.

It is thus possible to decompose each variable with these notation:

$$\phi = \overline{\phi} + \phi' \tag{2.27}$$

where by definition:

$$\overline{\overline{\phi}} = \overline{\phi} \tag{2.28a}$$

$$\overline{\phi'} = 0 \tag{2.28b}$$

This kind of decomposition is called *Reynolds decomposition* and, if applied to two variables ϕ and λ it fulfils the following two properties:

$$\overline{\phi'\overline{\lambda}} = \overline{\lambda'\overline{\phi}} = 0 \tag{2.29a}$$

$$\overline{\phi\lambda} = \overline{\lambda'\phi'} + \overline{\phi}\,\overline{\lambda} \tag{2.29b}$$

Moreover, the ensemble average concept grants that derivation and integration operators can commute with the average operator.

Let now use the Reynolds decomposition in the governing equations (2.5) and (2.17), and let average them. For the *continuity equation* we obtain:

$$\overline{\left(\overline{u_j} + u_j'\right)_{,j}} = \overline{\overline{u_{j,j}}} + \overline{u_{j,j}'} = \overline{u}_{j,j} + \overline{u_{j,j}'} = 0 \tag{2.30}$$

which means that

$$\overline{u}_{j,j} = 0 \tag{2.31}$$

This represents the *continuity equation for the mean flow*. Moreover subtracting it from (2.5b), it is possible to demonstrate that:

$$u_{j,j}' = 0 \tag{2.32}$$

which means that also the turbulent fluctuations are divergence-free. These results have been obtained in view of the linear structure of the continuity equation.

If we repeat the same procedure for the momentum equation (2.17), unfortunately some problems arise. Averaging each term, we obtain:

$$\overline{\frac{\partial}{\partial x_i}\left(\overline{P} + P'\right)} = \frac{\partial}{\partial x_i}\left(\overline{\overline{P} + P'}\right) = \frac{\partial \overline{P}}{\partial x_i} = \overline{P}_{,i} \tag{2.33a}$$

$$\overline{\mu \frac{\partial^2}{\partial x_j \partial x_j}\left(\overline{u_i} + u_i'\right)} = \mu \frac{\partial^2}{\partial x_j \partial x_j}\left(\overline{\overline{u_i} + u_i'}\right) = \mu \overline{u_i}_{,jj} \tag{2.33b}$$

$$\overline{\left(\overline{u_j} + u_j'\right)\frac{\partial}{\partial x_j}\left(\overline{u_i} + u_i'\right)} = \frac{\partial}{\partial x_j}\overline{\left(\overline{u_j} + u_j'\right)\left(\overline{u_i} + u_i'\right)} = \overline{u_j}\,\overline{u_i}_{,j} + \overline{u_i' u_j'}_{,j} \tag{2.33c}$$

where the average of the convective term has been obtained using the continuity property for the first passage and the Reynolds average properties for the second. The *non-linear* structure of the convective term is thus the origin of an additional term, that stems from the velocity fluctuations. More in particular this additional source of stress is related to the correlation of two velocity fluctuations at the same point, and is called *Reynolds stress* term. It is thus useful to put it on right-hand side, and after some simple developments it is possible to obtain the following *mean momentum equation*:

$$\rho \overline{u_j}\,\overline{u_i}_{,j} = -\overline{P}_{,i} + \left[\mu\left(\overline{u_i}_{,j} + \overline{u_j}_{,i}\right) - \rho \overline{u_i' u_j'}\right]_{,j} \tag{2.34}$$

where the diffusive term has been expressed in its original form in order to obtain a global right-hand side term which reads as:

$$\overline{\tau_{ij}}_{,j} = \left[-\overline{P}\delta_{ij} + \mu\left(\overline{u_i}_{,j} + \overline{u_j}_{,i}\right) - \rho \overline{u_i' u_j'}\right]_{,j} \tag{2.35}$$

The additional stress acting on the mean field of a turbulent flow is much larger than the diffusive (or viscous) one, except near the solid walls, where velocity gradients are relevant. It is thus useful to define the following Reynolds stress tensor $\boldsymbol{R}$:

$$\boldsymbol{R} = \begin{bmatrix} -\rho\overline{u'u'} & -\rho\overline{u'v'} & -\rho\overline{u'w'} \\ -\rho\overline{v'u'} & -\rho\overline{v'v'} & -\rho\overline{v'w'} \\ -\rho\overline{w'u'} & -\rho\overline{w'v'} & -\rho\overline{w'w'} \end{bmatrix} \tag{2.36}$$

It is a symmetric tensor, with diagonal components representing *normal stresses*, and non-diagonal terms representing *shear stresses*. If the flow tends to an *homogeneous isotropic* turbulent behavior, the normal stresses dominate and $\overline{u'} = \overline{v'} = \overline{w'}$. Even in this simplified setting, that is widely used in experimental studies, it is worth noting the intrinsic three-dimensionality of turbulence.

Eqs. (2.31) and (2.34) are the basis of the *RANS - Reynolds Averaged Navier-Stokes* approach to turbulence, which is nowadays the most widespread strategy for simulating turbulent flows, due to the enormous computational cost of direct simulation of complex turbulent flows.

Although the process of Reynolds decomposition permits to avoid the complete resolution of a turbulent motion, its drawback is that it introduces unknown single-point, higher-order correlations, which need to be included in the number of variables of the system of equations (Gatski and Rumsey (2002)). The need to model these correlations is what is called *closure problem*, and will be issued in the next Chapter, where different strategies to obtain a closed system of *RANS equations* will be presented.

As a conclusive remark, it is worthwhile mentioning that the high Reynolds number flows, with their *non-linearity* and their complex differential structure in modeling both the mean *continuity and momentum equation* and the effect of *turbulent correlations*, introduce a lot of numerical drawbacks, that must be addressed with an advanced stabilized finite element method. This issue will become clearer in the next Chapter and will be addressed in the fourth Chapter of the work.

References

Batchelor G. K., "An introduction to Fluid Dynamics", *Cambridge University Press*, (1967).

Chung T. J., "Finite Element Analysis in Fluid Dynamics", *McGraw-Hill*, (1978).

Cohen I. M., Kundu P. K., "Fluid Mechanics", *Academic press*, (2002).

Corsini A., "Analisi del flusso tridimensionale turbolento nei canali di una turbina idraulica. Previsione delle prestazioni con tecnica agli elementi finiti a matrice di rigidezza non assemblata" *(in italian), Ph D thesis, University of Rome "La Sapienza"*, (1996).

Gatski T. B. and Rumsey C. L., "Linear and Nonlinear Eddy Viscosity Models", in *Closure Strategies for Turbulent and Transitional Flows*, eds. Launder B. and Sandham N. D., pp. 9-46, *Cambridge University Press*, (2002).

Gresho P. M. and Sani R. L., "Incompressibile Flow and the Finite Element Method", *John Wiley and Sons*, (1998).

Hoffman J. and Johnson C., "Adaptive DNS/LES: a new agenda in CFD", in *Finite Element Methods: 1970's and beyond*, eds. Franca L. P., Tezduyar T. E. and Masud A., pp. 277-291, *CIMNE*, (2004).

Lentini D., "Applicazione di modelli di turbolenza avanzati a flussi in convezione naturale e forzata " *(in italian), University of Rome "La Sapienza",* (1996).

Löhner R., "Applied CFD Techniques", *John Wiley and Sons*, (2001).

Pope S. B., "Turbulent flows", *Cambridge University Press*, (2000).

Sandham N. D., "Introduction to Direct Numerical Simulation", in *Closure Strategies for Turbulent and Transitional Flows*, eds. Launder B. and Sandham N. D., pp. 248-266, *Cambridge University Press*, (2002).

Tezduyar T. E., Aliabadi S. K., Behr M., Johnson A. and Mittal S., "Parallel Finite Element Computation of 3D Flows", *Computer*, v. 26, pp. 27-36, (1993).

Tezduyar T. E., Aliabadi S. K., Behr M. and Mittal S., "Massively Parallel Finite Element Simulation of Compressible and Incompressible Flows", *Computer Methods in Applied Mechanics and Engineering*, v. 119, pp. 157-177, (1994).

Tezduyar T. E., Aliabadi S., Behr M., Johnson A., Kalro V. and Litke M., "Flow Simulation and High Performance Computing", *Computational Mechanics*, v. 18, pp. 397-412, (1996).

Tritton D. J., "Physical Fluid Dynamics", *Clarendon Press*, (1998).

Chapter 3

TURBULENT FLOW COMPUTATIONS

3.1 Introduction

Let recall the mean continuity and momentum equation, obtained in the previous Chapter:

$$\overline{u_j}_{,j} = 0 \tag{3.1}$$

$$\rho \overline{u_j}\,\overline{u_i}_{,j} = -\bar{P}_{,i} + \left[\mu \left(\overline{u_i}_{,j} + \overline{u_j}_{,i} \right) - \rho \overline{u_i' u_j'} \right]_{,j} \tag{3.2}$$

These equations represent the basis of the RANS approach to turbulent flows, and appear in all the turbulence models presented in the following. Notwithstanding, the presence of six more unknowns, namely the Reynolds stress components $R_{ij} = -\rho \overline{u_i' u_j'}$, introduces the necessity of additional equations in order to reach the closure of the system.

In this Chapter a description of the most used *closure strategies* within the RANS approach will be proposed, focusing on *first moment* closures, the ones adopted for the simulations reported at the end of the work, but also including a brief discussion on the recent LES and hybrid LES/RANS strategies. *Second Moment closures* won't be considered, being out of the scope of this research work, even if the *multiscale formulations* that will be derived in the next Chapter could be applied with beneficial effects in that context.

It is worth mentioning that First Moment closures, Second Moment closures and LES are based on *models*, which imply that a good numerical solution of the system of governing equations will be near to the real flow behavior depending on the quality of the model itself.

3.2 Moments and turbulent kinetic energy budget

At first sight, a good strategy to obtain the closure of the RANS system of equations is to deduce explicitly a conservation equation for each of the six unknown components of the Reynolds stress tensor. This procedure is called *direct closure,* and after some analytical passages, well described in Lentini (1996), leads to the following expression for the R_{ij} component governing equation:

$$\begin{aligned}\rho\overline{u_k}(\overline{u_i'u_j'})_{,k} &= -\rho(\overline{u_i'u_j'u_k'})_{,k} - \rho\overline{u_j'u_k'}\,\overline{u_i}_{,k} - \rho\overline{u_i'u_k'}\,\overline{u_j}_{,k} + \\ &+\overline{P'u_{j,i}'} + \overline{P'u_{i,j}'} - (\overline{P'u_j'})_{,i} - (\overline{P'u_i'})_{,j} + \mu(\overline{u_i'u_j'})_{,kk} - 2\mu\overline{u_{i,k}'u_{j,k}'}\end{aligned} \tag{3.3}$$

It is thus possible to understand that the attempt to obtain a conservation equation for a *second order moment*, that is an average of the product between two fluctuation components (i.e. $\overline{u_i'u_j'}$), gives rise to higher order moments and other unknowns such as the interaction moments between velocity and pressure fluctuations. In this way, the number of unknowns would progressively grow up, thus demonstrating the impracticability of the direct closure. The problem could be described by two key words: *non-linearity* and *non-locality* (Durbin and Petterson Reif (2001)). Non-linearity is represented by the fact that *n+1-th* moments appear in the governing equation of a *n-th* order moment, while non-locality is related to the terms containing pressure fluctuations, which are expression of two-point velocity fluctuation correlations, being pressure governed by elliptic operators, thus introducing the influence of the velocity field behavior in the surrounding of the point considered. Non-locality is nowadays out of any closure capabilities, and in the following it will be granted that only *single-point closures* will be issued, discarding or modeling all the terms introducing two-point correlations.

Concerning non-linearity and moments, it is possible to distinguish between formulations with *first moment closure*, where only the first order moments (mean velocity and pressure) are solved for, and formulations with *second moment closure*, where specific equations are written for the Reynolds stress components. Therefore the difference lays in the fact that first moment closures contain a *totally modeled* effect of Reynolds stress components, while second moment closures try to solve for them explicitly, and model only higher order moments.

In order to have a quick but complete comparison between first and second moment closures, it must be noted that second moment closures include the four scalar equations stemming from mean continuity and momentum, six equations for the second moments, and some equations modeling the effect of non-locality and/or higher order moments. On the other hand, first moment closures solve only for mean continuity and momentum equation, where the effect of Reynolds stress components is modeled by means of some empirical law or additional equation. Therefore, even if second moment closures are potentially more accurate in the description of complex turbulent flows, their computational cost is much higher.

Despite the difference in number and type of closure equations, generally the turbulence models share a common analytical basis, related to the representation of turbulence production and dissipation mechanisms. These physical aspects could be understood with the aid of the *turbulent kinetic energy* budget. The *turbulent kinetic energy k* (per unit mass) is defined as follows:

$$k = \frac{1}{2}\left(\overline{u'^2} + \overline{v'^2} + \overline{w'^2}\right) \tag{3.4}$$

The equation that governs its evolution could be obtained by subtracting the mean momentum equation (3.2) from the "instantaneous" momentum equation (2.17), thus obtaining the governing equation for each u_i', multiplying it for u_i' (performing also the sum due to the *repeated indices*) and averaging (i.e. see Cohen and Kundu (2002)). The equation reads as follows:

$$\overline{u}_j k_{,j} = -\overline{u_l' u_j'} \overline{u}_{l,j} - \nu \overline{u_{l,j}' u_{l,j}'} - \left(k\overline{u_j'} + \overline{\frac{P'}{\rho} u_j'} - \nu k_{,j} \right)_{,j} \tag{3.5}$$

It is possible to understand the nature and the function of each of the three right-hand side terms, that could be written synthetically as:

$$-\overline{u_l' u_j'} \overline{u}_{l,j} = P_k \tag{3.6a}$$

$$\nu \overline{u_{l,j}' u_{l,j}'} = \varepsilon \tag{3.6b}$$

$$-\left(k\overline{u_j'} + \overline{\frac{P'}{\rho} u_j'} - \nu k_{,j} \right)_{,j} = d_k \tag{3.6c}$$

Starting from the last one, namely d_k, it governs the spatial re-distribution of the turbulent kinetic energy, as demonstrated by its flux divergence form; the first two terms of it represent the turbulence transport by itself, the third one the turbulence transport due to molecular viscosity. The ε term is exactly the *viscous rate of turbulent kinetic energy dissipation*, already introduced but now analytically defined; it is worth noting that ε must be positive and its role in the k budget is to destroy the smaller fluctuation structures by means of viscous production of heat. Finally the P_k term must necessarily represent the turbulent kinetic energy production, which extract energy from the mean flow in order to give it to turbulent structures. The turbulent kinetic energy governing equation could thus be re-written in a more intuitive way as follows:

$$\overline{u}_j k_{,j} = P_k - \varepsilon + d_k \tag{3.7}$$

It contains some additional unknowns related to the fluctuations of velocity and pressure, that must be modeled in terms of the mean flow features in order to solve for k, as will be shown later.

From this discussion, it is possible to draw some important conclusions on the turbulence governing mechanisms, useful for the modeling of the Reynolds stress tensor components:

- The viscous dissipation ε contribution is relevant (see for example the dimensional analysis performed in Lentini (1996), which compares it with the molecular viscosity effect) and takes into account information from all the directions in the neighboring of the point considered, thus being difficult to be modeled and numerically computed;
- The d_k term does not contribute globally to the turbulent kinetic energy balance, but tends to redistribute it due to its viscous-like analytical structure. It contains a pressure-velocity term that must be modeled in order to pursue a single-point closure;
- The turbulence production P_k is active only in presence of mean velocity fluctuations, which means that this is the mechanism that enable turbulence to persist. This consideration suggest that the mean velocity gradient could be an important parameter for the definition of turbulence models;
- The k budget equation gives a lot of information about the turbulent behavior of a flow, thus it could be useful to include it in a turbulence closure, after having modeled all the terms containing additional unknowns.

As a final introductory remark to the turbulence models analysis that follows, the writer wants to highlight the fact that the main address of this work has been the study of first moment closures, for several reasons that could be summarized as follows:

- On a turbomachinery *R&D* point of view, the computational load is a fundamental issue for the industrial application of CFD results, since a new product could be out of market if competitors are faster. Quick answers are thus needed in order to *Develop* the *Research* results as soon as possible;
- On the numerical point of view, Second Moment Closures introduce a turbulent transport mechanism based on a source term in the mean momentum equation, namely the Reynolds stress tensor, which could introduce some difficulties. On the other hand, the following Section will demonstrate that First Moment Closures model the effect of Reynolds stress as an additional viscosity, which is beneficial for the numerical solution because it *artificially reduces the computational Reynolds number*;
- Considering the modeling difficulties, the challenge of First Moment Closures is to enclose the physics of Reynolds stress in a simple analytical form that could be representative of most of the situations encountered in the real flow behavior. In this regard, Second Moment Closures could be considered as a good basis to understand the underlying mechanisms that

permit a better choice of the parameters to be included in an advanced first order closure. These argumentations are in agreement with a more *research employment* of Second Moment formulations and a more *development employment* of First Moment ones.

3.3 First Moment Closures

As already explained in the preceding Section, *first moment closures (*or *first order closures)* are based on the solution of the mean flow equations (3.1, 3.2) and avoid specific equations for the Reynolds stress tensor components. This end is pursued by means of some modeling, based on empirical laws and/or on the solution of additional equations (such as the one for the *turbulent kinetic energy*), of the effect of Reynolds stress terms in the mean momentum equation.

From a physical standpoint, the cornerstone behind the development of a good first order turbulence model is to adequately describe the velocity and length characteristic scales associated with a turbulent flow (Gatski and Rumsey (2002)), and to introduce them in the term that models the Reynolds stress effect in the mean momentum equation. This operation could be done through an additional viscosity, which dimensionally is *length x velocity*, that from now on will be called *turbulent eddy viscosity* and will be described by ν_t.

All the models presented in this Section share the eddy viscosity approach, with an analytical operator which generally reads like this:

$$\overline{u_i' u_j'} = \nu_t [l^*(\mathbf{x},t), u^*(\mathbf{x},t)] \cdot f(S_{ij}, W_{ij}) \tag{3.8}$$

where l^* and u^* are function of *space* (and in general of *time*), and represent, respectively, the *local* characteristic length and velocity scale of the turbulent flow, and S_{ij} and W_{ij} are, respectively the *mean strain and rotation rate tensor*, reading as follows:

$$S_{ij} = \frac{1}{2}\left(\overline{u}_{i,j} + \overline{u}_{j,i}\right) \tag{3.9a}$$

$$W_{ij} = \frac{1}{2}\left(\overline{u}_{i,j} - \overline{u}_{j,i}\right) \tag{3.9b}$$

Depending on the expression used for $\nu_t(l^*,u^*)$ and for $f(S_{ij},W_{ij})$, it is possible to derive all the closures presented in this work, but a preliminary classification could be done with respect to the order of the tensor representation *f*: *linear eddy viscosity models* (*EVMs*) adopt a linear relationship between the turbulent stresses and the strain rate tensor S_{ij}, *non-linear eddy viscosity models* (*NLEVMs*) feature polynomial relationships involving generally combinations of S_{ij} and W_{ij}. The expansion coefficients could be

related to empirical or numerical rules, or could be derived directly from the closure coefficients of Second Moment Closures, whose usefulness as basis of First Moment Closures is thus demonstrated.

Concerning the expression of the turbulent eddy-viscosity $\nu_t(l^*,u^*)$, the definition of the length and velocity scales could be done with algebraic relations, thus avoiding additional equations (*zero equation models*), or solving differential transport equations (*one, two and more equations models*).

Over the years, there has been a multitude of EVMs and NLEVMs proposed for the RANS equations, each more suitable (or *calibrated*) for certain applications, thus being not worthwhile (and probably useless) to consider all the formulations. Notwithstanding, if the turbomachinery field is considered, some turbulence closures are usually preferred, in view of their better compromise between the quality of the results and computational load, which is relevant for this CFD application due to the complex geometries of the flows. Between the most used turbulence models for turbomachinery CFD, this work deals with the *mixing length* zero equation model (Prandtl (1925)), the *linear k-ε* two equations model (Launder and Sharma (1974)), the *linear k-ε-v²-f* four equations model (Durbin (1995)), and the *non-linear cubic k-ε* two equations model (Craft et al. (1996)). The models here considered permit thus to have a comprehensive panoramic on first moment closures with both linear and non-linear eddy viscosity models, and have shown good performance for the test cases reported in the last Chapter of this work.

3.3.1 Linear eddy viscosity models

The idea behind the linear eddy viscosity models (EVMs) is to express the Reynolds stress term in the mean momentum equation as a first order function of the rate of strain S_{ij} tensor (*gradient diffusion hypothesis*), with a proportionality coefficient, namely the eddy viscosity ν_t (*eddy viscosity hypothesis*), related to the local flow conditions. In this way the resulting expression for the modeled Reynolds stress term is equivalent to an additional diffusive operator. This choice could be first justified considering that one of the major effects of turbulence is to magnify the momentum transport, which is related to the diffusion mechanism. A detailed explanation of this concept could be inferred from the analysis of a geometrically simple turbulent statistically steady flow, namely a two-dimensional channel flow with axial velocity component *u* and crosswise *v*. Fig. 3.1 shows the possible relationships between the distributions of mean velocity components and the Reynolds stress.

Fig. 3.1a and 3.1b show the effects of *v'* fluctuations, while Fig. 3.1c and 3.1d show the effects of *u'* fluctuations. Considering the first ones, Fig. 3.1a is the situation of *u* velocity component decreasing in *y* direction, which means that $\overline{u}_{,y} < 0$; in this case, if a fluid particle moves in the positive *y* direction due to a fluctuation $v' > 0$, then it will be in a position in which the *u* velocity component is smaller, and its axial fluctuation is positive, i.e. $u' > 0$. On the contrary, if it moves in the negative y direction, due to a fluctuation $v' < 0$, then its other fluctuation will be $u' < 0$. In both the situations the resulting non-diagonal component of the Reynolds stress tensor is positive, i.e. $\overline{u'v'} > 0$,

which is opposite in sign with respect to $\overline{u}_{,y} < 0$. Same considerations could be done for Fig. 3.1b, where $\overline{u}_{,y} > 0$ and $\overline{u'v'} < 0$. Switching to the effects of *u'* fluctuations, Fig. 3.1c and 3.1d suggest that $\overline{u'v'}$ is opposite in sign with respect to $\overline{v}_{,x}$.

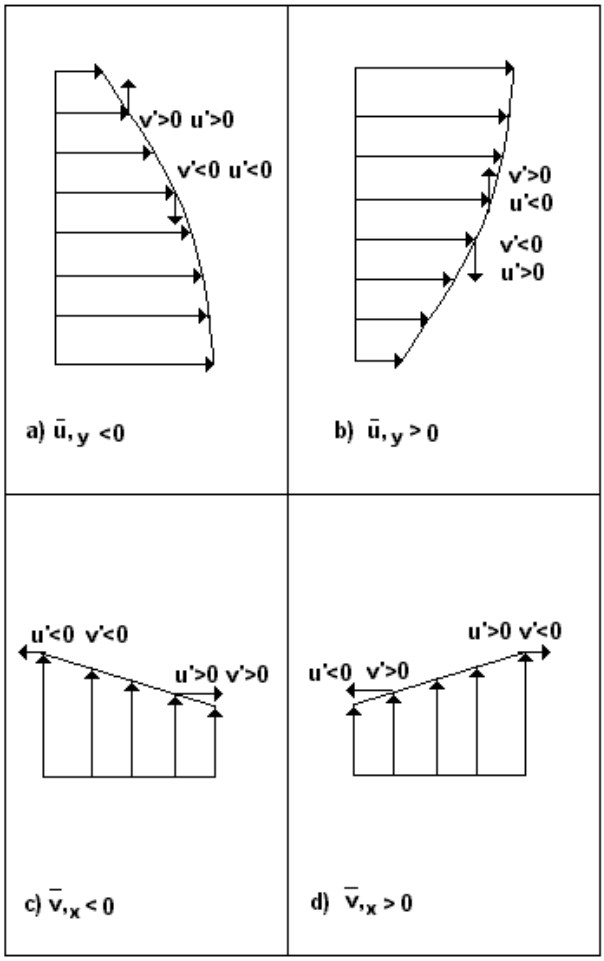

Fig. 3.1. Turbulent channel flow; Reynolds stress and velocity gradient.

These short considerations lead to the following *gradient diffusion* hypothesis:

$$\overline{u_i' u_j'} \propto -S_{ij} \tag{3.10}$$

The proportionality parameter is chosen, following the *Boussinesq hypothesis*, as a turbulent viscosity $\nu_t(l^*,u^*)$, and the resulting expression is:

$$\overline{u_i' u_j'} = -2\nu_t S_{ij} = -\nu_t \left(\overline{u}_{i,j} + \overline{u}_{j,i} \right) \tag{3.11}$$

Eq. (3.11) is based on an analogy with the *Newtonian flow* stress – rate of strain relationship and was derived by *Boussinesq* in 1877. Unfortunately this kind of expression is not correct for the diagonal components of the Reynolds stress, for which it would read as:

$$\overline{u_i' u_i'} = -2\nu_t S_{ii} = -\nu_t \left(\overline{u}_{i,i} + \overline{u}_{i,i} \right) \tag{3.12}$$

It is obvious to understand that in this case the sign of the modeled diagonal Reynolds stress would be related to the sign of $\overline{u}_{i,i}$, while it must be semi-positive defined and related to the turbulent kinetic energy k, which is half the sum of the three diagonal Reynolds stress components. In order to avoid unphysical behaviors and to fulfil the turbulent kinetic energy definition, the final expression proposed for the Reynolds stress term in a *linear eddy viscosity model* is:

$$\overline{u_i' u_j'} = -2\nu_t S_{ij} + \frac{2}{3}\delta_{ij} k \tag{3.13}$$

If we re-write the mean momentum equation, it reads now as:

$$\rho \overline{u}_j \overline{u}_{i,j} = -\overline{P}^*_{,i} + \left[\rho \left(\nu + \nu_t \right) \left(\overline{u}_{i,j} + \overline{u}_{j,i} \right) \right]_{,j} \tag{3.14}$$

where the isotropic part of (3.13) has been included in the pressure term, which reads as:

$$\overline{P}^* = \overline{P} + \frac{2}{3}\rho k \tag{3.15}$$

Eq. (3.14) represents the mean momentum equation for all the linear eddy viscosity models. Each of them could be identified by means of its definition of the turbulent viscosity $\nu_t(l^*,u^*)$. More in particular, the attention should be focused on how to determine l^* and u^*, and on the type of function relating u^*, l^* and ν_t. In the following, first a description of the mean features of the simplest turbulence model, namely the *zero equation mixing length* closure, will be proposed; then the classical *two equations k-ε model* will be issued; finally the linear first moment closures Sub-Section will be completed with the presentation of the *four equations k-ε-v²-f* model. It is worth noting that both the *k-ε* and *k-ε-v²-f* model will be considered in the *low-Reynolds* version, which permits an analytical near wall treatment (i.e see Patel and Rodi (1985) for a complete understanding of near wall treatments).

3.3.1.1 The mixing length

The simplest turbulence models add no equations to the RANS system (they are called *zero equation* models), and define the turbulent viscosity on the basis of physical and empirical laws. Amongst them, the oldest is the *mixing length theory* by Prandtl (1925) (founded on the analogy with kinetic theory of gases), which expresses the turbulent viscosity as product of the velocity and length scale of the turbulent motion, namely:

$$\nu_t = u^* l^* \tag{3.16}$$

In order to determine u^* and l^*, an analogy between the molecular and the turbulent diffusion mechanism is done: let consider again the simple channel flow of Fig. 3.1; in particular let focus on a position characterized by crosswise coordinate y and streamwise velocity fluctuation with root mean square equal to $\sqrt{\overline{u'^2}}$. If a particle moves due to a crosswise fluctuation (Fig. 3.1a and 3.1b) and reaches a position characterized by a velocity whose difference from the undisturbed one is equal to $\sqrt{\overline{u'^2}}$, then the distance from the starting position is called *mixing length*, and reads as l_m. The value of l^* is imposed as equal to l_m, and the value u^* is imposed as equal to $\sqrt{\overline{u'^2}}$, which in view of the preceding considerations is equal to $l_m \left|\overline{u}_{,y}\right|$. The turbulent eddy viscosity of the mixing length model reads as:

$$\nu_t = l_m{}^2 \left|\overline{u}_{,y}\right| \tag{3.17}$$

The first implication of (3.17) is that the velocity scale u^* is calculated with the mean streamwise velocity gradient projected normal to the wall, thus when it is zero there is no turbulent viscosity. This fact is in contrast with lots of real situations (Pope (2002)) in which $\left|\overline{u}_{,y}\right| = 0$ but turbulent scales exist (i.e. this is the case of the decaying turbulence grid). Another important drawback is that l_m is dependent on the "*geometric features of the flow considered"*, thus there are some typical situations in which one is able to choose a correct value for it, and other situations in which a lot of guesswork is needed, in addition to a relevant experience in judging the results.
The mixing length model is the simplest closure and, though the several drawbacks due to its incompleteness, the lack of additional computational load and the ease of implementation in computer codes led many authors to develop some variants, with the Baldwin and Lomax one (1978) being the most widespread.

3.3.1.2 The linear k-ε model and the Low Reynolds extension

At the zero equation level, the models usually focus on the specification of a turbulent eddy viscosity to be used directly in the RANS equations (3.14), and no importance is given to the transport of the turbulent velocity and length scales of the flow.

When introducing turbulent flows, it is always underlined the importance of the transport of the *turbulent kinetic energy k*, first because its underlying mechanisms are the basis for a better understanding of turbulence, and second because of its property of being the major indicator of the evolution of the flow. Following these ideas, one equation models started to appear (first by Prandtl himself and Kolmogorov), including typically a transport equation for *k*, that is used to determine the turbulent velocity scale, while still some empiricism remains in the determination of the turbulent length scale.

Up to this point, it should be more clearly highlighted the nature of the drawbacks related to the "*geometric features of the flow considered"*, already exposed in the mixing length presentation. The problem is not only due to the lack of specifications of characteristic turbulent length scales for complex flows, but also and primarily to the fact that *l** should be determined locally, as expressed by its definition in (3.8), without any *algebraic* relationship with other portions of the flow, or the use of *distance functions* to the nearest wall, that could be limiting in the development of the grid for the computations. On the contrary, a local approach to the calculation of the turbulent length scale is easily usable with any type of grid: structured, unstructured, single- or multi-block (Gatski and Rumsey (2002)), that are needed for the discretization of aerodynamics and turbomachinery flows.

In this viewpoint, a further step is represented by two equations models, that develop a specific equation for both the turbulent velocity and length scales. More in particular, the equation for the turbulent velocity scale is the turbulent kinetic energy transport equation, while the equation for determining the turbulent length scale, or a parameter in strong relationship with it, has been matter of discussion and several solutions have been proposed. Between these, the simplest and more widespread solution is to design a transport equation for the viscous dissipation rate ε, a concept that gave rise to the two equations *k-ε model* (i.e. see Launder and Sharma (1974) or Launder et al. (1977)).

For the sake of clarity, let consider again the definition used in First Moment Closures for the Reynolds stress components:

$$\overline{u_i' u_j'} = \nu_t [l^*(\mathbf{x},t), u^*(\mathbf{x},t)] \cdot f(S_{ij}, W_{ij}) \tag{3.8}$$

Since an *EVM* approach is under consideration, the definition (3.8) adopts the *gradient diffusion* hypothesis and turns to the already introduced relation:

$$\overline{u_i' u_j'} = -2\nu_t S_{ij} = -\nu_t \left(\overline{u_i}_{,j} + \overline{u_j}_{,i} \right) \tag{3.11}$$

The rationale of the *k-ε model* is to consider the following expressions for *l**, *u**, and for the function that permits to calculate the eddy viscosity ν_t:

$$l^* = \frac{k^{3/2}}{\varepsilon} \tag{3.18}$$

$$u^* = \sqrt{k} \tag{3.19}$$

$$\nu_t(l^*,u^*) = c_\mu l^* u^* = c_\mu \frac{k^2}{\varepsilon} \tag{3.20}$$

with c_μ being a model constant, whose value will be presented in the following Tab. 3.1. Retaining in mind the synthetic expression (3.7) for the turbulent kinetic energy transport equation, it is now possible to re-write its complete expression (3.5) in the form proposed in the Launder and Sharma (1974) *k-ε model*:

$$\overline{u_j} k_{,j} = 2\nu_t S_{ij} \overline{u_i}_{,j} - \varepsilon + \left[\left(\nu + \frac{\nu_t}{\sigma_k} \right) k_{,j} \right]_{,j} \tag{3.21}$$

where the production, dissipation and diffusion terms in right hand side are evident, and the σ_k parameter used in the diffusive term is an effective Prandtl number for diffusion, taken as constant for incompressible flows and explicated in Tab. 3.1. Concerning the transport equation for the viscous rate of turbulent kinetic energy dissipation ε, the rather general expression from which some variants have been determined is the one proposed in Jones and Launder (1972), which reads as:

$$\overline{u_j} \varepsilon_{,j} = C_{\varepsilon 1} \frac{1}{\tau} 2\nu_t S_{ij} \overline{u_i}_{,j} - C_{\varepsilon 2} \frac{1}{\tau} \varepsilon + \left[\left(\nu + \frac{\nu_t}{\sigma_\varepsilon} \right) \varepsilon_{,j} \right]_{,j} \tag{3.22}$$

where $C_{\varepsilon 1}$ is fixed from calibrations with homogeneous shear flows, $C_{\varepsilon 2}$ is determined from the decay rate of homogeneous isotropic turbulence, σ_ε is an effective Prandtl number for dissipation diffusion, and τ is the time scale of turbulence (for a description of all the parameters, see Tab. 3.1).

In order to complete the presentation of the Launder and Sharma (1974) *k-ε model*, two issues must be addressed, the first being the *near wall integration*, and the second being the *rationale* of the coefficients and parameters, which will drive to a general synthetic expression of the complete system of RANS equations.

Concerning *near wall integration*, the research community started in 1980s' a wide discussion about some ambiguities in the results obtained with turbulence closure models for wall-bounded shear flows. The original versions of many turbulence models were in

fact designed for *high Reynolds* number flows, and their near wall behavior was governed by the application of *near wall functions*. This kind of procedure has demonstrated to be unsuitable for low and transitional Reynolds number flows, separated flows, and complex three-dimensional flows.

In order to enable the use of turbulence closures at low Reynolds number and to describe near wall behavior, there has been an intense research work, preceded by some pioneer idea, such as the Van Driest (1956) *damping function* for the mixing length. The great amount of information from calculations and experiments available in the last twenty years, led to some modifications of the original fashion of the models, that gave rise to their *Low Reynolds extension*. These could be obtained adding or modifying some terms of the closure equations, in view of some fundamental discoveries, which are well described in Patel et al. (1985). More in particular, the most important modifications in the *k-ε model* are related to the near wall experimental behavior of k and ε, characterized by homogeneous surface boundary conditions for k and a finite ε at the wall. This condition causes a null turbulent time scale τ, which is defined for this model as k/ε, and a singular behavior of both the production and dissipation terms in the dissipation rate equation.

The *k-ε model* in its *Low Reynolds* extension is able to circumvent these singularities in the near wall integration, and is well behaved for both high and low Reynolds number flows. The associated closure equations solve for k and for a *modified* dissipation rate $\tilde{\varepsilon}$, that has homogeneous boundary conditions on solid walls, and reads as:

$$\tilde{\varepsilon} = \varepsilon - 2\nu(\partial\sqrt{k}/\partial x_i)^2 = \varepsilon - D \tag{3.23}$$

The governing equations for k and $\tilde{\varepsilon}$ read as:

$$\overline{u}_j k_{,j} = 2\nu_t S_{ij}\overline{u}_{i,j} - \tilde{\varepsilon} + \left[\left(\nu + \frac{\nu_t}{\sigma_k}\right)k_{,j}\right]_{,j} - D \tag{3.24}$$

$$\overline{u}_j \tilde{\varepsilon}_{,j} = C_{\varepsilon 1} f_{\varepsilon 1} \frac{1}{\tau} 2\nu_t S_{ij}\overline{u}_{i,j} - C_{\varepsilon 2} f_{\varepsilon 2} \frac{1}{\tau}\tilde{\varepsilon} + \left[\left(\nu + \frac{\nu_t}{\sigma_\varepsilon}\right)\tilde{\varepsilon}_{,j}\right]_{,j} + E \tag{3.25}$$

The meaning of each of the parameters and coefficients included in (3.24) and (3.25) is explained in detail in Patel et al. (1985), where it is underlined the presence of some differences in the choices of the quoted authors. For the *Low Reynolds k-ε model* implemented in the XENIOS code, that will be labeled as *LS74* (Launder & Sharma (1974)), the coefficients and parameters expressions are summarized in Table 3.1.

ν_t	$c_\mu f_\mu \frac{k^2}{\tilde{\varepsilon}}$
c_μ	0.09
f_μ	$exp[-3.4/(1+Re_t/50)^2]$
Re_t	$k^2/(\nu\tilde{\varepsilon})$
σ_k	1
σ_ε	1.3
$C_{\varepsilon 1}$	1.44
$C_{\varepsilon 2}$	1.92
$f_{\varepsilon 1}$	1
$f_{\varepsilon 2}$	$[1-0.3exp(-Re_t^2)]$
D	$2\nu(\partial\sqrt{k}/\partial x_i)^2$
E	$2\nu\nu_t(\partial^2\overline{u}_i/\partial x_j\partial x_k)^2$
τ	$k/\tilde{\varepsilon}$

Table 3.1. Closure Coefficients of Low Reynolds *k-ε model.*

It is noticeable that no additional terms have been included in (3.24), while (3.25) contains a term E used to correct the near wall behavior of the modified dissipation rate variable.

The complete system of RANS equations, including mean momentum, continuity and closure equations, could be recast in a more synthetic form, first introduced in Borello et al. (1997) and more evident in Corsini and Rispoli (2002), that is very general and will be used for presenting the other turbulence closures addressed in this work. The formulation makes use of fluxes vectors, and the resulting boundary value problem reads as:

$$\begin{aligned} &\boldsymbol{F}_a\left(\tilde{\boldsymbol{U}}\right)_{,j} + \boldsymbol{F}_d\left(\tilde{\boldsymbol{U}}, \nabla\tilde{\boldsymbol{U}}\right)_{,j} - \rho\boldsymbol{f} = \boldsymbol{0} \ \text{ in } \Omega \in \mathbb{R}^{nsd} \\ &\overline{\boldsymbol{U}} = \overline{\boldsymbol{U}}_D \qquad \text{on } \Gamma_D \\ &\boldsymbol{F}_{d,n} = \boldsymbol{\theta}_N \qquad \text{on } \Gamma_N \end{aligned} \tag{3.26}$$

where $\overline{\boldsymbol{U}}$ is the vector of the averaged unknowns related to $\tilde{\boldsymbol{U}}$ by

$$\overline{\boldsymbol{U}} \equiv \left[\overline{u_1},\ \overline{u_2},\ \overline{u_3},\ \overline{P},\ k,\ \tilde{\varepsilon}\right]^T = \tilde{\boldsymbol{U}} + \left[0,\ 0,\ 0,\ \overline{P}-1,\ 0,\ 0\right]^T \qquad (3.27)$$

which could be interpreted in terms of the primary-turbulent flow properties $\overline{\boldsymbol{U}}_p \equiv \left[\overline{u_1},\overline{u_2},\overline{u_3},0,k,\tilde{\varepsilon}\right]^T$ and of the constrained variables $\overline{\boldsymbol{U}}_c \equiv \left[0,0,0,\overline{P},0,0\right]^T$. The boundary conditions, specified along the computational domain boundary, generally include inflow Dirichlet conditions ($\overline{\boldsymbol{U}}_D$) and outflow Neumann conditions ($\boldsymbol{\theta}_N$). On solid boundaries, homogeneous Dirichlet conditions are imposed for $\overline{\boldsymbol{U}}_p$.

The flux vectors appearing in (3.26) read as:

$$\boldsymbol{F}_a\left(\tilde{\boldsymbol{U}}\right) = \left[\overline{u_j}\rho\overline{u_1},\overline{u_j}\rho\overline{u_2},\overline{u_j}\rho\overline{u_3},\overline{u_j},\overline{u_j}\rho k,\overline{u_j}\rho\tilde{\varepsilon}\right]^T \qquad (3.28a)$$

$$\boldsymbol{F}_d\left(\tilde{\boldsymbol{U}},\nabla\tilde{\boldsymbol{U}}\right) = \left[\bar{\sigma}_{1j},\bar{\sigma}_{2j},\bar{\sigma}_{3j},0,-\rho\left(\nu+\frac{\nu_t}{\sigma_k}\right)k_{,j},-\rho\left(\nu+\frac{\nu_t}{\sigma_\varepsilon}\right)\tilde{\varepsilon}_{,j}\right]^T \qquad (3.28b)$$

with

$$\bar{\sigma}_{ij} = \overline{P}*\delta_{ij} - \rho\left(\nu+\nu_t\right)\left(\overline{u_{i,j}}+\overline{u_{j,i}}\right) \qquad (3.28c)$$

and the source vector reads as:

$$\boldsymbol{f} \equiv -\left[0,\ 0,\ 0,\ 0,\ -P_k+\tilde{\varepsilon}+D,\ -c_{\varepsilon 1}f_{\varepsilon 1}P_k\tilde{\varepsilon}/k + c_{\varepsilon 2}f_{\varepsilon 2}\tilde{\varepsilon}^2/k - E\right]^T \qquad (3.28d)$$

with $P_k = 2\nu_t S_{ij}\overline{u_{i,j}} = \nu_t\left(\overline{u_{i,j}}+\overline{u_{j,i}}\right)\overline{u_{i,j}}$, and all the coefficients defined in Tab. 3.1. The loosely explicit coupling between the turbulence scale determining equations is strengthened by means of the following decomposition of the source vector $\boldsymbol{f}$:

$$-\rho\boldsymbol{f} = -\rho\tilde{\boldsymbol{f}} + \boldsymbol{F}_r(\tilde{\boldsymbol{U}}) \qquad (3.29)$$

where

$$\tilde{\boldsymbol{f}} \equiv -\left[0,\ 0,\ 0,\ 0,\ -P_k+D,\ -c_{\varepsilon 1}f_{\varepsilon 1}P_k\tilde{\varepsilon}/k - E\right]^T \qquad (3.30a)$$

$$\boldsymbol{F}_r(\tilde{\boldsymbol{U}}) = \left[0,0,0,0,c_k k, c_\varepsilon\tilde{\varepsilon}\right]^T \qquad (3.30b)$$

with

$$c_k = \frac{\tilde{\varepsilon}}{k}$$
$$c_\varepsilon = c_{\varepsilon 2} f_{\varepsilon 2} \frac{\tilde{\varepsilon}}{k} \tag{3.30c}$$

By that way the dissipation-destruction budget components in $\boldsymbol{F}_r(\tilde{\boldsymbol{U}})$ establish a direct non-linear coupling between the turbulence variables. Moreover this kind of representation will be useful for the numerical developments of the next Chapter, because it introduces the concepts of advective fluxes, namely $\boldsymbol{F}_a\left(\tilde{\boldsymbol{U}}\right)$, diffusive fluxes, namely $\boldsymbol{F}_d\left(\tilde{\boldsymbol{U}}, \nabla\tilde{\boldsymbol{U}}\right)$, and reactive fluxes, namely $\boldsymbol{F}_r(\tilde{\boldsymbol{U}})$, which are related respectively to first, second and zero order derivatives to the unknowns.
The final expression of the problem statement reads as:

$$\boldsymbol{F}_a\left(\tilde{\boldsymbol{U}}\right)_{,j} + \boldsymbol{F}_d\left(\tilde{\boldsymbol{U}}, \nabla\tilde{\boldsymbol{U}}\right)_{,j} + \boldsymbol{F}_r(\tilde{\boldsymbol{U}}) - \rho\tilde{\boldsymbol{f}} = \boldsymbol{0} \quad \text{in } \Omega \in \mathbb{R}^{nsd}$$
$$\overline{\boldsymbol{U}} = \overline{\boldsymbol{U}}_D \qquad \text{on } \Gamma_D \tag{3.31}$$
$$\boldsymbol{F}_{d,n} = \boldsymbol{\theta}_N \qquad \text{on } \Gamma_N$$

The reader should note that formulation (3.31) is very smart and features a relevant ease of implementation in a computer code.

3.3.1.3 The k-ε-v^2-f model

Starting from 1990s', a growing request for accurate simulations of complex turbulent flows, featuring massively separated boundary layers and non-equilibrium effects. This necessity led to develop some new turbulence closures with the scope of eliminating some of the drawbacks encountered with linear zero, one and two equations model.

It was first noted by Launder (1986) that the standard *k-ε model* features an inappropriate velocity scale (i.e. k) for the turbulent transport toward the wall. In the simulation of wall-bounded flows a better choice would be to use the mean square of the turbulence fluctuation in the wall-normal direction, namely $\overline{v'^2}$. In this respect, one of the major shortcomings of using k instead of $\overline{v'^2}$ as velocity scale for turbulent transport toward the wall is a too early prediction of transition phenomena for complex geometries, related to the stagnation point anomaly (see Durbin (1996)). As a remedial strategy Durbin (1995) proposes the employment of the k-ε-v^2-f turbulence model, which consists of three closure equations respectively for the turbulent kinetic energy k, the dissipation

rate ε, and the energy of the turbulence fluctuations normal to the streamlines $\overline{v'^2}$. An additional elliptic relaxation equation is written for the variable f, which models the pressure-strain term for $\overline{v'^2}$.

The adopted version of the model refers to Lien et al. (1998) (i.e. it is called the code-friendly version of the k-ε-v^2-f turbulence model), with a modified elliptic relaxation variable $\tilde{f}$ that has homogeneous boundary condition on solid walls. It has been implemented in its *Low Reynolds extension* in Corsini et al. (2004). The linear nature of the model arises from the adoption of the Boussinesq approximation of the stress-strain relation (3.13), where the turbulent eddy viscosity is now defined as:

$$\nu_t = c_\mu \overline{v'^2} \, k / \varepsilon \tag{3.32}$$

The RANS complete formulation is obtained in terms of: momentum components $\rho\overline{u_i}$ ($i=1,...,3$) (where ρ is the density, and $\overline{u_i}$ the Cartesian averaged velocity components), static pressure $\overline{P}$, turbulent kinetic energy k, homogeneous dissipation variable $\tilde{\varepsilon} = \varepsilon - 2\nu(\partial\sqrt{k}/\partial x_i)^2$, average of the square of turbulence fluctuation in the wall-normal direction, namely $\overline{v'^2}$, and modified elliptic relaxation variable $\tilde{f}$. The boundary value problem reads as:

$$\begin{aligned} &\boldsymbol{F}_a\left(\tilde{\boldsymbol{U}}\right)_{,j} + \boldsymbol{F}_d\left(\tilde{\boldsymbol{U}}\right)_{,j} + \boldsymbol{F}_r(\tilde{\boldsymbol{U}}) - \boldsymbol{B} = \boldsymbol{0} \quad \text{in } \Omega \in \mathbb{R}^{nsd}, j = 1,\ldots 3 \\ &\overline{\boldsymbol{U}} = \overline{\boldsymbol{U}}_D \qquad \text{on } \Gamma_D \\ &\boldsymbol{F}_{d,n} = \boldsymbol{\theta}_N \quad \text{on } \Gamma_N \end{aligned} \tag{3.33}$$

where $\Gamma = \Gamma_D \cup \Gamma_N$, with $\Gamma_D \cap \Gamma_N = \varnothing$, n is the direction normal to the boundary, and $\overline{\boldsymbol{U}}$ is the vector of the averaged unknowns related to $\tilde{\boldsymbol{U}}$ by

$$\begin{aligned} &\overline{\boldsymbol{U}} \equiv \left[\overline{u_1},\ \overline{u_2},\ \overline{u_3},\ \overline{P},\ k,\ \tilde{\varepsilon},\ \overline{v'^2},\ \tilde{f}\right]^T = \\ &= \tilde{\boldsymbol{U}} + \left[0,\ 0,\ 0,\ \overline{P}-1,\ 0,\ 0,\ 0,\ 0\right]^T \end{aligned} \tag{3.34}$$

and could be interpreted in terms of primary-turbulent flow properties $\overline{\boldsymbol{U}}_p \equiv \left[\overline{u_1},\overline{u_2},\overline{u_3},0,k,\tilde{\varepsilon},\overline{v'^2},\tilde{f}\right]^T$ and constrained variable $\overline{\boldsymbol{U}}_c \equiv \left[0,0,0,\overline{p},0,0,0,0\right]^T$. The boundary conditions, specified along the computational domain boundary, generally

include inflow Dirichlet conditions ($\bar{\boldsymbol{U}}_D$) and outflow Neumann conditions ($\boldsymbol{\theta}_N$). On solid boundaries, homogeneous Dirichlet conditions are imposed for $\overline{\boldsymbol{U}}_p$. The flux vectors appearing in (3.34) are defined as:

$$\boldsymbol{F}_a\left(\tilde{\boldsymbol{U}}\right)=\left[\overline{u_j}\rho\overline{u_1},\overline{u_j}\rho\overline{u_2},\overline{u_j}\rho\overline{u_3},\overline{u_j},\overline{u_j}\rho k,\overline{u_j}\rho\tilde{\varepsilon},\overline{u_j}\rho\overline{v'^2},0\right]^T \tag{3.35a}$$

$$\begin{aligned}\boldsymbol{F}_d\left(\tilde{\boldsymbol{U}}\right)=&[\bar{\sigma}_{1j},\bar{\sigma}_{2j},\bar{\sigma}_{3j},\\ &,-\rho\left(\nu+\frac{\nu_t}{\sigma_k}\right)k_{,j},-\rho\left(\nu+\frac{\nu_t}{\sigma_\varepsilon}\right)\tilde{\varepsilon}_{,j},-\rho\left(\nu+\frac{\nu_t}{\sigma_k}\right)\overline{v'^2}_{,j},-L_s^2\tilde{f}_{,j}]^T\end{aligned} \tag{3.35b}$$

where L_s is the turbulent length scale, defined in Table 3.2, and the stress tensor is as defined in (3.28c) for the k-ε model. The reactive terms are described by

$$\boldsymbol{F}_r(\tilde{\boldsymbol{U}})=\left[0,0,0,0,c_k k,c_\varepsilon\tilde{\varepsilon},c_{v^2}\overline{v'^2},c_{\tilde{f}}\right]^T \tag{3.35c}$$

with

$$\begin{aligned}&c_k=\rho\frac{\tilde{\varepsilon}}{k},\ \ c_\varepsilon=\rho c_{\varepsilon 2}f_{\varepsilon 2}\frac{1}{T_s},\\ &c_{v^2}=6\rho\frac{\varepsilon}{k},\ \ c_{\tilde{f}}=1\end{aligned} \tag{3.35d}$$

Finally the source vector reads as:

$$\boldsymbol{B}=\begin{bmatrix}0,\ \ 0,\ \ 0,\ \ 0,\ \ P_k-\rho D,\ \ c_{\varepsilon 1}f_{\varepsilon 1}P_k\tilde{\varepsilon}/k,\\ \rho k\tilde{f},\ \ -\left[(C_1-1)(\overline{v'^2}/k-2/3)\right]/T_s+(5/T_s)\overline{v'^2}/k+(C_2/\rho)P_k/k\end{bmatrix}^T \tag{3.35e}$$

Tab. 3.2 shows the $k-\varepsilon-v^2-f$ closure coefficients, according to the formulation implemented in the XENIOS code, well documented in Corsini et al. (2004).

σ_k	1
σ_ε	1.3
$c_{\varepsilon 1}$	$1.4(1+0.05\sqrt{k/\overline{v'^2}})+0.4exp(-0.1\,Re_t)$
$c_{\varepsilon 2}$	1.9
$f_{\varepsilon 1}$	1
$f_{\varepsilon 2}$	$[1-0.3exp(-Re_t^2)]$
Re_t	$k^2/(\nu\tilde{\varepsilon})$
c_μ	0.22
P_k	$-\rho\overline{u'_i u'_k}\bar{u}_{i,k}$
D	$2\,\nu(\partial\sqrt{k}/\partial x_i)^2$
L_s	$C_L\,max\left(k^{3/2}/\varepsilon, C_\eta \nu^{3/4}/\varepsilon^{1/4}\right)$
T_s	$max\left(k/\varepsilon, 6\sqrt{\nu/\varepsilon}\right)$
C_1	1.4
C_2	0.3
C_L	0.23
C_η	70

Table 3.2. Closure coefficients of the adopted k-ε-v^2-f closure.

3.3.2 Limits of linear closures and non-linear k-ε model

The linear EVM approach to turbulent flows represents a valuable tool, both for industrial studies, for which it represents the state of the art, and for research investigations, where it provides benchmark solutions for the assessment of the results of newer models. Unfortunately it suffers from a certain number of drawbacks, with some of them resolvable retaining a gradient diffusion point of view, as done with the *k-ε-v^2-f* closure, that uses a more reliable turbulent velocity scale toward to the walls. It is also

possible to elaborate strategies that permit case by case to modify a linear model, in order to avoid some drawbacks, but this procedure is in contrast of the necessity of turbulence modeling to be a predictive tool (i.e. the reader could consider the *intermittency factor* γ, which is used as a constraint for the transition phenomena).

Even in presence of *ad-hoc* tools, such as the *intermittency factor*, there are still some deficiencies that could not be cured remaining in a linear EVM framework. To mention but a few, the most important ones are the *isotropy of the eddy viscosity,* that is evident in definition (3.13), and the material frame-indifference (Gatski and Rumsey (2002)). Moreover the standard linear modelling of turbulence is not adequate in presence of strong curvature and features a relevant *overproduction* of turbulence in stagnating flow cores (Durbin (1996)), that are a typical feature of turbomachinery flow fields.

Several studies have been performed in order to remove these deficiencies, without abandoning a first moment closure approach, overturning the structure of the equations and increasing their number. The most widespread idea is to turn to non-linear relations between Reynolds stress components and velocity gradient, as suggested by the non-Newtonian fluids analogy proposed by Rivlin (1957). Such relationships may be arrived at by simplifying stress-transport models (so-called *algebraic stress models*) (Pope (1975)) or by tensor representations, generally routed on the invariant theory in continuum mechanics (Lumley (1970)), which are kinematic relations that mimic the functional dependencies of *stress anisotropies*.

Here an approach belonging to the latter family of models will be addressed, namely the *cubic* formulation proposed by Craft et al. (1996), which gives rise to the *non-linear k-ε model*, labeled *CLS96 (Craft, Launder & Suga)*. To be more precise, let consider again the expression of the Reynolds stress components for a first moment closure:

$$\overline{u_i' u_j'} = \nu_t [l^*(\mathbf{x},t), u^*(\mathbf{x},t)] \cdot f(S_{ij}, W_{ij}) \tag{3.8}$$

Linear eddy viscosity models are characterized by definition (3.13), which establish a linear relation between the Reynolds stress and the S_{ij} tensor. On the contrary, in the *non-linear k-ε*, the authors state that in a polynomial sense, in order to have a correct flexibility of the function *f*, it should be at least of the third order in S_{ij} and W_{ij}. The non-isotropic constitutive relation is thus modeled in the form of a third-order polynomial of the *mean strain* and *vorticity tensors*, and scalar turbulent viscosity ν_t, where cubic terms are able to sensitize the model to streamline curvature effects (Chen and Leschziner (1999)). By adopting the Reynolds averaging, the full tensor functional form is:

$$\begin{aligned}
&\overline{u'_i u'_j} = \frac{2}{3}k\delta_{ij} - 2\nu_t S_{ij} - 0.1\nu_t \frac{k}{\varepsilon}\left(2S_{ik}\,2S_{kj} - 2S_{kl}\,2S_{kl}\frac{1}{3}\delta_{ij} \right) \\
&+0.1\nu_t \frac{k}{\varepsilon}\left(2W_{ik}\,2S_{kj} + 2W_{jk}\,2S_{ki} \right) + 0.26\nu_t \frac{k}{\varepsilon}\left(2W_{ik}\,2W_{kj} - 2W_{kl}\,2W_{kl}\frac{1}{3}\delta_{ij} \right) \\
&-10c_\mu^2\nu_t\left(\frac{k}{\varepsilon}\right)^2 \left(2S_{ki}\,2W_{lj} + 2S_{kj}\,2W_{li} \right) 2S_{kl} \\
&-5c_\mu^2\nu_t\left(\frac{k}{\varepsilon}\right)^2 2S_{ij}\,2S_{kl}\,2S_{kl} + 5c_\mu^2\nu_t\left(\frac{k}{\varepsilon}\right)^2 2S_{ij}\,2W_{kl}\,2W_{kl}
\end{aligned} \tag{3.36}$$

where it is noticeable that $W_{ij} = \frac{1}{2}\left(\overline{u}_{i,j} - \overline{u}_{j,i}\right) + e_{mji}\omega_m$ is the *absolute vorticity tensor*, ω_m is the frame angular velocity, e_{mji} is the permutation tensor. The non-isotropic model under investigation is coupled with a two-equation closure. The turbulent velocity- and length-scales are determined by solving conservation equations for the turbulent kinetic energy (k) and the commonly used homogeneous turbulent dissipation rate ($\tilde{\varepsilon}$), that read as:

$$\overline{u}_j k_{,j} = -\overline{u'_i u'_j}\,\overline{u}_{i,j} - \tilde{\varepsilon} + \left[\left(\nu + \frac{\nu_t}{\sigma_k} \right) k_{,j} \right]_{,j} - D \tag{3.37}$$

$$\overline{u}_j \tilde{\varepsilon}_{,j} = -C_{\varepsilon 1} f_{\varepsilon 1} \frac{1}{\tau}\overline{u'_i u'_j}\,\overline{u}_{i,j} - C_{\varepsilon 2} f_{\varepsilon 2} \frac{1}{\tau}\tilde{\varepsilon} + \left[\left(\nu + \frac{\nu_t}{\sigma_\varepsilon} \right) \tilde{\varepsilon}_{,j} \right]_{,j} + E \tag{3.38}$$

where

$$\nu_t = c_\mu f_\mu \tau k \tag{3.39}$$

with $\tau = k/\tilde{\varepsilon}$. It is now clear how the *CLS96* model features a strong relationship with the standard *LS74* model, the only difference being the definition of the Reynolds stress term, and the expressions and values of the coefficients, reported in Table 3.3, where a comparison is done with respect to the linear k-ε (i.e. the reader could consider the argumentations of Corsini and Rispoli (2005)). It is worth noting that both models are considered in their *Low Reynolds extension*, and that the acronyms *S* and *W* stand for *strain* and *vorticity invariants*, which read respectively as $S = \tau\sqrt{2S_{ij}S_{ij}}$ and $W = \tau\sqrt{2W_{ij}W_{ij}}$.

	CLS96	*LS74*
ν_t	$c_\mu f_\mu \frac{k^2}{\tilde{\varepsilon}}$	$c_\mu f_\mu \frac{k^2}{\tilde{\varepsilon}}$
c_μ	$\frac{0.3\left[1-exp\left[-0.36/exp\left[-0.75\max(S,W)\right]\right]\right]}{1+0.35\left[\max(S,W)\right]^{1.5}}$	0.09
f_μ	$1-exp\left[-\left(Re_t/90\right)^{0.5}-\left(Re_t/400\right)^2\right]$	$exp[-3.4/(1+Re_t/50)^2]$
Re_t	$k^2/(\nu\tilde{\varepsilon})$	$k^2/(\nu\tilde{\varepsilon})$
σ_k	1	1
σ_ε	1.3	1.3
$C_{\varepsilon 1}$	1.44	1.44
$C_{\varepsilon 2}$	1.92	1.92
$f_{\varepsilon 1}$	1	1
$f_{\varepsilon 2}$	$[1-0.3exp(-Re_t^2)]$	$[1-0.3exp(-Re_t^2)]$
D	$2\nu(\partial\sqrt{k}/\partial x_i)^2$	$2\nu(\partial\sqrt{k}/\partial x_i)^2$
E	$0.0022\,S\,k\,\tau\nu_t(\partial^2\overline{u}_i/\partial x_j\partial x_k)^2$	$2\nu\nu_t(\partial^2\overline{u}_i/\partial x_j\partial x_k)^2$
τ	$k/\tilde{\varepsilon}$	$k/\tilde{\varepsilon}$
P_k	$-\overline{u'_i u'_j}\overline{u}_{i,j}$	$2\nu_t S_{ij}\overline{u}_{i,j}$

Table 3.3. Closure coefficients of non-linear k-ε closure compared with linear k-ε.

The RANS complete formulation with the *CLS96 closure* in its *Low Reynolds extension*, is obtained in terms of: momentum components $\rho\overline{u_i}$ ($i=1,...,3$) (where ρ is the density, and $\overline{u_i}$ the Cartesian averaged velocity components), static pressure $\overline{P}$, turbulent kinetic energy k and homogeneous dissipation variable $\tilde{\varepsilon}=\varepsilon-2\nu(\partial\sqrt{k}/\partial x_i)^2$. The boundary value problem reads as:

$$\begin{aligned} &\boldsymbol{F}_a\left(\tilde{\boldsymbol{U}}\right)_{,j}+\boldsymbol{F}_d\left(\tilde{\boldsymbol{U}},\nabla\tilde{\boldsymbol{U}}\right)_{,j}-\rho\boldsymbol{f}=\boldsymbol{\theta} \ \text{ in } \Omega\in\mathbb{R}^{nsd} \\ &\overline{\boldsymbol{U}}=\overline{\boldsymbol{U}}_D \qquad \text{on } \Gamma_D \\ &\boldsymbol{F}_{d,n}=\boldsymbol{\theta}_N \qquad \text{on } \Gamma_N \end{aligned} \tag{3.40}$$

where $\overline{\boldsymbol{U}}$ is the vector of the averaged unknowns related to $\tilde{\boldsymbol{U}}$ by

$$\overline{\boldsymbol{U}} \equiv \left[\overline{u_1},\ \overline{u_2},\ \overline{u_3},\ \overline{P},\ k,\ \tilde{\varepsilon}\right]^T = \tilde{\boldsymbol{U}} + \left[0,\ 0,\ 0,\ \overline{P}-1,\ 0,\ 0\right]^T \tag{3.41}$$

which could be interpreted in terms of the primary-turbulent flow properties $\overline{\boldsymbol{U}}_p \equiv \left[\overline{u_1},\overline{u_2},\overline{u_3},0,k,\tilde{\varepsilon}\right]^T$ and of the constrained variables $\overline{\boldsymbol{U}}_c \equiv \left[0,0,0,\overline{P},0,0\right]^T$. The boundary conditions, specified along the computational domain boundary, generally include inflow Dirichlet conditions ($\overline{\boldsymbol{U}}_D$) and outflow Neumann conditions ($\boldsymbol{\theta}_N$). On solid boundaries, homogeneous Dirichlet conditions are imposed for $\overline{\boldsymbol{U}}_p$. Up to this point no differences are noticeable between the CLS96 problem statement and the LS74 one, they will appear now in the definition of the flux vectors appearing in (3.40), which read as:

$$\boldsymbol{F}_a\left(\tilde{\boldsymbol{U}}\right) = \left[\overline{u_j}\rho\overline{u_1},\overline{u_j}\rho\overline{u_2},\overline{u_j}\rho\overline{u_3},\overline{u_j},\overline{u_j}\rho k,\overline{u_j}\rho\tilde{\varepsilon}\right]^T \tag{3.42a}$$

$$\boldsymbol{F}_d\left(\tilde{\boldsymbol{U}},\nabla\tilde{\boldsymbol{U}}\right) = \left[\bar{\sigma}_{1j},\bar{\sigma}_{2j},\bar{\sigma}_{3j},0,-\rho\left(\nu+\frac{\nu_t}{\sigma_k}\right)k_{,j},-\rho\left(\nu+\frac{\nu_t}{\sigma_\varepsilon}\right)\tilde{\varepsilon}_{,j}\right]^T \tag{3.42b}$$

with

$$\bar{\sigma}_{ij} = \overline{P}*\delta_{ij} - \rho\left(\nu+\nu_t\right)\left(\overline{u_{i,j}}+\overline{u_{j,i}}\right) \tag{3.42c}$$

and the source vector reads as:

$$\boldsymbol{f} \equiv -\left[P_{M1},\ P_{M2},\ P_{M3},\ 0,\ -P_k+\tilde{\varepsilon}+D,\ -c_{\varepsilon 1}f_{\varepsilon 1}P_k\frac{\tilde{\varepsilon}}{k}+c_{\varepsilon 2}f_{\varepsilon 2}\frac{\tilde{\varepsilon}^2}{k}-E\right]^T \tag{3.42d}$$

Concerning the momentum source components P_{Mi}, they account for volume sources originating from square and cubic terms in the assumed constitutive relation (3.36). As for the other closures presented, the loosely explicit coupling between the turbulence scale determining equations is strengthened by means of the following decomposition of the source vector $\boldsymbol{f}$:

$$-\rho\boldsymbol{f} = -\rho\tilde{\boldsymbol{f}} + \boldsymbol{F}_r(\tilde{\boldsymbol{U}}) \tag{3.43}$$

where

$$\tilde{\boldsymbol{f}} \equiv -\left[0, \quad 0, \quad 0, \quad 0, \quad -P_k + D, \quad -c_{\varepsilon 1} f_{\varepsilon 1} P_k \tilde{\varepsilon} / k - E\right]^T \tag{3.44a}$$

$$\boldsymbol{F}_r(\tilde{\boldsymbol{U}}) = \left[0,0,0,0,c_k k, c_\varepsilon \tilde{\varepsilon}\right]^T \tag{3.44b}$$

with

$$\begin{aligned} c_k &= \frac{\tilde{\varepsilon}}{k} \\ c_\varepsilon &= c_{\varepsilon 2} f_{\varepsilon 2} \frac{\tilde{\varepsilon}}{k} \end{aligned} \tag{3.44c}$$

In terms of advective $\boldsymbol{F}_a\left(\tilde{\boldsymbol{U}}\right)$, diffusive $\boldsymbol{F}_d\left(\tilde{\boldsymbol{U}}, \nabla\tilde{\boldsymbol{U}}\right)$ and reactive $\boldsymbol{F}_r(\tilde{\boldsymbol{U}})$ fluxes, the final expression of the problem statement reads as:

$$\begin{aligned} &\boldsymbol{F}_a\left(\tilde{\boldsymbol{U}}\right)_{,j} + \boldsymbol{F}_d\left(\tilde{\boldsymbol{U}}, \nabla\tilde{\boldsymbol{U}}\right)_{,j} + \boldsymbol{F}_r(\tilde{\boldsymbol{U}}) - \rho\tilde{\boldsymbol{f}} = \boldsymbol{0} \quad \text{in } \Omega \in \mathbb{R}^{nsd} \\ &\overline{\boldsymbol{U}} = \overline{\boldsymbol{U}}_D \qquad \text{on } \Gamma_D \\ &\boldsymbol{F}_{d,n} = \boldsymbol{\theta}_N \qquad \text{on } \Gamma_N \end{aligned} \tag{3.45}$$

3.4 Hints on LES and Hybrid RANS/LES

One of the main characteristics of turbulent flows is the dominant non-linearity and the continuous and wide spectrum of observed scales. In a DNS calculation no model is applied to turbulent scales so that motions of all sizes could be resolved, but the price that must be paid is in terms of a too expensive grid. On a practical point of view, probably this limit is not the main shortcoming of DNS, or not the only one, because another main issue is that a great number of points generates a large amount of data, that is unaffordable and sometimes useless to manage with. Probably this is the major drawback that reduces the reliability of DNS for many applications (mostly in the industrial field), as well described in Frölich and Rodi (2002).

An approach that permits to adopt a *coarser grid*, able to capture the *larger eddies* of the flow, would be a very good compromise between the DNS and the RANS, which is characterized by some difficulties in the computation of more complex flows, probably due to the necessity of improved models. In order to accurately resolve the larger scales, it is of fundamental importance to model the effect of the finer ones on them.

The idea behind *LES (Large Eddy Simulation)* is to develop a method which needs a coarser grid with respect to DNS, and is able to resolve larger eddies taking into account the effect of the smaller scales by means of a *subgrid-scale (SGS)* model. The starting point is the Navier-Stokes equations system, including the time dependent term:

$$u_{j,j} = 0$$
$$\rho u_{i,t} + \rho u_j u_{i,j} = -P_{,i} + [\mu(u_{i,j} + u_{j,i})]_{,j} \tag{3.46}$$

In order to have a quick look at the method (for a more detailed description and references the reader could consult for example the book from Pope (2000)), the approach to obtain the LES system of equations is conceptually different from the one adopted in RANS, because now an operation of *filtering* is pursued, which decomposes the velocity field as follows:

$$\boldsymbol{U}(\boldsymbol{x},t) = \underline{\boldsymbol{U}}(\boldsymbol{x},t) + \dot{\boldsymbol{u}}(\boldsymbol{x},t) \tag{3.47}$$

where $\underline{\boldsymbol{U}}(\boldsymbol{x},t)$ represents the *filtered velocity field*, which is three-dimensional and time-dependent, while $\dot{\boldsymbol{u}}(\boldsymbol{x},t)$ is the *subgrid scale component*. The procedure followed to obtain the closure of the system is to include this decomposition in the Navier-Stokes equations, and to model the subgrid contribution arising from the convective term. In this respect, there have been a lot of works on the argument of *SGS modeling*, but here only two milestones will be quoted, namely the first pioneer work on LES by Smagorinsky (1963) and the more recent *dynamic SGS* by Germano et al. (1991). After having included the SGS model in the filtered Navier-Stokes equation, it is possible to solve for the filtered velocity field, which permits to obtain the evolution of the large eddies of the motion.

Unfortunately, for accurate predictions of wall-bounded flows, LES imposes severe near-wall grid resolution constraints (very close to those imposed by DNS) in all the directions, while RANS needs a proper resolution only in wall-normal direction. Moreover there is no sufficient confidence in the LES performance on *unstructured* grids, which are necessary to discretize the complex geometries and wall topologies pertinent to industrial CFD (Hanjalic (2005)). Finally, it should be noted that LES is defined as a three-dimensional time-dependent tool, thus needing three-dimensional grids and long time calculations.

In the work by Hanjalic (2005) it is claimed that LES will be more and more useful in a research context in parallel with DNS, but for the daily industrial application the RANS approach will be preferred, because of several reasons, including the necessity of shortening design and market time, and the continuous broadening of the applicability of CFD, that must handle more and more complex problems and would require prohibitive computer resources for LES calculations.

As a compromise solution for realistic engineering and environmental flows, an attractive proposition is to combine LES and RANS, into an *Hybrid RANS/LES approach*.

In this context, among the different proposed strategies, the most popular is the *zonal approach*, where LES on coarse grid is applied far from the wall, while RANS is used to compute the near wall flow field. The key problem of this approach is to find an appropriate location for the interface between the two zones and to find proper matching conditions between the two flow fields. Several investigations have been developing in the framework of Hybrid RANS/LES, and their results are expected to give also some answers about how to improve advanced RANS closures.

3.5 Structure of turbulence closure equations and Finite Element algorithm

After the description of the adopted turbulence closures, a complete understanding of a CFD method could be reached only if some key ingredients are explained in detail. More in particular it is necessary to discuss the analytical structure of the mathematical operators and how they fit in the numerical formulation implemented in the computer code, the solution algorithm adopted and the numerical tools that permit to obtain *accurate* and *stable* solutions. In the following, a short presentation of the main computational features of the *XENIOS* code is done, except for the subject of accuracy and stability, considered a key point of this work and widely discussed in the next Chapter.

All the turbulence closures considered in this work share a common RANS problem statement structure, which reads as:

$$\begin{aligned} &\boldsymbol{F}_a\left(\tilde{\boldsymbol{U}}\right)_{,j} + \boldsymbol{F}_d\left(\tilde{\boldsymbol{U}}, \nabla\tilde{\boldsymbol{U}}\right)_{,j} + \boldsymbol{F}_r(\tilde{\boldsymbol{U}}) - \rho\tilde{\boldsymbol{f}} = \boldsymbol{0} \quad \text{in } \Omega \in \mathbb{R}^{nsd} \\ &\overline{\boldsymbol{U}} = \overline{\boldsymbol{U}}_D \qquad \text{on } \Gamma_D \\ &\boldsymbol{F}_{d,n} = \boldsymbol{\theta}_N \qquad \text{on } \Gamma_N \end{aligned} \tag{3.48}$$

It is important to stress again on the fact that the flux vectors represent advective $\boldsymbol{F}_a\left(\tilde{\boldsymbol{U}}\right)$, diffusive $\boldsymbol{F}_d\left(\tilde{\boldsymbol{U}}, \nabla\tilde{\boldsymbol{U}}\right)$ and reactive $\boldsymbol{F}_r(\tilde{\boldsymbol{U}})$ contributions. In this respect, the next Chapter will focus attention on the numerical difficulties introduced by *advective* and *reactive* operators.

On the computational point of view, an incompressible Navier-Stokes fixed point problem (i.e. see Corsini and Rispoli (2002) for more details) is solved with a fully-coupled *Oseen-like* form that contains linearized operators with respect to the ones in (3.48), reading as follows:

$$\mathcal{F}_a\left(\tilde{\boldsymbol{U}}\right)_{,j} + \mathcal{F}_d\left(\tilde{\boldsymbol{U}}, \nabla\tilde{\boldsymbol{U}}\right)_{,j} + \mathcal{F}_r(\tilde{\boldsymbol{U}}) - \rho\tilde{\boldsymbol{f}} = \boldsymbol{0} \text{ in } \Omega \in \mathbb{R}^{nsd} \tag{3.49}$$

where $\mathcal{F}_a\left(\tilde{\boldsymbol{U}}\right)_{,j}$ is linearized with a given velocity field (i.e. the velocity field itself evaluated at the preceding equilibrium iteration), and $\mathcal{F}_d\left(\tilde{\boldsymbol{U}}, \nabla\tilde{\boldsymbol{U}}\right)_{,j}$, $\mathcal{F}_r(\tilde{\boldsymbol{U}})$, $\tilde{\boldsymbol{f}}$ are the linearized version of their corresponding operators.

The solution procedure features the possibility of data decomposition using an in-house made code developed to guarantee both the minimization of the message passing requirements and the load balancing, with MPI libraries used for the message passing operations (i.e. see *overlapping Domain Decomposition* procedure in Borello et al. (2003)). This characteristic of the XENIOS code permits to manage with "large" grids, with reference to both the spatial domain and the nodes quantity attributes.

Finally, the fully coupled solution of the RANS equations involves a *Flexible Generalized Minimal Residual (FGMRES)* solver (Saad (1993)) with convergence thresholds imposed on both the relative residual *r norm* ($R_{res} = \|r_k\|_2 / \|r_0\|_2$), where k indicates the current iteration, and the relative difference between two consecutive norms ($R_{sol} = \|U_k\|_2 - \|U_{k-1}\|_2 / \|U_k\|_2$) of the solution.

References

Baldwin B. S., Lomax H., "Thin layer approximation and algebraic model for separated turbulent flows", *AIAA 16th Aerospace sciences meeting, paper 78-257,* (1978).

Borello D., Corsini A., Rispoli F., "A 3D stabilized finite element technique with compact stiffness matrix treatment. Application to internal flows", *1997 ASME Fluids Engineering Division Summer Meeting and Fluids Engineering Conference, Vancouver*, (1997).

Borello D., Corsini A. and Rispoli F., "A finite element overlapping scheme for turbomachinery flows on parallel platforms", *Computers and Fluids*, v. 32/7, pp. 1017-1047, (2003).

Chen W.L., Leschziner M.A., "Modeling turbomachine-blade flows with non-linear eddy-viscosity models and second moment closure", *IMechE Paper C557/131/99, A,* pp. 189-199, (1999).

Cohen I. M., Kundu P. K., "Fluid Mechanics", *Academic press*, (2002).

Corsini A., Rispoli F., "Anisotropic turbulence modelling of near wall effects pertinent to turbomachinery flows", *FEDSM'02 Proceedings*, paper FEDSM2002-31206, pp. 1-10, (2002).

Corsini A., Rispoli F., "Flow analyses in a high-pressure axial ventilation fan with a non-linear eddy viscosity closure", *Int. J. Heat and Fluid Flow* , v. 26-3, pp. 349-361, (2005).

Corsini A., Rispoli F., Santoriello A., "A VMS/Stabilized formulation for the k-ε-v^2-f turbulence closure: application to turbomachinery CFD", *ECCOMAS 2004*, paper 1872, (2004).

Craft T. J., Launder B. E., Suga K., "Development and application of a cubic eddy-viscosity model of turbulence", *Int. J. Heat and Fluid Flow*, v. 17, pp. 108-115 (1996).

Durbin P. A., "Separated flow computations with the k-ε-v^2 model", *AIAA J.*, v. 33, pp. 659-664, (1995).

Durbin P. A., "On the k-ε stagnation point anomaly", *Int. J. Heat and Fluid Flow*, v. 17, pp. 89-90, (1996).

Durbin P. A., Petterson Reif B. A., "Statistical Theory and Modeling for Turbulent Flows", *John Wiley and Sons*, (2001).

Frölich J., Rodi W., "Introduction to Large Eddy Simulation of Turbulent Flows", in *Closure Strategies for Turbulent and Transitional Flows*, ed. Launder B. and Sandham N. D., pp. 267-297, *Cambridge University Press*, (2002).

Gatski T. B. and Rumsey C. L., "Linear and Nonlinear Eddy Viscosity Models", in *Closure Strategies for Turbulent and Transitional Flows*, ed. Launder B. and Sandham N. D., pp. 9-46, *Cambridge University Press*, (2002).

Germano M., Piomelli U., Moin P., Cabot W. H., "A dynamic subgrid-scale eddy viscosity model", *Physics of Fluids A,* v. 3, pp. 1760-1765, (1991).

Hanjalic K., "Will RANS survive LES? A View of Perspectives", *Journal of Fluids Engineering*, v. 127, pp. 831-839, (2005).

Jones W. P. and Launder B. E., "The prediction of laminarization with a two-equation model of turbulence", *Int. Journal Heat and Mass Transfer*, v. 15, pp. 301-314, (1972).

Launder B. E., "Low Reynolds Number Turbulence Near Walls", *UMIST Mechanical Engineering Dept.*, Rept. TFD/86/4, *University of Manchester*, (1986).

Launder B. E. and Sharma B. I., "Application of the energy dissipation model of turbulence to the calculation of flow near a spinning disc", *Lett. In Heat and Mass Transfer*, v. 1, pp. 131-138 (1974).

Launder B.E., Priddin C. H., Sharma B. I., "The calculation of Turbulent Boundary Layers on Spinning and Curved Surfaces", *Journal of Fluids Engineering*, pp. 231-239, (1977).

Lentini D., "Applicazione di modelli di turbolenza avanzati a flussi in convezione naturale e forzata " *(in italian), University of Rome "La Sapienza"*, (1996).

Lien F. S., Kalitzin G., Durbin P. A., "RANS modeling for compressible and transitional flows", *Proceedings of the Summer Program 1998*, *Center for Turbulence Research - Stanford University*, pp. 267-286, (1998).

Lumley J.L., "Toward a turbulent constitutive relation", *J. Fluid Mech.*, v. 41, pp. 413-434, (1970).

Patel V. C., Rodi W., Scheurer G., "Turbulence Models for Near-Wall and Low Reynolds Number flows: A Review", *AIAA Journal*, v. 23 n. 9, pp 1308-1319, (1985).

Pope S.B., "A more general effective-viscosity hypothesis", *J. Fluid Mech.*, v. 72, pp. 331-340, (1975).

Pope S. B., "Turbulent flows", *Cambridge University Press*, (2000).

Prandtl L., "Report on investigation of developed turbulence", *ZAMM*, v.5, pp.136-139, (1925).

Rivlin R.S., "The relation between the flow of non-Newtonian fluids and turbulent Newtonian fluids", *Quarterly of Applied Mathematics*, v. 15, pp. 212-215, (1957).

Saad Y., "A Flexible inner-outer Preconditioned GMRes algorithm", *SIAM J. Sci. Statistical Comput*., v. 14, pp. 461-469, (1993).

Smagorinsky J., "General circulation experiments with the primitive equations: I. The basic equations", *Mon. Weather Rev.*, v. 91, pp. 99-164, (1963).
Van Driest E. R., "On Turbulent Flow Near a Wall", *Journal of the Aeronautical Sciences*, v. 23, pp. 1007-1011, (1956).

Chapter 4

STABILIZED FINITE ELEMENT METHODS

4.1 Introduction

It is a matter of fact that most of the differential equation systems that model the real physics don't have a known analytical solution, mainly due to complex geometries and particular sets of boundary conditions. In order to circumvent these difficulties computational science arose and has been growing up for at least three decades, in parallel with the performance of computers, introducing several numerical techniques to obtain *approximate* solutions of the original problems. Among these numerical tools, the Finite Element method (FEM) represents a valuable choice in the solution of many engineering problems, fluid dynamics being one of the most important fields of application. The most common FEM is the *weighted residual Galerkin* formulation, already described in Chapter 1, which revealed as an optimal method for structural problems but showed some deficiencies for computational fluid dynamics (CFD), where in presence of "certain conditions" the solution becomes oscillating and *unstable,* and loses *accuracy*.

In this Chapter an investigation on the origins of *instability of the numerical behavior* will be performed, showing how it fits in fluid dynamics of turbulent flows, and describing some parameters of the discretized system of equations that govern this issue. After that an extensive analysis of the most common formulations proposed in literature to overcome instabilities will be pursued, focusing on both the well established *Petrov-Galerkin (PG)* framework and the newer *Variational MultiScale (VMS)* approach. The discussion will be enriched by some original contributions from the author and the research team to which he belongs, that have given rise to some new *stabilized finite element methods* for advection-diffusion-reaction operators, subject of recent publications and widely tested in the final Chapters of this work on both model problems and real turbomachinery flows.

Nonetheless, before addressing the theme of *stabilization*, it is necessary a preliminary short discussion to clarify the concepts of *convergence, stability* and *consistency*. To this end, let consider a simple first order differential equation in one-dimension, described by this *Cauchy problem*:

$$\begin{cases} y'(x) = f(x, y(x)) \\ y(x_0) = y_0 \end{cases} \tag{4.1}$$

Suppose the exact solution is the function $y(x_i)$ and the domain of the problem is $I = [x_0, x_0 + \beta]$. Its discretization is obtained by means of $n+1$ nodes, which define n intervals of the same length, labeled h,. The numerical solution of the original problems is computed with the following system of difference equations:

$$y_{i+k} = G(x_i, y_{i+k}, ..., y_i; h; f), \Rightarrow 0 \le i \le n-k \tag{4.2}$$

where k is the order of the difference equations, which depends on the previous k *computed* values of the solution, the characteristic dimension h of the grid, and the original differential operator f. If we define the *error* or *residual* as:

$$e_{i+k} = y(x_{i+k}) - y_{i+k} \tag{4.3}$$

we could isolate two contributions as follows:

$$\begin{aligned} e_{i+k} &= y(x_{i+k}) - G(x_i, y_{i+k}, ..., y_i; h; f) = R(x_i, y(x_i); h; f) + \\ &+ \left[G(x_i, y(x_{i+k}), .., y(x_i); h; f) - G(x_i, y_{i+k}, .., y_i; h; f) \right] \end{aligned} \tag{4.4}$$

the first one, labeled as R, is the *local truncation error* of the generic *i-th* step of the method, while the second is the *propagation error* due to the fact that the determination of y_{i+k} is obtained in terms of approximated values on the preceding nodes. The numerical method is said to be convergent when:

$$\lim_{h->0} \left(\max_{1 \le i \le n} |e_i| \right) = 0 \tag{4.5}$$

The first *necessary condition for convergence* is that all the *local truncation error* are infinitesimal with the characteristic dimension h of the grid, which means that the method must be *consistent*, as stated in the following relationship:

$$\lim_{h->0} \frac{R(x, y(x); h; f)}{h} = 0 \tag{4.6}$$

Unfortunately this is not sufficient, because the *propagation error* could corrupt the method step by step during the calculations. The concept of *stability* stems from the *propagation error*, and could be well described stating that if the *propagation error* does not corrupt the solution, the method is said to be *stable*. *Stability* and *consistency* together

define a *sufficient condition* for the *convergence* of the numerical solution to the exact one. For a more detailed discussion about errors and *"best approximation" property*, focused on the Galerkin method, the reader could consult the book from Hughes (2000).

4.2 Numerical instabilities in CFD and classical remedial strategies

Let recall the general *Oseen-like* form of the RANS system of equations, used to implement the governing equations that model turbulent flows into a CFD code:

$$\begin{gathered}\boldsymbol{\mathcal{F}}_a\left(\tilde{\boldsymbol{U}}\right)_{,j}+\boldsymbol{\mathcal{F}}_d\left(\tilde{\boldsymbol{U}},\nabla\tilde{\boldsymbol{U}}\right)_{,j}+\boldsymbol{\mathcal{F}}_r(\tilde{\boldsymbol{U}})-\tilde{\boldsymbol{\mathcal{B}}}=\boldsymbol{0}\ \text{ in }\ \Omega\in\mathbb{R}^{nsd}\\ \overline{\boldsymbol{U}}=\overline{\boldsymbol{U}}_D\ \text{ on }\ \Gamma_D\\ \boldsymbol{\mathcal{F}}_{d,n}=\boldsymbol{\theta}_N\ \text{ on }\ \Gamma_N\end{gathered}\tag{4.7}$$

where $\boldsymbol{\mathcal{F}}_a\left(\tilde{\boldsymbol{U}}\right)_{,j}$ is linearized with a given velocity field (i.e. the velocity field itself evaluated at the preceding equilibrium iteration), and $\boldsymbol{\mathcal{F}}_d\left(\tilde{\boldsymbol{U}},\nabla\tilde{\boldsymbol{U}}\right)_{,j}$, $\boldsymbol{\mathcal{F}}_r(\tilde{\boldsymbol{U}})$, $\tilde{\boldsymbol{\mathcal{B}}}$ are the linearized version of their corresponding operators. By introducing the following *vector function spaces* for *n* degrees of freedom:

$$\begin{gathered}\boldsymbol{H}^{1h}(\Omega)=\left[H^{1h}(\Omega)\right]^n\\ \boldsymbol{H}_0^{1h}(\Omega)=\left[H_0{}^{1h}(\Omega)\right]^n\\ \boldsymbol{H}^{(1/2)h}(\Omega)=\left[H^{(1/2)h}(\Omega)\right]^n\end{gathered}\tag{4.8}$$

By adopting the same notation used in the preceding Chapters, the finite dimensional spaces of *trial* and *test vector functions*, for primary and constrained (i.e. *pressure*) variables, are defined as:

$$\begin{gathered}\boldsymbol{S}_p^h=\left\{\overline{\boldsymbol{U}}_p^h\,\middle|\,\overline{\boldsymbol{U}}_p^h\in\boldsymbol{H}^{1h}(\Omega),\ \overline{\boldsymbol{U}}_p^h=\boldsymbol{U}_D\quad\text{on }\Gamma_D,\quad\boldsymbol{U}_D\in\boldsymbol{H}^{(1/2)h}(\Gamma_D)\right\}\\ \boldsymbol{W}_p^h=\left\{\boldsymbol{w}_p^h\,\middle|\,\boldsymbol{w}_p^h\in\boldsymbol{H}_0^{1h}(\Omega),\ \boldsymbol{w}_p^h=0\quad\text{on }\Gamma_D\right\}\\ S_c^h=W_c^h=\left\{\overline{U}_c^h\,\middle|\,\overline{U}_c^h\in H_0^{1h}(\Omega),\ w_c^h\,\middle|\,w_c^h\in H_0^{1h}(\Omega)\right\}\end{gathered}\tag{4.9}$$

where the Galerkin test functions could be the ones for *mixed elements*, namely *quadratic* for primary variables and *linear* for constrained ones (in the following a description of some problems related to the combination of interpolation spaces will be performed). The associated weights functions could be written in vector form as:

$$\boldsymbol{w}^h = \left[w_p^h, \quad w_p^h, \quad w_p^h, \quad w_c^h, \quad w_p^h, \quad w_p^h, \quad w_p^h, \quad w_p^h \right]^T \tag{4.10}$$

The approximated variational formulation of the linearized problem (4.7) could be thus written in a synthetic and meaningful way:

$$\textit{find } \overline{\boldsymbol{U}}^h \in \boldsymbol{H}^{1h} \;\; \forall \boldsymbol{w}_p^h \in \boldsymbol{W}_p^h, \;\; \forall w_c^h \in W_c^h, \textit{ such that}$$

$$c\left(\overline{\boldsymbol{V}}^h, \tilde{\boldsymbol{U}}^h, \boldsymbol{w}^h\right) + s\left(\tilde{\boldsymbol{U}}^h, \boldsymbol{w}^h\right) + r\left(\tilde{\boldsymbol{U}}^h, \boldsymbol{w}^h\right) = \left(\tilde{\boldsymbol{\mathcal{B}}}, \boldsymbol{w}^h\right) - \left(\boldsymbol{\theta}_N, \boldsymbol{w}_{|\Gamma_N}^h\right)_{\Gamma_N} \tag{4.11}$$

with the use of bi-linear and tri-linear forms:

$$s\left(\tilde{\boldsymbol{U}}^h, \boldsymbol{w}^h\right) = -\int_\Omega \boldsymbol{w}_{,j}^h \cdot \boldsymbol{\mathcal{F}}_d^h \, d\Omega$$

$$\left(\tilde{\boldsymbol{\mathcal{B}}}, \boldsymbol{w}^h\right) = \int_\Omega \boldsymbol{w}^h \cdot \tilde{\boldsymbol{\mathcal{B}}} \, d\Omega$$

$$\left(\boldsymbol{\theta}_N, \boldsymbol{w}_{|\Gamma_N}^h\right)_{\Gamma_N} = \int_{\Gamma_N} \boldsymbol{w}_{|\Gamma_N}^h \cdot \; \boldsymbol{\theta}_N \, d\Gamma \tag{4.12}$$

$$c\left(\overline{\boldsymbol{V}}^h, \tilde{\boldsymbol{U}}^h, \boldsymbol{w}^h\right) = \int_\Omega \boldsymbol{w}^h \cdot \boldsymbol{\mathcal{F}}_{a,j} \, d\Omega$$

$$r\left(\tilde{\boldsymbol{U}}^h, \boldsymbol{w}^h\right) = \int_\Omega \boldsymbol{w}^h \cdot \boldsymbol{\mathcal{F}}_r{}^h \, d\Omega$$

It is thus remarkable that generally the scalar equations that compose the RANS system appear in a complete advective-diffusive-reactive form. *Diffusion*, *advection* and *reaction* respectively refer to those terms in the partial differential equations *(PDE)* involving second, first and zero order derivatives of the unknowns.

In this viewpoint each of the equations composing (4.11) could be written, with respect to the corresponding unknown *U*, as follows:

$$F_a(U)_{,j} + F_d(U)_{,j} + F_r(U) = B \quad \text{in } \Omega \in \mathbb{R}^{nsd}, j = 1, \ldots, 3 \qquad (4.13)$$

$$U = U_D \quad \text{on } \Gamma$$

where for the sake of simplicity only Dirichlet boundary conditions have been considered, and the structure of the operators reads as:

$$\begin{aligned} F_a(U) &= u_j U \\ F_d(U) &= -kU_{,j} \\ F_r(U) &= cU \end{aligned} \qquad (4.14)$$

In (4.13) and (4.14), *nsd* is the number of space dimensions, $k > 0$ is a constant diffusivity, u_j are solenoidal velocity components, $c \geq 0$ is a reaction coefficient, and B the source term. According to these choices, that are representative of all the conditions encountered in RANS framework, the solution behavior for each of the scalar unknowns U is *exponential* (Corsini et al. (2005a)). Even if the reader should be aware of the fact that there is an *intrinsic coupling* between these equations, the problem of stabilization could be more easily addressed considering the problem statement (4.13), because it is a generalized form that could be simply specialized for each of the variables appearing in the turbulence closures presented in this work.

The numerical discretization of (4.13) must adequately tackle the instability origins that stem from the *advective* (Leonard (1979)) or *diffusive limit for incompressible fluid* (Gresho (1981)), as well that related to the *reaction dominated flow conditions* (Tezduyar and Park (1986), Harari and Hughes (1994)). The next Subsections deal with all these numerical difficulties, in the attempt to give an explanation for each of them and to obtain some *qualitative* and *quantitative* parameters that permit to define the conditions under which the *Galerkin method* is stable or not. Moreover a discussion about the instabilities due to the presence of *shocks* and relevant *solution gradients* will be included.

Each of the Subsections here included will be completed by the presentation of the *classical* approaches to tackle the related instability origin. Actually it must be recalled that a multitude of stabilized formulations could be found in the open literature, and probably a specialized text on the subject of stabilization would not be sufficient to include all of them. However, here for *"classical"* the author intends the methods based on the *Petrov-Galerkin* approach, which is characterized by a modification of the weight functions, and represents a well-established framework. In this work the *PSPG* method will be considered for the incompressibility constraint, the non-consistent *Streamline Upwind* and the *SUPG* for advection effects, the *SPG* for reactive features, and the *Discontinuity Capturing* for the treatment of gradients and shocks. It is worth noting that from now on, where possible, the superscript *h* will be removed from weight and trial functions, in order to have simpler expressions, even if it will be granted that finite

dimensional functional spaces are considered, in accordance to the concepts explained in Chapter 1.

4.2.1 Interpolation spaces and incompressibility constraint

The *continuity equation* for *incompressible flows* expresses a constraint for the velocity field, called *incompressibility constraint*, due to its equivalence with the *Poisson's equation* for the *pressure* field. In practice, pressure becomes a sort of *Lagrange multiplier* for this constraint, that must be fulfilled iteration after iteration by the computed velocity filed. In this way the number of equations is less than the total unknowns because conservation of mass has been degraded to a constraint, and there is an indetermination that makes the solution unstable. Babuska and Brezzi explained in detail this problem and found (i.e. see Babuska (1971) or Brezzi (1976)) that it can be avoided using certain pair of interpolation spaces for velocity and pressure fields, that fulfil the so-called *div-stab* or *Babuska-Brezzi* conditions.

Among these stable combinations of velocity and pressure interpolation spaced used in CFD computations, probably the most widespread is the mixed *Q2Q1* one, that uses *quadratic* functions for velocity components and *linear* for pressure. This choice features several benefits for the calculations, because it permits to avoid the *pressure checkerboarding effects* related to the incompressibility constraint, and in parallel enables a more accurate description of the velocity field. Notwithstanding, some problems could arise due to its coding complexity related to the non-negligibility of *second-order derivatives*, and due to its more demanding computational load.

4.2.1.1 PSPG stabilization

The *Q2Q1* element will be widely used in the rest of this work, and *ad-hoc* stabilized formulations will be derived for quadratic spaces of interpolations, for avoiding the oscillations due to advection, reaction and gradient effects. Nonetheless the equal order *Q1Q1* element, which employs linear interpolation functions for both velocity and pressure, is simpler and less demanding, so there has been a lot of research effort to circumvent the *Babuska-Brezzi condition* without using mixed finite elements. A good solution to this problem is represented by the *PSPG stabilization (Pressure Stabilizing Petrov-Galerkin)* that creates a relaxation of the incompressibility constraint and introduces in it a term that is proportional to the residual of the momentum equation. This procedure is well explained in Tezduyar et al. (1992), and the resulting perturbation of the continuity equation, which is made proportional to the momentum residual, makes use of a function π_c that reads as:

$$\pi_c = \frac{h}{2\|U\|} z w_{c,j} \tag{4.15}$$

where U is the global scaling velocity, h is the *geometric* characteristic length of the element considered, namely the diameter of the area-equivalent circle (in the following other definitions will be proposed for h), and the intensity of the stabilization parameter is defined by means of the z *magic function* proposed in Tezduyar et al. (1992):

$$z(Re_U^{\#}) = coth(Re_U^{\#}) - \frac{1}{Re_U^{\#}} \tag{4.16}$$

.

where $Re_U^{\#}$ is a local Reynolds number, calculated with the global scaling velocity and the local length scale h.

It has been demonstrated that the introduction of *PSPG* is beneficial also in presence of mixed Q2Q1 formulations, due to the elimination of zero diagonal entries in the resulting matrices (Borello et al. (2003)). It is therefore worth explaining the modifications that it introduces in the variational formulation of the RANS system. In practice a new contribution must be added to the weighted residual form of the *continuity equation*, that reads as:

$$\Pi\left(\pi_c\right) = \sum_{e=1}^{nel} \int_{\Omega_e} \left(\mathcal{F}_{a,j} + \mathcal{F}_{d,j} + \mathcal{F}_r - \tilde{\mathcal{B}} \right)^{(M)} \pi_c \, d\Omega \tag{4.17}$$

where the superscript $^{(M)}$ refers to the momentum residual, and the stabilizing contributions are confined on the element interior according to the continuity properties of the lower order perturbation function. In the next Sections, it will be clarified that (4.17) gives rise, together with other stabilization integrals, to a *global stabilization vector* that could be interpreted as a *perturbation of the weight functions* of the Galerkin formulation, thus explaining the attribute of *Petrov-Galerkin* formulations, which are characterized by weight and trial functions which differ.

4.2.2 Advection induced instabilities

Since the appearance of the first works by Hughes and Brooks (1982a, 1982b), the subject of *advection* (or *convection*) induced instabilities, mainly appearing in fluid flows computation, has been widely studied, with enormous production of literature and theories, speculating on both the origin of this numerical drawback and the possible solutions. In the following a short description of the problem will be performed, enriched by some helpful mathematical explanations, that will be recalled later, when presenting the stabilized formulations for advection effects.

Early computations of convective transport problems with the Galerkin method gave rise to unsatisfactory results (Hughes and Brooks (1982a)), also on simple configurations, such as the following *second order linear* differential equation in one-dimension for the scalar unknown U (i.e. it could represent the temperature field):

$$uU_{,x} = kU_{,xx} \tag{4.18}$$

on the domain *(0,L)*, with boundary conditions *U(0)=0, U(L)=1*. It is worth mentioning that (4.18) could be seen as a specialized *homogeneous* counterpart of (4.13) in one-dimension with null reaction. The exact solution has a known exponential behavior and reads as follows:

$$U(x) = \frac{1 - e^{ux/k}}{1 - e^{uL/k}} \tag{4.19}$$

It was noted that for a dominating convection effect, the numerical solution featured node to node oscillations (or wiggles), that ruined the quality of the result. The explanation to this behavior is that the convection term leads to a *non-symmetric* (or *skew-symmetric*) matrix, with a lack of diagonal terms. As a first remedial strategy, it is possible to *extremely refine the mesh*, with the counterpart of a rapidly increasing computational load. The fact that the quality of the results is related to the grid refinement could be helpful in defining a mathematical non-dimensional parameter that governs the solution behavior, namely the *element (or local) Peclet number (Pe)*, which reads as:

$$Pe = \frac{\|u\| h}{2k} \tag{4.20}$$

where the *euclidean norm* of the velocity has been considered, in order to have a definition valid for the multi-dimensional context too. It is thus possible to have a quantitative evaluation of the *advection-to-diffusion* ratio, with respect to the adopted grid. Fig. 4.1 shows in a qualitative way that when *Pe* number grows up, the solution of the proposed problem with the *Galerkin method* on *linear finite elements* starts to feature more and more oscillations. It is worth noting that in this discussion *u* has been considered as positive.

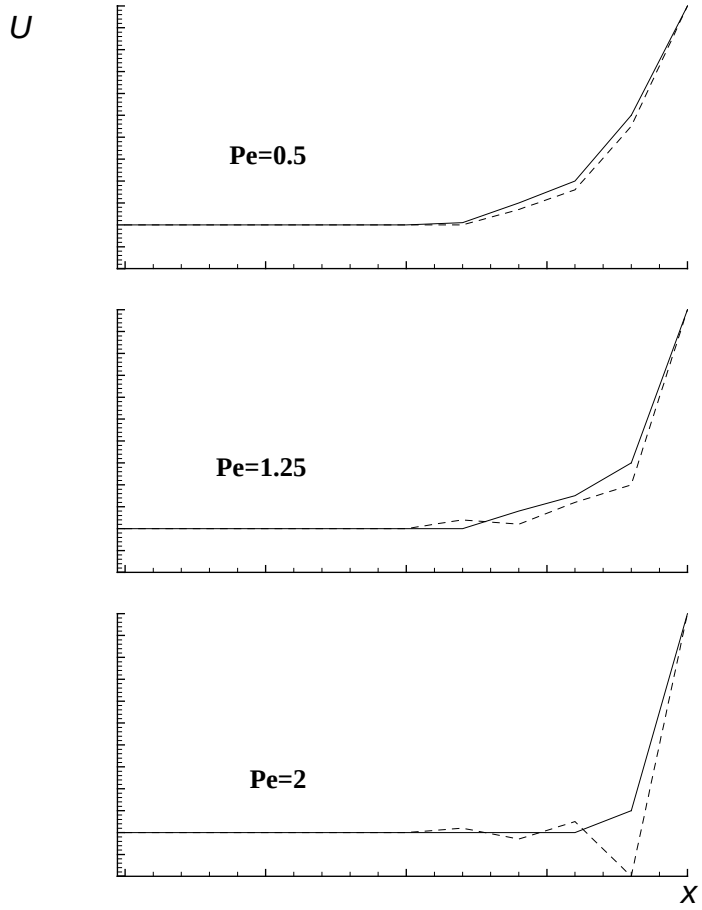

Fig. 4.1. Effect of increasing *Pe*; solid line=exact, dashed=Galerkin.

As a matter of fact the shown oscillations (or wiggles) often corrupt all the solution field, especially for multidimensional problems, thus corrupting the convergence of iterative solution procedures and leading to poor results. Therefore it is of fundamental importance to determine which is the cut-off value that separates the stable region of *Pe* values from the unstable one, let consider the *i-th* equation of the tri-diagonal system arising from the application of the Galerkin method, in case of $u>0$:

$$\left[-U_{i-1}+2U_i-U_{i+1}\right]+Pe\left[-U_{i-1}+U_{i+1}\right]=0 \tag{4.21}$$

Following argumentations similar to those used in Corsini et al. (2005b) for a more general context (i.e. the *advection-diffusion-reaction* problem, that will be addressed in the following), it could be demonstrated that the so-called *Galerkin nodal amplification factors* (see Harari and Hughes (1994)), which are the solutions of the characteristic equation associated to Eq. (4.21), purely depend on the magnitude of *Peclet:*

$$\rho = \frac{-1 \pm Pe}{-1 + Pe} \tag{4.22}$$

The influence exerted on ρ shows that the exact solution exponential behavior could be preserved only with $Pe < 1$, because both the nodal amplification factors are positive. On the contrary, if Pe grows up, that could be interpreted as a *coarsening* of the mesh while velocity and diffusion remain constant, no stability is guaranteed, and oscillatory behavior starts to appear. This circumstance confirms the need of designing a stabilized scheme with built-in component to preclude oscillatory behavior in advection dominated cases.

Before starting the description of the stabilization techniques addressed in this work, let point out an important concept about oscillations (or wiggles): a possible interpretation of numerical instabilities in general (i.e. both due to advection and to reaction effects) could be that they signal a grid space too coarse to resolve certain features (Gresho and Lee (1979)), such as boundary layers. In this way they could be used as an input for adapting meshing tools, but this argumentations are not acceptable for two major reasons: first, the most complex problems, such as turbomachinery flows, would require an exaggerate number of nodes, and second, not all the flow features must be well resolved, the important being that their unsatisfactory computation must not ruin the rest of the solution.

4.2.2.1 Streamline Upwind non-consistent stabilization

Originating from the concept of *upwind differences*, the first solution proposed for advection induced instabilities has been the use of *upwind differencing* the convective term, which means writing it in terms of the central value and the one *upstream*, as follows:

$$uU_{,x} \approx u\frac{U_i - U_{i-1}}{\Delta x} \tag{4.23}$$

In this way the matrix recovers a diagonal dominance, and instabilities disappear. This operation could be interpreted as an additional *"artificial viscosity"* to the original differential problem, namely:

$$\tilde{k} = \frac{uh}{2} \tag{4.24}$$

An early recognized drawback of this procedure, called *upwind* method, is a resulting *overly diffuse solution*, and a lose in accuracy (i.e. upwind differences are only first-order accurate, as well explained in Hughes and Brooks (1982a)). The interpretation of upwind

differences as additional viscosity generated extensive criticism on the upwind method as it was, thus leading to more research on the argument. A first improving solution was recognized to be the addition of a stabilization term, depending on the *Peclet* magnitude, with a resulting artificial viscosity equal to:

$$\tilde{k} = \frac{uh}{2}\xi$$
$$\xi = coth[sgn(u)Pe] - {sgn(u)}/{Pe} \tag{4.25}$$

where the *sgn* function permits to correctly take into account the sign of u and to upwind the convective term, while the stabilization coefficient ξ damps the artificial viscosity, as shown in Fig. 4.2.

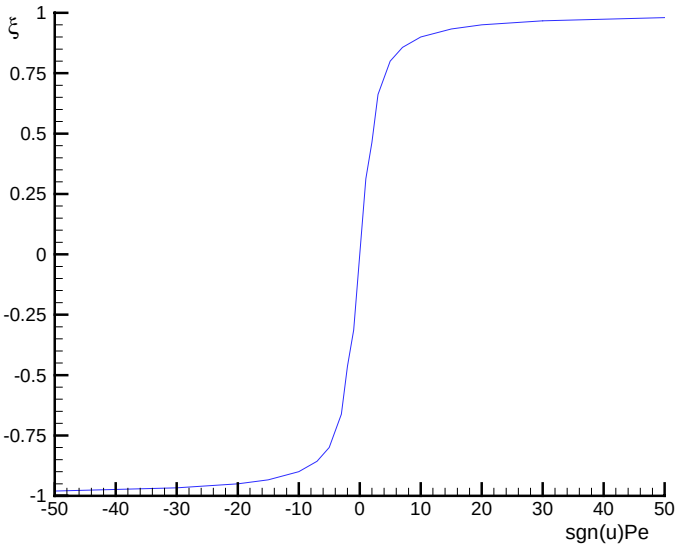

Fig. 4.2. Upwind magic function behavior.

Nonetheless, for multidimensional problems, still some difficulties were encountered due to the *isotropic* nature of the operator introduced, generalized by means of the euclidean norm of the velocity as:

$$\tilde{k} = \frac{\|u\| h}{2} \xi$$
$$\xi = coth(Pe) - 1/Pe \tag{4.26}$$

The results obtained with these expression of the additional viscosity are characterized by an excessive *crosswind diffusion*, and this circumstance led to the development of the *Streamline Upwind* formulation, which makes use of a *non-isotropic* additional viscosity, and results in an equivalent *perturbation of the weight of the convective term* that reads as:

$$\pi_p = \frac{h}{2} \xi \frac{1}{\|u\|} (u_k w_{,k}) \tag{4.27}$$

In this way both the crosswind and streamline components of the additional diffusion are limited, thus leading to quite satisfactory results. The resulting variational formulation for the RANS system of equations reads generally as:

$$find\ \overline{\boldsymbol{U}}^h \in \boldsymbol{H}^{1h}\ \ \forall \boldsymbol{w}_p^h \in \boldsymbol{W}_p^h,\ \forall w_c^h \in W_c^h,\ such\ that$$

$$c\left(\bar{\boldsymbol{V}}^h, \tilde{\boldsymbol{U}}^h, \boldsymbol{w}^h\right) + s\left(\tilde{\boldsymbol{U}}^h, \boldsymbol{w}^h\right) + r\left(\tilde{\boldsymbol{U}}^h, \boldsymbol{w}^h\right) + \Pi(\boldsymbol{\pi}) = \left(\tilde{\boldsymbol{\mathcal{B}}}, \boldsymbol{w}^h\right) - \left(\boldsymbol{\theta}_N, \boldsymbol{w}^h_{|\Gamma_N}\right)_{\Gamma_N} \tag{4.28}$$

where a stabilization integral has been added to (4.11), which reads as:

$$\Pi\left(\pi_p\right) = \sum_{e=1}^{nel} \int_{\Omega_e} \mathcal{F}_{a,j}\, \pi_p\, d\Omega \tag{4.29a}$$

$$\Pi\left(\pi_c\right) = \sum_{e=1}^{nel} \int_{\Omega_e} \left(\mathcal{F}_{a,j} + \mathcal{F}_{d,j} + \mathcal{F}_r - \tilde{\mathcal{B}}\right)^{(M)} \pi_c\, d\Omega \tag{4.29b}$$

where (4.29a) is added to the equations of the *primary variables*, and (4.29b) represents the *PSPG* contribution to continuity equation.

4.2.2.2 SUPG stabilization

The *Streamline Upwind* represents a smart solution for improving Galerkin finite elements in solving advection diffusion problems with relevant *Peclet number*. Notwithstanding the results continue to show an excessive diffusion, and upwinding the convection term is *not consistent* with the centrally weighted reaction and transient terms. For these reasons, Hughes and Brooks (1982a, 1982b) developed a *Petrov-Galerkin* method, based on an *upwinding procedure* for all the terms of the equation, and named *SUPG* (i.e. *Streamline Upwind Petrov-Galerkin*). In this way, the recovered consistency of the numerical scheme enabled the definitive separation between numerics of finite elements and finite differences.

SUPG is probably the most famous stabilized formulation, and finds application in commercial as well as research codes. It consists in applying to all the terms of the equations the weight perturbation π_p already defined in (4.27).

In this work we would like to approach the *SUPG* in such a way to understand how the final expression of the magic function ξ, which from now on will be called ζ_a, due to the fact that it tackles advection effects, could be rigorously obtained. To this end, let consider the *modified* weight function that is possible to obtain for the *i-th* node of the numerical scheme:

$$\tilde{w}_i = w_i + \pi_p = w_i + \zeta_{a_i} P_i \tag{4.30}$$

It is worth noting that the perturbation π_p could be decomposed in two factors:

$$\pi_p = \tau_{SUPG}(u_k w_{,k}) = \frac{h}{2\|u\|}\zeta_a(u_k w_{,k}) \tag{4.31}$$

In (4.31) the τ_{SUPG} parameter is called intrinsic time scale, due to its physical dimension. Let now consider the perturbed form assumed by (4.21) if we apply *SUPG* on *linear finite elements*:

$$\frac{k + u\frac{\zeta_a}{2}h}{h}\left[-U_{i-1} + U_i - U_{i+1}\right] + \frac{u}{2}\left[-U_{i-1} + U_{i+1}\right] = 0 \tag{4.32}$$

If we impose the exact exponential behavior on the discrete nodal solutions appearing in (4.32), it turns to an equation in the unknown ζ_a, that has the following solution:

$$\zeta_a = coth(Pe) - 1/Pe \tag{4.33}$$

No surprise with the fact that the obtained expression is equal to the one proposed by Hughes and Brooks in their early works on *Petrov-Galerkin upwind finite elements*. The

magic function, that assumes the character of a *stabilization function*, permits to obtain nodal exact solution in the advection-diffusion homogeneous one-dimensional counterpart of problem (4.13), and has the behavior shown in Fig. 4.2, tuning the stabilization effect in view of the *Peclet* value, that represents the relative importance of advection with respect to diffusion. The conditions fulfilled by ζ_a are summarized in the so-called *super-convergence* feature (i.e. nodal exactness for the discrete solution of the one-dimensional homogeneous linear differential equation), well described in Corsini et al. (2005b), that represents the basis for all the *Petrov-Galerkin* formulations presented in the following.

The final expression of *SUPG* stabilized formulation for linear elements, obtained including (4.33) in (4.31) could be easily *generalized to multi-dimensional problems* by choosing an adequate estimate of the element characteristic length. In the open literature, several expression appears, but for this work the author decided to restrict the choice between three different possibilities:

1. the *geometric element characteristic length h*, equal to the diameter of the circle equivalent to the considered element;
2. the *streamline element characteristic length*

$$h = 2(\sum_a |\boldsymbol{s} \cdot \nabla N_a|)^{-1} \tag{4.34}$$

   where $\boldsymbol{s}$ represents the unit vector in direction of the streamlines and N_a is the interpolation function associated to the *a-th* node of the element considered. This kind of length has been defined and applied with success in several works from Tezduyar and coauthors, starting from Tezduyar and Park (1986), and labeled h_{UGN} in Tezduyar and Osawa (2000)*;*
3. the gradient element characteristic length

$$h = 2(\sum_a |\boldsymbol{r} \cdot \nabla N_a|)^{-1} \tag{4.35}$$

   where $\boldsymbol{r}$ represents the unit vector in direction of the gradient, as proposed in Tezduyar (2003), where this length is labelled $h_{RGN.}$, which is very useful for problems with relevant reaction or where gradients are predominant, as will be clarified in the following.

Before presenting the formulation of the RANS problem stabilized with SUPG and PSPG formulations, a further capital question must be addressed: is this SUPG suitable for higher order elements, in particular *Q2* ones? The answer is negative, because the nodal exactness (based on the *super-convergence* condition) of the discrete solution must be imposed on all the nodes of the grid. Provided that different equations could be obtained for the extreme and central nodes of a quadratic three-nodes one-dimensional element (see Codina et al. (1992)), it is possible to find two optimal modified weights, one for

central nodes, labelled ζ_{a2}, and one for extreme nodes, labelled ζ_{a1}, on the basis of the following discrete equations for central nodes:

$$\begin{aligned}&[-4-2Pe-4\zeta_{a2}Pe]U_{i-1}+[8+8\zeta_{a2}Pe]U_i+\\&+[-4+2Pe-4\zeta_{a2}Pe]U_{i+1}=0\end{aligned} \tag{4.36}$$

and for extreme (or corner) nodes:

$$\begin{aligned}&[1+Pe-6\zeta_{a1}+\zeta_{a1}Pe]U_{i-2}+[-8-4Pe+12\zeta_{a1}-8\zeta_{a1}Pe]U_{i-1}+\\&+[14+14\zeta_{a1}Pe]U_i+[-8+4Pe-12\zeta_{a1}-8\zeta_{a1}Pe]U_{i+1}\\&+[1-Pe+6\zeta_{a1}+\zeta_{a1}Pe]U_{i+2}=0\end{aligned} \tag{4.37}$$

Imposing nodal exactness of the discrete solution and following the simple manipulations described in Codina et al. (1992), it is possible to obtain the following expression for the stabilization functions of the *SUPG Q2 stabilization*:

$$\zeta_{a2}(Pe)=\frac{1}{2}[\coth(Pe/2)-2/Pe] \tag{4.38a}$$

$$\zeta_{a1}(Pe)=\frac{(3+3\zeta_{a2}Pe)\tanh(Pe)-(3Pe+Pe^2\zeta_{a2})}{[2-3\zeta_{a2}\tanh(Pe)]Pe^2} \tag{4.38b}$$

It is worth noting that the stabilization function for extreme nodes depends on the one for central nodes, due to the fact that for quadratic elements the shape functions associated to corner nodes involve adjacent elements (e.g. for the influence of interpolation space order on stabilization parameters, see Akin and Tezduyar (2004)). The behavior of these magic functions for the SUPG Q2 formulation is shown in Fig. 4.3.

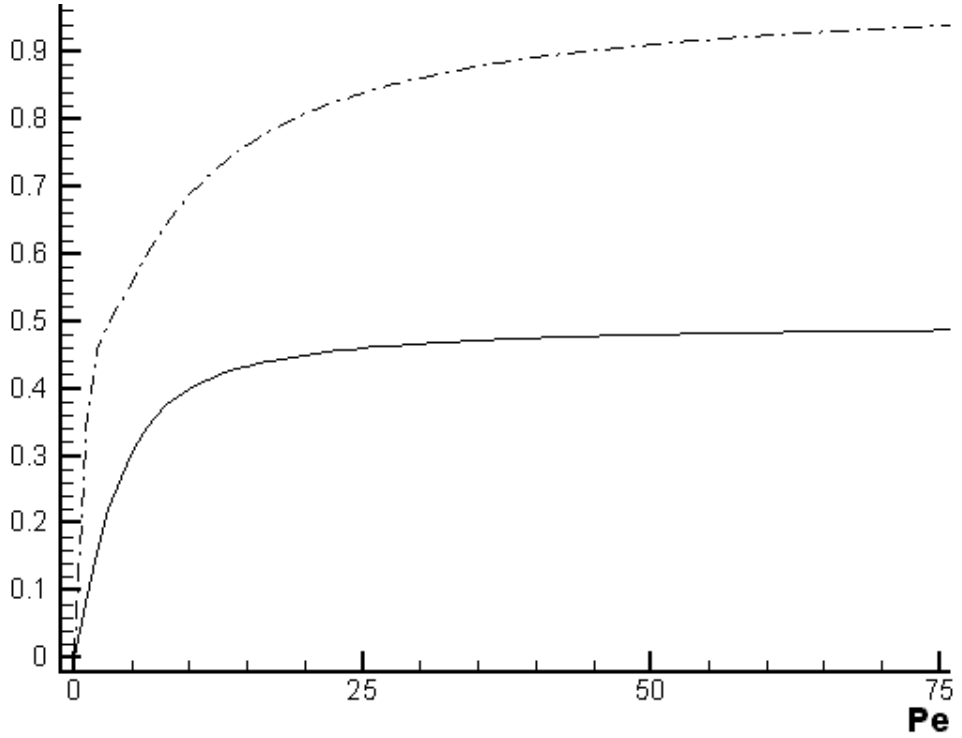

Fig. 4.3. Stabilization functions for SUPG Q2; solid line: ζ_{a2}, dashed line: ζ_{a1}.

For the multi-dimensional extension of *SUPG Q2*, it is important to define which are the central nodes and which the extreme nodes. This operation could be performed by means of the knowledge of the streamline direction with respect to the axes of the logic system of coordinates for the element considered, and is explained in Codina et al. (1992), where it is clarified that some nodes are of intermediate nature, i.e. their stabilization function is a combination of ζ_{a1} and ζ_{a2}.

It is now possible to present the global formulation of the *SUPG/PSPG* stabilized formulation of the RANS system of equations, that could be applied for all the turbulence closures presented in this work:

$$find\ \overline{\boldsymbol{U}}^h \in \boldsymbol{H}^{1h}\ \ \forall \boldsymbol{w}_p^h \in \boldsymbol{W}_p^h,\ \forall w_c^h \in W_c^h,\ such\ that$$

$$c\left(\overline{\boldsymbol{V}}^h, \tilde{\boldsymbol{U}}^h, \boldsymbol{w}^h\right) + s\left(\tilde{\boldsymbol{U}}^h, \boldsymbol{w}^h\right) + r\left(\tilde{\boldsymbol{U}}^h, \boldsymbol{w}^h\right) + \Pi(\boldsymbol{\pi}) = \left(\tilde{\mathcal{B}}, \boldsymbol{w}^h\right) - \left(\boldsymbol{\theta}_N, \boldsymbol{w}^h_{|\Gamma_N}\right)_{\Gamma_N} \quad (4.39)$$

where all the bi-linear and tri-linear forms are as defined in (4.11) and (4.12), while the stabilization integral is now consistent and reads as:

$$\Pi\left(\pi_p\right)=\sum_{e=1}^{nel}\int_{\Omega_e}\left(\mathcal{F}_{a,j}+\mathcal{F}_{d,j}+\mathcal{F}_r-\tilde{\mathcal{B}}\ \right)\pi_p\, d\Omega \tag{4.40a}$$

$$\Pi\left(\pi_c\right)=\sum_{e=1}^{nel}\int_{\Omega_e}\left(\mathcal{F}_{a,j}+\mathcal{F}_{d,j}+\mathcal{F}_r-\tilde{\mathcal{B}}\ \right)^{(M)}\pi_c d\Omega \tag{4.40b}$$

where (4.40b) is added to the continuity equation, as described in the *PSPG* Subsection, while for the *primary variables* (4.40a), namely the *SUPG* contribution, adopts this weight:

$$\pi_p=\tau_{SUPG}(u_k w_{,k})=\frac{h}{2\|u\|}\zeta_{ai}(u_k w_{,k}) \tag{4.41}$$

and the stabilization function must be chosen according to the order of the element, and in case of quadratic one, it differs for central and extreme nodes.

The resulting RANS stabilized formulation could be thus interpreted as a modification of the weight function vector $\tilde{\boldsymbol{w}}\equiv\boldsymbol{w}\ +\boldsymbol{\pi}$ as follows:

$$\boldsymbol{w}\ =\left[w_p,\ \ w_p,\ \ w_p,\ \ w_c,\ \ w_p,\ \ w_p\right]^T \tag{4.42a}$$

$$\boldsymbol{\pi}\ =\left[\pi_p,\ \ \pi_p,\ \ \pi_p,\ \ \pi_c,\ \ \pi_p,\ \ \pi_p\right]^T \tag{4.42b}$$

4.2.3 Reaction induced instabilities

Moving towards turbomachinery CFD, an additional origin of numerical deficencies stems from the reaction or zero order derivative terms. These terms are usually related to the rotation of turbomachinery frame of reference (e.g. in the modelling of Coriolis forces), but they also appear in the turbulence closure equations (e.g., eddy viscosity models). In this ambit, they are related to dissipation terms and play a critical role in the development of boundary layers in the case of vanishing advection effects, such as in the transitional region, or in the stagnation and separation flow cores (i.e. see Corsini et al. (2005b)). Whenever the reaction is present, local oscillations, near boundaries or solution discontinuities, may be originated but they typically do not degrade the global solution accuracy (Codina (2001)). As a matter of fact, in this case it is not possible to obtain a global stability estimate in the H^1 norm, though it could be evaluated in L^2, thus explaining the local scale of the oscillations.

In order to better understand these concepts, let recall the general *advective-diffusive-reactive* problem statement that could be written for each of the scalar unknowns of the RANS system of equations:

$$\begin{aligned} F_a(U)_{,j} + F_d(U)_{,j} + F_r(U) &= B \quad \text{in } \Omega \in \mathbb{R}^{nsd}, j = 1, \ldots, 3 \\ U &= U_D \quad \text{on } \Gamma \end{aligned} \tag{4.13}$$

where for the sake of simplicity only Dirichlet boundary conditions have been considered, and the structure of the operators reads as:

$$\begin{aligned} F_a(U) &= u_j U \\ F_d(U) &= -kU_{,j} \\ F_r(U) &= cU \end{aligned} \tag{4.14}$$

In (4.13) and (4.14), *nsd* is the number of space dimensions, $k > 0$ is a constant diffusivity, u_j are solenoidal velocity components, ., B the source term, and *c,* now considered as non-zero, is the positive *reaction coefficient*. It is clear that now the solution will be governed by two parameters, the first one being the already introduced element *Peclet* number, relating advection to diffusion, and the second being the *element reaction number r*, which reads as:

$$r = \frac{ch^2}{k} \tag{4.43}$$

The new non-dimensional parameter introduced in (4.43) relates the reaction magnitude to the diffusion. The solution behavior, governed by both *Pe* and *r*, is always exponential, therefore if we restrict our attention to the one-dimensional linear homogeneous context, the nodal amplification factors should be both positive (see Corsini et al. (2005b)).

In order to have a first insight on the instability origin of the reaction dominated case, let now consider the null advection limit of the studied problem, focusing for instance on element central nodes of a *quadratic* Galerkin finite element, as in the analysis performed in Corsini et al. (2003) (for a similar discussion on linear elements, the reader could consult Harari and Hughes (1994)). In this condition, the equation for the *i-th* node reads as:

$$\begin{aligned} &U_{i-1}\,[-4 + r/10] + U_i\,[8 + r\,4/5] + \\ &+ U_{i+1}\,[-4 + r/10] = 0 \end{aligned} \tag{4.44}$$

The solutions of the characteristic equation associated to Eq. (4.44), the so-called Galerkin nodal amplification factors, in absence of advection purely depend on the magnitude of reaction:

$$\rho = \frac{-(8+\frac{4}{5}r) \pm \sqrt{(8+\frac{4}{5}r)^2 - 4(-4+\frac{r}{10})^2}}{2(-4+\frac{r}{10})} \tag{4.45}$$

The influence exerted on ρ shows that the exact solution exponential behavior is preserved only with $r < 40$. This circumstance confirms the need of designing a stabilized scheme with built-in component to preclude oscillatory behavior in reaction dominated cases (Corsini et al. (2003)).

A criticism that typically is moved against reaction controlling numerical tools is that the reaction instabilities appear in very limited zones of the solution field and that a simple *mass lumping technique* (for *mass lumping* rationale see Hughes (2000)) could be sufficient to control them. Actually this way of thinking doesn't take into account two main concepts: first, the *mass lumping* is a non-consistent numerical trick (and in the following Chapters its inaccuracy will be demonstrated), and second, high reaction flow cores are physically meaningful, especially in the turbomachinery context. In this respect, let consider for example the CLS96 turbulence closure, described with Eqs. (3.40-3.45) (same discussions could be performed for *LS74* and *k-ε-v²-f*). The reaction numbers for the *k-ε* equations, reads as:

$$r_k = \frac{c_k h^2}{\nu + \frac{\nu_t}{\sigma_k}} \tag{4.46a}$$

$$r_\varepsilon = \frac{c_\varepsilon h^2}{\nu + \frac{\nu_t}{\sigma_\varepsilon}} \tag{4.46b}$$

where the reaction coefficients have been defined in Chapter 3. It is remarkable that the magnitudes of the reaction-to-advection ratios (r_k/Pe_k , $r_\varepsilon/Pe_\varepsilon$) become relevant in the near-wall region, mainly within the viscous and buffer sub-layers (Corsini et al. (2005b)). Moreover, reaction-driven effects are emphasized in presence of non-equilibrium phenomena such as stagnation region, transition or separation. To this end it is possible to express the relative magnitude of reaction with respect to advection in terms of time scale ratio:

$$\frac{r_k}{Pe_k} \sim \frac{r_\varepsilon}{Pe_\varepsilon} \sim \frac{\varepsilon}{k}\frac{h}{\left\|\bar{u}\right\|} \sim \frac{T}{\tau} \tag{4.47}$$

where $T = h/\left\|\bar{u}\right\|$ is the element mean time scale and $\tau = k/\varepsilon$ is the modeled turbulence time scale. For instance, in case of a fully developed plane channel flow it is easy to show that approaching the wall T/τ behaves as:

$$\frac{T}{\tau} \sim \frac{1}{\delta^2} \tag{4.48}$$

where δ is the distance from the solid wall. The turbulence model related reactivity is thus expected to dramatically affect the boundary layer simulation in turbomachinery configurations, where the presence of stagnation, separation or adverse pressure gradient phenomena gives rise to local reaction-to-advection ratio of order $o(10^5)$ (Corsini et al. (2003)).

4.2.3.1 SPG stabilization

Two alternative routes could be found in literature to build-up classical stabilization schemes for the reactive limit. The first one includes the earlier attempts, mainly based on the extension of existing advective-diffusive stabilization concepts to the reactive case. To mention but a few, the work of Tezduyar and Park (1986) that used a discontinuity capturing like operator (to this method, called *DRD*, in the following a Subsection will be dedicated), or the gradient GLS formulation proposed by Harari and Hughes (1994). More recently, in the framework of Petrov-Galerkin methods, Idelsohn and co-workers (1996) proposed a Centered PG formulation for linear elements involving two different stabilizing parameters, the first to control advection induced instabilities and the second, based on a second-order polynomial, for reaction induced ones. To the best of the authors' knowledge, most of the consistent formulations proposed for advective-diffusive-reactive flow problems have been designed for linear equations and linear elements, and only few works concern with reactive problems pertinent to turbomachinery fluid dynamics (e.g. Codina and Soto (1997)).

In this Subsection, dedicated to reaction controlling Petrov-Galerkin methods, the author would like to introduce the *SPG (Spotted Petrov-Galerkin)* formulation, recently developed by the team at University "La Sapienza" (i.e. the reader could see Corsini et al. (2003), (2004a), (2004b) and (2005b)), and formulated on a quadratic finite element space of approximation. We advocate the use of a higher order stabilized formulation (despite of its coding complexity, due to non-negligible second order derivatives) that guarantees the best compromise between solution stability and accuracy (as shown by Borello et al. (2003)). The proposed method, namely the *Spotted Petrov-Galerkin* (*SPG*), possesses some distinctive features. For advection-diffusion problems it behaves like a *SUPG Q2* method, whereas in the reactive-diffusive limit it turns to a space invariant

perturbation able to give rise to spot-like weight functions, symmetric and concentrated around each nodal position. In intermediate situations, the scheme combines the advective and reactive perturbation integrals using nodal *stabilization* or *upwind* coefficients that depend on element *Peclet* and *reaction* numbers and are designed to circumvent any compounding effect (Corsini et al. (2005b)).

The discretization of the one-*dimensional homogeneous counterpart* of (4.13-14), for constant physical properties (*k, c, u*), using the Galerkin method on a quadratic space of interpolation, with uniform element of length *h*, gives rise to the following difference equations:

$$\begin{aligned} &U_{i-1}\,[-4-2Pe+r/10]+U_i\,[8+r\,4/5]+\\ &+U_{i+1}\,[-4+2\,Pe+r/10]=0 \end{aligned} \tag{4.49}$$

for (*i*) element central node, and

$$\begin{aligned} &U_{i-2}\,[1+Pe-r/10]+U_{i-1}\,[-8-4Pe+r/5]+\\ &+U_i\,[14+r\,4/5]+U_{i+1}\,[-8+4Pe+r/5]+\\ &+U_{i+2}\,[1-Pe-r/10]=0 \end{aligned} \tag{4.50}$$

for (*i-2*, *i*, *i+2*) element extreme nodes.

Provided that different equations have been obtained for the extreme and central nodes, as already said for *SUPG Q2*, it is possible to find two optimal modified weights, on the basis of the discrete Eqs. (4.49) and (4.50) separately. Each of these resulting PG weight functions is obtained from the addition to the Galerkin one w_i of two perturbation functions, the first one to control advection induced oscillations and the second for reaction induced ones (as first suggested for linear elements by Idelsohn et al. (1996)), and for each element node (*i*) read as:

$$\tilde{w}_i = w_i + \zeta_{a_i} P_{a_i} + \zeta_{r_i} P_{r_i} \tag{4.51}$$

where ζ_{a_i} and ζ_{r_i} the stabilization coefficients for the two perturbation functions, respectively P_{a_i} for advection induced instabilities and P_{r_i} for reaction induced ones. The first perturbation is formally similar to a SUPG one and reads as:

$$P_{a_i} = \frac{h}{2\|u\|} u_k w_{i,k} \tag{4.52}$$

On the other hand, the design of the perturbation function that controls reaction effects is based on the following constraints. First, in the *null advection* case the invariance of the equation under coordinate inversion suggests to adopt symmetric weight

$\widetilde{w}_i$ (Idelsohn et al. (1996)). Moreover, in the *pure reaction* limit ($r \to \infty$), the optimal weight would be a Dirac's delta. On this basis, the perturbation suggested by the authors is a *symmetric and negative definite polynomial* (Corsini et al. (2004a)), and must fulfil at least six constraints, i.e. it must be zero with zero first-order derivative on the element nodes. The lowest order polynomial with these features is a sixth order one; the seventh constraint imposed by the authors is represented by the C_{SPG} value which sets the magnitude of the weight reduction between two neighbouring nodes:

$$P_{r_i} = P_r = -\frac{C_{SPG}}{l_\xi^{\,6}}\left[\xi^6 - \frac{l_\xi^{\,2}}{2}\xi^4 + \frac{l_\xi^{\,4}}{16}\xi^2\right] \tag{4.53}$$

where ξ represents the coordinate in the master or logic space and l_ξ its dimension (in our case equal to 2). It is remarkable that the periodic-like behaviour of this function permits to use the same analytical expression for each node. The coefficient C_{SPG} is used to set the asymptotic values of the stabilization functions ζ_{r_i}, without affecting ζ_{a_i}.

The expression for the stabilization functions are consequent to the super-convergence condition (Codina et al., 1992, Idelsohn et al., 1996), that requires the identity between the discrete and the exact solution in case of a homogeneous linear one-dimensional problem**.** In particular, the use of the SPG method to solve the considered problem statement on a quadratic space of interpolation, with uniform elements of length *h*, gives rise to the following difference equations:

$$-a_6 \cdot U_{i-1} + d_8 \cdot U_i - a_7 \cdot U_{i+1} = 0 \tag{4.54}$$

for (*i*) element central node, and

$$\begin{aligned} & U_{i-2}\,[a_2 + b_2\zeta_{a_1} + e_2\zeta_{r_1}] + \\ +U_{i-1}\,& [a_1 + b_1\zeta_{a_1} + e_1\zeta_{r_1}] + \\ +U_i\,& [a_4 + b_4\zeta_{a_1} + e_4\zeta_{r_1}] + \\ +U_{i+1}\,& [a_3 + b_3\zeta_{a_1} + e_3 4.55\zeta_{r_1}] + \\ +U_{i+2}\,& [a_5 + b_5\zeta_{a_1} + e_5\zeta_{r_1}] = 0 \end{aligned} \tag{4.55}$$

for (*i-2*, *i*, *i+2*) element extreme nodes. It should be remarked that in (4.54) the coefficients are linear function of the unknowns, namely ζ_{a_2}, ζ_{r_2}, and equation (4.55) provides $\zeta_{a_1} = \zeta_{a_3}$, $\zeta_{r_1} = \zeta_{r_3}$. The complete expressions of the coefficients are given in Table 4.1.

$$a_{7=}\ [-4-2Pe+r/10-4Pe\zeta_{a_2}+\frac{r}{2}\zeta_{a_2}+\frac{C_{SPG}}{280}\zeta_{r_2}Pe+\frac{C_{SPG}}{140}\zeta_{r_2}-\frac{53C_{SPG}}{26880}r\zeta_{r_2}]$$

$$d_8=[8+r\,4/5+8Pe\zeta_{a_2}-\frac{C_{SPG}}{70}\zeta_{r_2}-\frac{C_{SPG}}{840}r\zeta_{r_2}]$$

$$a_6=[-4+2\,Pe+r/10-4Pe\zeta_{a_2}-\frac{r}{2}\zeta_{a_2}-\frac{C_{SPG}}{280}\zeta_{r_2}Pe+\frac{C_{SPG}}{140}\zeta_{r_2}-\frac{53C_{SPG}}{26880}r\zeta_{r_2}]$$

$$a_1=-8-4Pe+r/5, \qquad b_1=-8Pe+12+r,$$

$$a_2=1+Pe-r/10, \qquad b_2=Pe-6-r/4,$$

$$a_3=-8+4Pe+r/5, \qquad b_3=-8Pe-12-r,$$

$$a_4=14+r\,4/5, \qquad b_4=14Pe,$$

$$a_5=1-Pe-r/10, \qquad b_5=Pe+6+r/4,$$

$$e_1=-C_{SPG}(1/35+r/420),$$

$$e_2=-C_{SPG}(53r/13440-Pe/140-1/70),$$

$$e_3=-C_{SPG}(1/35+r/420),$$

$$e_4=-C_{SPG}(53r/6720-1/35),$$

$$e_5=-C_{SPG}(53r/13440+Pe/140-1/70),$$

$$C_{SPG}=(2^{12}/3^2)\cdot 0.35.$$

Table 4.1. Coefficients adopted in SPG stabilization functions determination.

The substitution of the analytical solution into Eqs. (4.54) and (4.55), permits to obtain first ζ_{a_2}, ζ_{r_2} and as a consequence ζ_{a_1}, ζ_{r_1}. For the sake of completeness the analytical expressions of the stabilization functions are summarized in Table 4.2.

$$\zeta_{a_2} = \frac{4}{5} r \cdot \frac{\begin{bmatrix} (450+49r)\cdot(aa_2 - aa_1) + \\ +Pe\cdot(241aa_3 + 241aa_4 - 16aa_1 - 16aa_2) \end{bmatrix}}{\begin{bmatrix} (192r+768Pe^2)\cdot(aa_1 + aa_2 - aa_3 - aa_4) + \\ +r^2\cdot(16aa_1 + 16aa_2 + 53aa_3 + 53aa_4) + 552Pe\cdot r\cdot(aa_1 - aa_2) \end{bmatrix}},$$

$$\zeta_{r_2} = 16.875 \cdot \frac{\begin{bmatrix} (40r+160Pe^2)\cdot(aa_1 + aa_2 - aa_3 - aa_4) + \\ +r^2\cdot(4aa_1 + 4aa_2 + aa_3 + aa_4) + 40r\cdot Pe\cdot(aa_1 - aa_2) \end{bmatrix}}{\begin{bmatrix} (192r+768Pe^2)\cdot(aa_1 + aa_2 - aa_3 - aa_4) + \\ +r^2\cdot(16aa_1 + 16aa_2 + 53aa_3 + 53aa_4) + 552Pe\cdot r\cdot(aa_1 - aa_2) \end{bmatrix}},$$

$$aa_1 = e^{Pe+0.5\sqrt{Pe^2+r}},\quad aa_2 = e^{0.5\sqrt{Pe^2+r}},\quad aa_3 = e^{0.5Pe+\sqrt{Pe^2+r}},\quad aa_4 = e^{0.5Pe},$$

$$\begin{aligned}
\zeta_{a_1} = [\, & P_1\cdot(a_6{}^2e_3a_1 + e_5d_8{}^2a_4 - a_6{}^2a_3e_1 - a_5d_8{}^2e_4 + a_6e_5d_8a_1 + a_3a_7e_5d_8 + a_6e_3a_4d_8 - e_3a_7a_5d_8 + \\
& - a_6a_3e_4d_8 - a_6a_5d_8e_1) + P_2\cdot(e_5d_8{}^2a_2 - a_5d_8{}^2e_2 - a_6a_3a_7e_1 + a_1a_7e_5d_8 + a_6e_3a_2d_8 + \\
& - a_5d_8a_7e_1 + a_6e_3a_7a_1 - a_6a_3e_2d_8) + P_3\cdot(-a_6a_3e_2d_8 - a_6a_3a_7e_1 + a_6e_3a_2d_8 + \\
& + a_6e_3a_7a_1 + e_5d_8a_7a_1 - a_5d_8a_7e_1 + e_5d_8{}^2a_2 - a_5d_8{}^2e_2) + P_4\cdot(-e_1a_7{}^2a_3 - a_4d_8{}^2e_2 + \\
& + e_4d_8{}^2a_2 + a_7{}^2e_3a_1 - a_4d_8a_7e_1 - a_7a_3e_2d_8 + e_4d_8a_7a_1 + a_7e_3a_2d_8 - a_6a_1e_2d_8 + \\
& + a_6e_1a_2d_8)] / [\, P_1\cdot(-a_7b_3e_5d_8 - a_6b_1e_5d_8 + b_5d_8a_6e_1 + b_5d_8a_7e_3 - b_4d_8{}^2e_5 + \\
& - a_6{}^2b_1e_3 + b_5d_8{}^2e_4 + a_6{}^2b_3e_1 - b_4d_8a_6e_3 + a_6b_3e_4d_8) + P_2\cdot(a_7b_3a_6e_1 + e_2d_8a_6b_3 + \\
& - a_6b_1a_7e_3 + e_1a_7b_5d_8 - b_1a_7e_5d_8 - b_2d_8{}^2e_5 + e_2d_8{}^2b_5 - b_2d_8a_6e_3) + P_3\cdot(-b_1a_7e_5d_8 + \\
& - a_6b_1a_7e_3 + e_2d_8a_6b_3 + e_1a_7b_5d_8 + a_7b_3a_6e_1 - b_2d_8{}^2e_5 + e_2d_8{}^2b_5 - b_2d_8a_6e_3) + \\
& + P_4\cdot(-b_2d_8a_7e_3 - b_1a_7e_4d_8 + e_2d_8a_7b_3 + e_2d_8a_6b_1 + e_1a_7b_4d_8 - b_2d_8a_6e_1 + \\
& + e_1a_7{}^2b_3 - b_1a_7{}^2e_3 + e_2d_8{}^2b_4 - b_2d_8{}^2e_4)],
\end{aligned}$$

$$\begin{aligned}
\zeta_{r_1} = -[\, & P_1\cdot(-b_4d_8a_6a_3 + b_5d_8a_6a_1 - a_7b_3a_5d_8 - a_6b_1a_5d_8 + b_5d_8a_7a_3 - a_6{}^2b_1a_3 - b_4d_8{}^2a_5 + \\
& + a_6{}^2b_3a_1 + b_5d_8{}^2a_4 + a_6b_3a_4d_8) + P_2\cdot(a_1a_7b_5d_8 - b_1a_7a_5d_8 - b_2d_8a_6a_3 - a_6b_1a_7a_3 + \\
& + a_2d_8a_6b_3 + a_7b_3a_6a_1 - b_2d_8{}^2a_5 + a_2d_8{}^2b_5) + P_3\cdot(a_2d_8{}^2b_5 - b_2d_8{}^2a_5 + a_2d_8a_6b_3 + \\
& - b_2d_8a_6a_3 + a_1a_7b_5d_8 - a_6b_1a_7a_3 - b_1a_7a_5d_8 + a_7b_3a_6a_1) + P_4\cdot(-b_2d_8a_7a_3 + a_2d_8a_6b_1 + \\
& + a_2d_8a_7b_3 - b_1a_7a_4d_8 + a_1a_7b_4d_8 - b_2d_8a_6a_1 + a_1a_7{}^2b_3 - b_1a_7{}^2a_3 - b_2d_8{}^2a_4 + \\
& + a_2d_8{}^2b_4)] / [\, P_1\cdot(-a_7b_3e_5d_8 - a_6b_1e_5d_8 + b_5d_8a_6e_1 + b_5d_8a_7e_3 - b_4d_8{}^2e_5 - a_6{}^2b_1e_3 + \\
& + b_5d_8{}^2e_4 + a_6{}^2b_3e_1 - b_4d_8a_6e_3 + a_6b_3e_4d_8) + P_2\cdot(a_7b_3a_6e_1 + e_2d_8a_6b_3 - a_6b_1a_7e_3 + \\
& + e_1a_7b_5d_8 - b_1a_7e_5d_8 - b_2d_8{}^2e_5 + e_2d_8{}^2b_5 - b_2d_8a_6e_3) + P_3\cdot(-b_1a_7e_5d_8 - a_6b_1a_7e_3 + \\
& + e_2d_8a_6b_3 + e_1a_7b_5d_8 + a_7b_3a_6e_1 - b_2d_8{}^2e_5 + e_2d_8{}^2b_5 - b_2d_8a_6e_3) + P_4\cdot(-b_2d_8a_7e_3 + \\
& - b_1a_7e_4d_8 + e_2d_8a_7b_3 + e_2d_8a_6b_1 + e_1a_7b_4d_8 - b_2d_8a_6e_1 + e_1a_7{}^2b_3 - b_1a_7{}^2e_3 + \\
& + e_2d_8{}^2b_4 - b_2d_8{}^2e_4)],
\end{aligned}$$

$$P_1 = e^{2Pe+\sqrt{Pe^2+r}},\quad P_2 = e^{Pe+2\sqrt{Pe^2+r}},\quad P_3 = e^{Pe},\quad P_4 = e^{\sqrt{Pe^2+r}}.$$

Table 4.2. SPG stabilization functions expressions.

Fig. 4.4 shows the perturbed weight function $\tilde{w}_i$, for one-dimensional quadratic elements in case of null advection with varying stabilization coefficients ζ_{r_i}, both for central and extreme nodes. The weights are plotted for $C_{SPG} = (2^{12}/3^2)\times 0.35$. This value stems from the fulfillment of seven constraints for the P_r perturbation on quadratic elements (e.g. see Corsini et al. (2004b)), including: null nodal values and derivatives, P_r intensity at $\xi = \pm\, l_\xi/4$.

a)

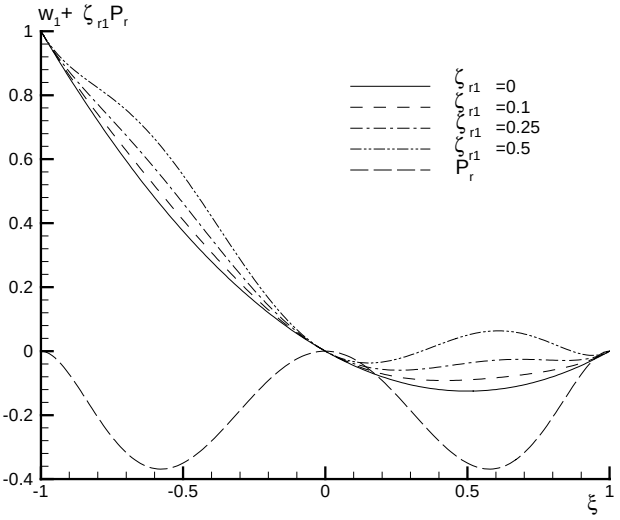

b)

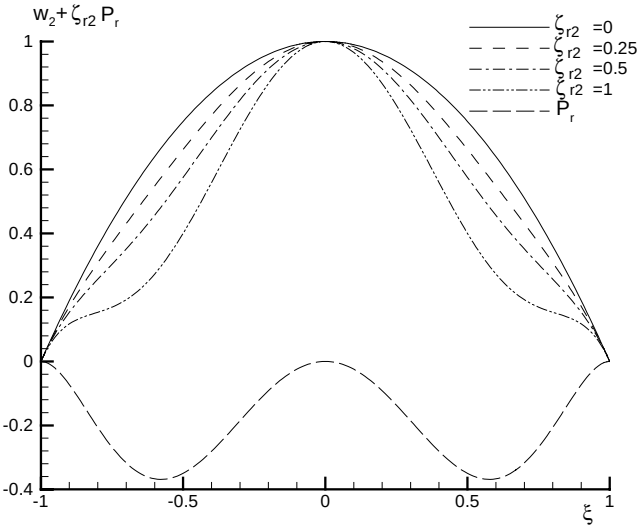

Fig. 4.4. 1-D null advection: resulting weight for a) extreme and b) central node.

Fig. 4.5a shows the behaviours of ζ_{a_i} for different combinations of *Pe* and *r*. Furthermore, Fig. 4.5b shows that of ζ_{r_i} stabilization functions.

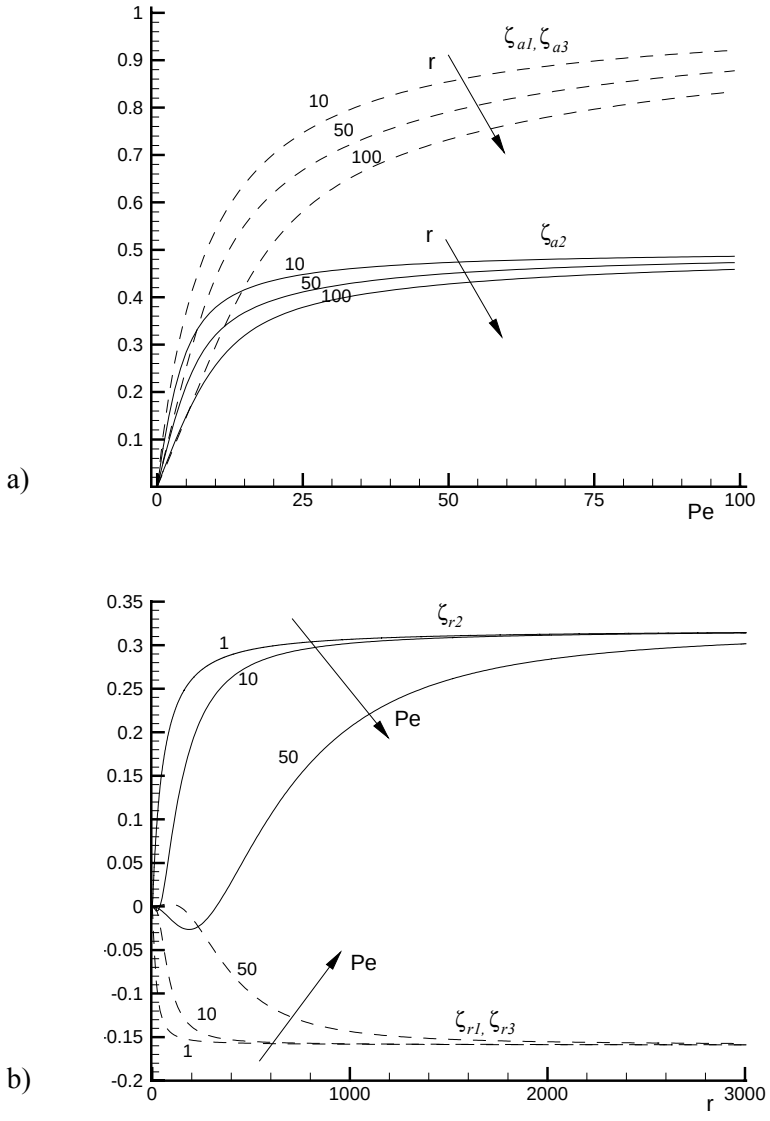

Fig. 4.5. SPG stabilization functions: a) advective and b) reactive controlling.

It is remarkable that the sensitivity to the reactive part of the differential operator gives rise to the stabilization functions ζ_{r_i} and the behaviour of the formulation in the null-reaction limit approaches the SUPG Q2 one proposed by Codina et al. (1992).

The two-dimensional (2D) extension of the P_r function is designed to preserve its 1D requirement, that is the isotropic concentration of the perturbed weight around the nodal positions. To this end, we designed a Cartesian product between the 1D counterparts of the second perturbation function, where the P_r spots are moved in the element portion closer to the corresponding nodes. This concept is depicted in Fig. 4.6 that shows the resulting geometries for the two-dimensional second perturbation functions on logic space. In such a way it is possible to maintain the continuity of the P_r on the inter-element boundary.

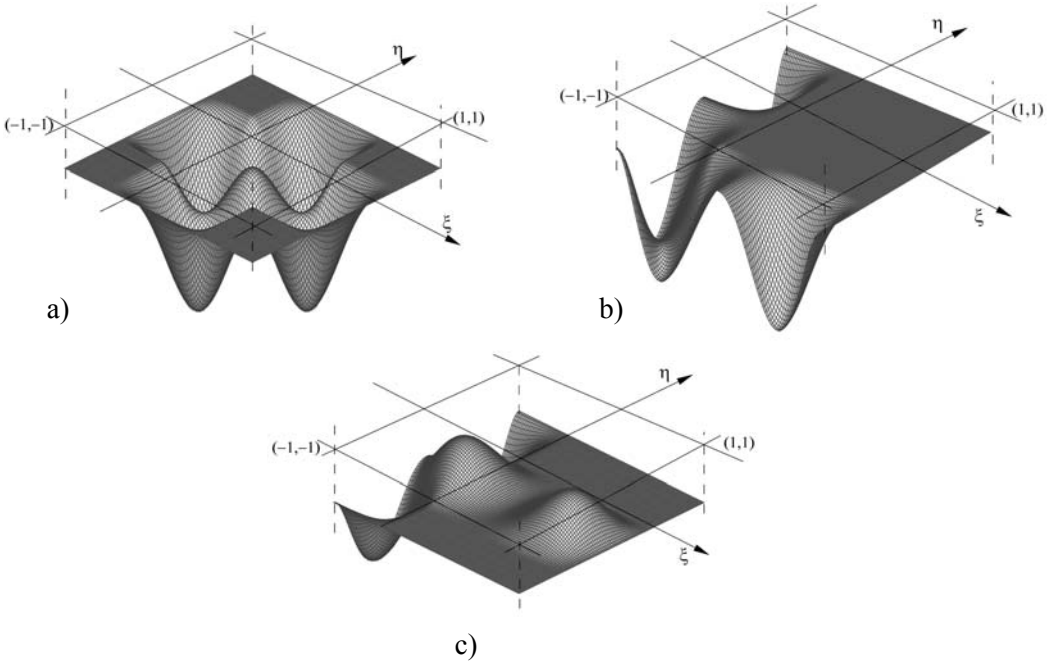

Fig. 4.6. 2D P_r functions in the logic space: a) central-central node (0,0); b) corner node (-1,-1); c) mid-side node (-1,0).

It is worth noting that the 2D stabilization functions ζ_{r_i} are obtained on the basis of a pure positional criterion on logic space. For example, in the case of the mid-side node of Fig. 4.6c the stabilization function is a linear combination of ζ_{r_1} and ζ_{r_2}.

The global formulation of the *SPG/PSPG* stabilized formulation of the RANS system of equations, that could be applied for all the turbulence closures presented in this work, is formally identical to the *SUPG/PSPG* one already proposed, namely:

$$find\ \overline{\boldsymbol{U}}^h \in \boldsymbol{H}^{1h}\ \ \forall \boldsymbol{w}_p^h \in \boldsymbol{W}_p^h,\ \forall w_c^h \in W_c^h,\ such\ that$$

$$c\left(\bar{\boldsymbol{V}}^h, \tilde{\boldsymbol{U}}^h, \boldsymbol{w}^h\right) + s\left(\tilde{\boldsymbol{U}}^h, \boldsymbol{w}^h\right) + r\left(\tilde{\boldsymbol{U}}^h, \boldsymbol{w}^h\right) + \Pi(\boldsymbol{\pi}) = \left(\tilde{\boldsymbol{\mathcal{B}}}, \boldsymbol{w}^h\right) - \left(\boldsymbol{\theta}_N, \boldsymbol{w}^h_{|\Gamma_N}\right)_{\Gamma_N} \quad (4.39)$$

with:

$$\Pi\left(\pi_p\right) = \sum_{e=1}^{nel} \int_{\Omega_e} \left(\mathcal{F}_{a,j} + \mathcal{F}_{d,j} + \mathcal{F}_r - \tilde{\mathcal{B}}\ \right) \pi_p\, d\Omega \quad (4.40a)$$

$$\Pi\left(\pi_c\right) = \sum_{e=1}^{nel} \int_{\Omega_e} \left(\mathcal{F}_{a,j} + \mathcal{F}_{d,j} + \mathcal{F}_r - \tilde{\mathcal{B}}\ \right)^{(M)} \pi_c\, d\Omega \quad (4.40b)$$

where (4.40b) is added to the continuity equation, as described in the *PSPG* Subsection, while for the *primary variables,* (4.40a) represents now the *SPG* contribution, and is defined using this weight:

$$\pi_p = \frac{h}{2\|u\|} \zeta_{ai}(u_k w_{,k}) + \zeta_{r_i} P_{r_i} \quad (4.56)$$

and the stabilization functions must be chosen according to the nature of the node considered.

4.2.4 Gradients and Shocks

PG-like stabilized formulations are able to effectively control advection induced instabilities and, if built-in tools for reaction are included, also reactive features. Notwithstanding they suffer in presence of *sharp solution layers*, as encountered in presence of particular sets of boundary conditions, or in the situations in which the flow is subject to compressibility effects and *shocks* (for an extensive discussion about compressible flows and stabilized finite elements, the reader could consult Saavedra (2004)).

Along discontinuities of the solution fields, the classical stabilized tools do not preclude some phenomena of *overshooting* and *undershooting*, due to their incapability of monotonic representations of sharp layers. In several applications, these oscillatory approximations of abrupt solution zones are not allowed, especially in turbomachinery CFD, and this instance led to some numerical solutions.

4.2.4.1 Discontinuity Capturing

In Hughes and Mallet (1986) and Hughes et al. (1986), a first solution to the problem of controlling sharp solution layers was given. The idea behind their *Discontinuity Capturing* method, was to enrich the numerical dissipation locally where the gradient of the solution is relevant and in the meanwhile the convection dominates on the diffusion. In this way the new term is added only where it is needed, without adding diffusion elsewhere.

The Discontinuity Capturing formulation is a consistent Petrov-Galerkin method that takes its origin from the SUPG, and it could be considered as a complementary part of the SUPG weight perturbation, thus a global perturbation function containing advection, discontinuity and reaction controlling tools, reads as follows:

$$\pi_p = [\frac{h}{2\|u\|}\zeta_{ai}(u_k w_{,k}) + \tau_{DC}(u_{II\,k} w_{,k})] + \zeta_{r_i} P_{r_i} \tag{4.57}$$

where the *Discontinuity Capturing* contribution contains an *intrinsic time scale* that reads as follows:

$$\tau_{DC} = \frac{h_{II}}{2\|u_{II}\|}\zeta_{aiII} \tag{4.58}$$

with

$$h_{II} = \frac{2\|u_{II}\|}{\sum_{a=1}^{nen}|\boldsymbol{u}_{II}\cdot\boldsymbol{\nabla}N_a|} \tag{4.59}$$

which represents an *element characteristic length* in direction of the $\boldsymbol{u}_{II}$ vector, that is the *projection of the streamlines along the solution gradient*, namely:

$$\begin{aligned} \boldsymbol{u}_{II} &= \frac{(\boldsymbol{u}\cdot\boldsymbol{\nabla}U)}{\|\boldsymbol{\nabla}U\|^2}\boldsymbol{\nabla}U \qquad for \qquad \boldsymbol{\nabla}U \neq \boldsymbol{0} \\ \boldsymbol{u}_{II} &= \boldsymbol{0} \qquad\qquad\qquad for \qquad \boldsymbol{\nabla}U = \boldsymbol{0} \end{aligned} \tag{4.60}$$

and a *stabilization function* ζ_{aiII} that has an expression identical to the one proposed for the stabilization function of SUPG, except for the governing parameter, that is the element Peclet number in the direction of the solution gradient, namely:

$$Pe_{II} = \frac{\|\boldsymbol{u}_{II}\| h_{II}}{2k} \tag{4.61}$$

In order to avoid compounding effects (see for example Tezduyar and Park (1986)), the Discontinuity Capturing contribution is reduced of a quantity equal to the SUPG contribution, that must not be doubled:

$$\tau_{DC} = max\left(0, \left(\frac{h_{II}}{2\|u_{II}\|}\zeta_{aiII} - \frac{h}{2\|u\|}\zeta_{ai}\right)\right) \tag{4.62}$$

4.2.4.2 DRD and DRDJ

For reaction dominated problems or when diffusive-reactive conditions appear, due to a vanishing velocity field (i.e. near stagnation points), Tezduyar and Park (1986), and Tezduyar et al. (1987), demonstrated that the presence of sharp solution layers could not be controlled with classical Discontinuity Capturing terms. In these two works, a new stabilizing term was introduced, the so-called *DRD* (*Diffusion* for *Reaction Dominated* problems), that is a second-order term that becomes significant only where reaction rate becomes high, in order to preserve numerical accuracy elsewhere.

The *DRD* method has been obtained for two limit cases of the general CFD problem structure: *convection-reaction* and *diffusion-reaction*. For both cases the analytical expression of the additional second-order term depends on the already introduced dimensionless numbers *r* and *Pe*, and on a dimensionless number that relates the reaction rate to the advection, retaining into account the quality of the grid adopted for the problem discretization. The resulting method for advection-reaction problems in one dimension adds a diffusivity as follows:

$$\tilde{k}_{AR} = \tilde{k}_{AR}(\gamma) = \frac{1}{2}uh(-coth\,\gamma + \gamma(1/sinh^2\,\gamma + 4r_{int})) \tag{4.63}$$

with

$$\gamma = \frac{1}{2}hc/u \tag{4.64}$$

and r_{int} is determined by the integration rule used for the element coefficient matrix corresponding to the reaction term (e.g. r_{int} equal to *1/6* for two point Gaussian quadrature).

The multi-dimensional extension is obtained by defining a numerical diffusivity tensor as follows:

$$\tilde{\boldsymbol{K}} = \tilde{k}_{AR}(\gamma)\boldsymbol{ss} + \tilde{k}_{AR}(\infty)(\boldsymbol{tt} + \boldsymbol{vv}) \tag{4.65}$$

where $\boldsymbol{s}$ is the unit vector in direction of the streamlines, $\boldsymbol{t}$ and $\boldsymbol{v}$ are two unit vectors orthogonal to $\boldsymbol{s}$ and each other, and (4.64) must be re-calculated with $\|\boldsymbol{u}\|$ instead of u. The chosen definition of the element characteristic length h is equal to h_{UGN} (i.e. the one contained in (4.34)).

In the diffusion-reaction limit the additional diffusive term reads like this:

$$\tilde{k}_{DR} = \tilde{k}_{DR}(\beta) = c(h/2)^2(4r_{int} + 1/sinh^2\beta - 1/\beta^2)) \tag{4.66}$$

where

$$\beta^2 = (c/k)(h/2)^2 \tag{4.67}$$

and the element characteristic length h is equal to h_{RGN} (i.e. the one contained in (4.35)). Both the expressions obtained for the additional diffusion share the same limit for pure reaction, namely:

$$\tilde{k}_{AR}(\infty) = \tilde{k}_{DR}(\infty) = 4r_{int}c(h/2)^2 \tag{4.68}$$

The DRD method is thus a very useful stabilization for situations in which classical Discontinuity Capturing terms are not able to work, and is well suited for Petrov-Galerkin formulations. Notwithstanding, it is not-consistent, and starting from these considerations, a new DRD concept has been recently developed in Corsini et al. (2005c), based not only on the reaction rate but also on the solution gradient, turning to a *DRD-like Discontinuity Capturing technique,* named *DRDJ* (*Diffusion* for *Reaction Dominated* problems with *Jump* factor).

The *DRDJ* additional diffusivities read as follows:

$$\tilde{k}_{AR} = \tilde{k}_{AR}(\gamma, J_e) = \frac{1}{2}uh_{UGN}J_e(-coth\gamma + \gamma(1/sinh^2\gamma + 4r_{int})) \tag{4.69a}$$

$$\tilde{k}_{DR} = \tilde{k}_{DR}(\beta, J_e) = c(h_{RGN}/2)^2 J_e(4r_{int} + 1/sinh^2\beta - 1/\beta^2)) \tag{4.69b}$$

where J_e is a normalized measure of the solution gradient intensity across each element e, that reads as:

$$J_e = \frac{|U_{max} - U_{min}|_e}{\|U\|_e} \tag{4.70}$$

with all the operators defined considering only a local point of view. In particular $\|U\|_e$ represents the local norm of the unknown, equal to a global scaling U for model problems, characterized by only one scale of the solution. On the contrary, turbulent variables are characterized by different orders of magnitude for different zones of the flow field, thus for turbulence computations $\|U\|_e$ must take into account the local features of the problem and has been chosen equal to the maximum value of the unknown into the element. With such a choice, that has been used for the calculations presented in the next Chapters, it is possible to assure that J_e ranges from *0* to *1*, thus leading to a diffusivity that is everywhere limited.

The resulting *DRDJ* could be generalized to a multi-dimensional diffusivity tensor:

$$\tilde{\boldsymbol{K}} = \tilde{k}_{AR}(\gamma, J_e)\boldsymbol{ss} + \tilde{k}_{DR}(\beta, J_e)(\boldsymbol{tt} + \boldsymbol{vv}) \tag{4.71}$$

It is worthwhile noting that along the ***t*** and ***v*** direction the additional diffusion is the one associated to a generic diffusion-reaction one-dimensional operator. For this reason, the element characteristic length measure is provided by the h_{RGN} defined with (4.35), as done in (4.69b).

Finally, as a conclusive remark that ensure the flexibility of *DRDJ*, it is remarkable that the typical structure of differential equations modeling the turbulence closure variables is convection-diffusion-reaction, but it is not unusual to find also diffusion-reaction equations modeling elliptic parameters, such as $\tilde{f}$ in the k-ε-v^2-f . For these situations the *DRDJ* expression is the following:

$$\tilde{\boldsymbol{K}} = \tilde{k}_{DR}(\beta, J_e)(\boldsymbol{tt} + \boldsymbol{vv} + \boldsymbol{zz}) \tag{4.72}$$

where **t**, **v** and **z** define a three-dimensional system of orthogonal axes.

4.3 Variational MultiScale approach to stabilization

Recently, a new route to build-up residual based stabilized formulations has been suggested on the basis of the *Variational MultiScale (VMS)* method, first proposed by Hughes (1995). This approach permits to obtain formulations with a more attractive mathematical background (i.e. see Roach (1970), or Oberai and Pinski (1998)), the so-called *sub-grid scale models (SGS)* able to deal with *multiscale phenomena* and to give a theoretical foundation of stabilized methods. The idea that lays behind the VMS methods is to obtain a residual based stabilization technique by computing analytically the effects of fine or sub-grid scale solution on the resolvable one by means of element residuals (Hughes (1995)). Brezzi et al. (1997) demonstrated the equivalence of the *RFB* (presented in several works, such as Brezzi et al. (1998)) and *VMS* approaches under certain hypotheses.

It is a matter of fact that fine scale structures, which are smaller than the characteristic length of the assigned grid and whose influence on coarse scales must be accounted for, can be captured by a classical Galerkin formulation only after a strong refinement of the mesh, that can quickly overload the computational resources. The SGS modeling strategy consists in obtaining a stabilization technique by computing the effect of the fine scale solution (i.e. the error in the coarse-scale solution) on the resolvable one by means of element residuals, without refining the mesh. The key ingredient of a VMS formulation is the design of the intrinsic time scale parameter τ, that appears in the stabilization integral containing the coarse scales residual.

In order to have an insight of the general approach followed in the VMS framework (well described in Hauke (2002)), let introduce the linear advection-diffusion-reaction operator L, and its adjoint operator L^*, acting on the scalar unknown variable U, that could represent one of the variables of the RANS problem:

$$\begin{aligned} LU &= F_a(U)_{,j} + F_d(U)_{,j} + F_r(U) \\ L^*U &= -F_a(U)_{,j} + F_d(U)_{,j} + F_r(U) \end{aligned} \tag{4.73}$$

The problem statement (4.13) can be thus recast in a compact form that reads as:

$$\begin{aligned} &LU = B \\ &U = U_D \qquad on \quad \Gamma \end{aligned} \tag{4.74}$$

Now let recall some of the already introduced notation: consider $S \subset H^1(\Omega)$ as the trial solution space and $W \subset H^1(\Omega)$ as the weighting function space, where $H^1(\Omega)$ is the Sobolev space of square integrable functions with square integrable derivatives.

The *variational formulation* of the problem could be written as:

$$\begin{aligned} &find\ U \in S\ \ such\ that\ \forall w \in W \\ &a(w,U) = (w,B) \end{aligned} \tag{4.75}$$

where $(\cdot,\cdot)$ is the $L_2(\Omega)$ inner product, and $a(\cdot,\cdot)$ is a bilinear form satisfying the following identity:

$$a(w,U) = (w,LU) \tag{4.76}$$

for all sufficiently smooth $w \in W, U \in S$.

Given a finite element partition of the domain, as defined in Chapter 1 (for a systematic approach the reader could consult Corsini et al. (2005a)), the Galerkin formulation of the boundary-value problem (4.74) could be written as follows:

$$find\ U^h \in S^h\ \ such\ that\ \forall w^h \in W^h$$

$$a(w^h, U^h) = (w^h, B) \tag{4.77}$$

It must be recalled that S^h and W^h are discrete finite-dimensional subsets of *S* and *W,* unable to capture the fine scales of the solution, characterized by structures which are smaller than the grid-spacing used for the discretization of the problem.

The sum decomposition of the solution $U = U^h + U'$ permits to distinguish the resolvable or coarse scales U^h and the unresolvable or fine or subgrid scales U', and in a Galerkin sense the same decomposition is applicable to the weight functions $w = w^h + w'$ (Corsini et al. (2004c)). By that way the *VMS* approach is aimed at solving a problem for U' and calculating the effect of the fine scales on the resolvable ones by means of their elimination in a variational sub-grid problem, as first proposed in Hughes (1995).

Let re-write the variational formulation (4.75) in terms of the decomposition in coarse and fine scales as:

$$a(w^h + w', U^h + U') = (w^h + w', B) \qquad \forall w^h \in W^h, w' \in W' \tag{4.78}$$

By means of the linear independence of w^h and w' (Hughes et al. (1998)), the formulation (4.78) splits into two sub-problems that, due to the linearity of the *L* differential operator, read as:

for the *coarse scales*

$$a(w^h, U^h) + a(w^h, U') = (w^h, B) \qquad \forall w^h \in W^h \tag{4.79}$$

and for the *sub-grid scales*

$$a(w', U^h) + a(w', U') = (w', B) \qquad \forall w' \in W' \tag{4.80}$$

This second sub-problem must be solved in terms of U' in order to describe the effect of fine scales on the coarse ones.

Let now make the quite strong assumption that subgrid scales vanish on element boundaries:

$$U' = 0 \qquad \text{on} \quad \Gamma_e \qquad e = 1,....,nel \tag{4.81}$$

Eq.(4.81) represents a widespread hypothesis in stabilized finite elements framework (e.g. Hughes (1995), Hauke and Garcia-Olivares (2001)), that avoids cumbersome mathematics, and means that unresolved scales could exert their influence in the limit of the coarse grid space discretization, thus reducing *non-locality* into individual elements. Hypothesis (4.81) thus discards the effect of fine scales pertaining to other elements onto the coarse ones of the element under consideration. This corresponds with the solution on each element domain of a problem, whose *Euler-Lagrange* equations read now as:

$$LU' = -(LU^h - B) \quad \text{in } \Omega_e \tag{4.82a}$$

$$U' = 0 \quad \text{on} \quad \Gamma_e \qquad e = 1,....,nel \tag{4.82b}$$

As proposed in Hughes (1995), Eq. (4.82) could be tackled introducing the element Green's function problem (for a complete theory of Green's function the reader could consult the book by Roach (1970) or the more recent one from Kythe et al. (2003)) that reads as:

$$L^* g_e(x,y) = \delta(x,y) \qquad \text{in } \Omega_e \tag{4.83a}$$

$$g_e = 0 \quad \text{on} \quad \Gamma_e \qquad e = 1,....,nel \tag{4.83b}$$

The element Green's function permits to obtain the following coarse scales residual dependent expression for the fine scales:

$$U'(y) = -\int_{\Omega_e} g_e(x,y)(LU^h - B)(x)d\Omega_x \qquad \forall y \in \Omega_e \tag{4.84}$$

The contribution of unresolved scales could be now substituted in the problem for coarse scales and by means of successive integrations by parts (Hughes et al. (1998)) reads as:

$$a(w^h, U') = (w^h, LU') = \sum_{e=1}^{nel} \int_{\Omega_e} w^h \cdot LU' d\Omega_e = \sum_{e=1}^{nel} \int_{\Omega_e} L^* w^h \cdot U' d\Omega_e \tag{4.85}$$

Substituting (4.85) into the coarse-scales problem, it turns to a *subgrid scales (SGS) model*:

$$a\left(w^h,U^h\right)-\sum_{e=1}^{nel}\int_{\Omega_e} L^* w^h(y)\int_{\Omega_e} g_e(x,y)(LU^h-B)(x)d\Omega_x d\Omega_y = \\ =\left(w^h,B\right) \qquad \forall w^h\in W^h \tag{4.86}$$

As remarkably noted in Corsini et al. (2005a), the obtained formulation contains an *alternative consistent technique* to build-up the residual stabilization term with respect to classical Petrov-Galerkin formulations, which in view of the introduced notations generally read as:

$$find\ U^h\in S^h\ \ such\ that\ \forall w^h\in W^h$$

$$a(w^h,U^h)+(\pi,LU^h-B)=(w^h,B) \tag{4.87}$$

A *Variational MultiScale* (or *SGS*) stabilized formulation models in a different way the residual term, by means of an adjoint based operator $(L^* w^h,U')$, that plays the role of the PG stabilization term (π,LU^h-B). The distinctive feature of each particular *SGS* method lays on the choice of a suitable approximated expression for the coarse scales residual based integral operator containing the element Green's function.

4.3.1 V-SGS formulation

The open literature usually features *adjoint-type stabilized methods* where the subgrid scales are approximated by an *intrinsic time scale* parameter τ that weights the coarse scales residual. The review of recent research papers shows that most of the proposed formulations work with element-wise constant definition of τ, either computed as average value of the exact element Green's function (i.e. see Hauke and Garcia-Olivares (2001)), or as classical in the Petrov-Galerkin context in terms of local length and velocity scales (Codina (2001)). Few works propose definitions tuned in order to fulfil the *Discrete Maximum Principle* (e.g. see Franca and Valentin (2001)). In this viewpoint *bubble function* based formulations constitute a vital background for the design of more accurate intrinsic time scale parameters, though their application is limited only to advective-diffusive problems (Brezzi et al. (1998)), or to linear elements (Franca and Fahrat (1995)).

With respect to the presented state-of-the-art, in Corsini et al. (2004c) and (2005a), an alternative residual based SGS stabilization technique, called *V-SGS* (*Variable - SubGrid Scale*) has been developed by the team at "La Sapienza" for second-order interpolation spaces, often applied in CFD near wall turbulence modelling. The use of higher order finite element spaces has been already justified in the preceding Sections, following the argumentations in Borello et al. (2003). In particular the use of the Q2Q1 element has been addressed, in which the *space-dependence of stabilization parameters* needs to be exploited. This feature has been a driving criterion in the design of the proposed SGS model, that here is shortly described.

The presented *V-SGS* formulation admits the following definition for the element Green's function:

$$g_e(x,y) = \tau^{V-SGS}(x)\delta(x,y) \tag{4.88}$$

where the *error distributor* is described by a function product including the *Dirac's delta* and a space-dependent intrinsic time scale parameter τ^{V-SGS}. On this basis the sub-grid scales could be modeled as:

$$U'(y) = -\int_{\Omega_e} g_e(x,y)(LU^h - B)(x)d\Omega_x = -\tau^{V-SGS}(y)(LU^h - B)(y) \tag{4.89}$$

where the time scale $\tau^{V-SGS}(y)$ is computed by the exact integration over each element of $g_e(x,y)$ as:

$$\tau^{V-SGS}(y) = \int_{\Omega_e} \tau^{V-SGS}(x)\delta(x,y)d\Omega_x = \int_{\Omega_e} g_e(x,y)d\Omega_x \tag{4.90}$$

It should be noted that the above $\tau^{V-SGS}(y)$ definition grants a-priori the suitability of the proposed approach for high order finite element interpolation spaces, such as quadratic ones. As a result of the proposed *V-SGS model*, the stabilization integral becomes:

$$\begin{aligned}&(w^h, LU^h - B) = (L^* w^h, U') = \\ &= -\sum_{e=1}^{nel} \int_{\Omega_e} L^* w^h(y)\tau^{V-SGS}(y)(LU^h - B)(y)d\Omega_y\end{aligned} \tag{4.91}$$

It is interesting to give more hints on the determination of $\tau^{V-SGS}(y)$, because it reveals to be a quite simple operation with meaningful results. To this end, let use a one-dimensional advective-diffusive-reactive model problem with constant physical properties. In this configuration the adjoint problem for the element Green's function reads as:

$$-kg_{e,xx} - ug_{e,x} + cg_e = \delta(x,y) \qquad \text{in } \Omega_e \tag{4.92a}$$

$$g_e = 0 \qquad \text{on} \qquad \Gamma_e \qquad e = 1,....,nel \tag{4.92b}$$

For both linear and quadratic isoparametric finite elements, the above problem could be reformulated in element parent domain taking into account the invariance of the properties of the Dirac's delta in the coordinate transformation (Roach (1970)):

$$-\left(\frac{2}{h}\right)^2 k g_{e,\xi\xi} - \left(\frac{2}{h}\right) u g_{e,\xi} + c g_e = \left(\frac{2}{h}\right)\delta(\xi,\zeta) \qquad \xi,\zeta \in (-1,1) \tag{4.93a}$$

$$\begin{aligned} g_e(-1,\zeta) &= 0 \\ g_e(+1,\zeta) &= 0 \end{aligned} \tag{4.93b}$$

here ζ is the auxiliary Dirac's delta space variable. The related element Green's function is found to have an exponential behaviour:

$$\begin{aligned} g_e(\xi,\zeta) &= C_1 e^{\lambda_1 \xi} + C_2 e^{\lambda_2 \xi} \qquad -1 \le \xi \le \zeta \\ g_e(\xi,\zeta) &= C_3 e^{\lambda_1 \xi} + C_4 e^{\lambda_2 \xi} \qquad \zeta < \xi \le +1 \end{aligned} \tag{4.94}$$

where λ_1 and λ_2 are the roots of the characteristic equation associated to problem (4.93). The four closure constants are determined by imposing on g_e the homogeneous boundary values, the continuity in ζ and the value of its first derivative jump in ζ, defined as in Kythe et al. (2003):

$$g_{e,\xi}(\zeta^+,\zeta) - g_{e,\xi}(\zeta^-,\zeta) = -\left(\frac{h}{2k}\right) \tag{4.95}$$

where the g_e first derivative discontinuity is related to the element length and to the diffusivity.

In Fig. 4.7 the behaviour of element Green's function is shown for a one-dimensional logic element focusing on the effect of *Pe* and *r* magnitudes, with ζ set equal to zero, $h = 10^{-1}$ and $k = 10^{-4}$.

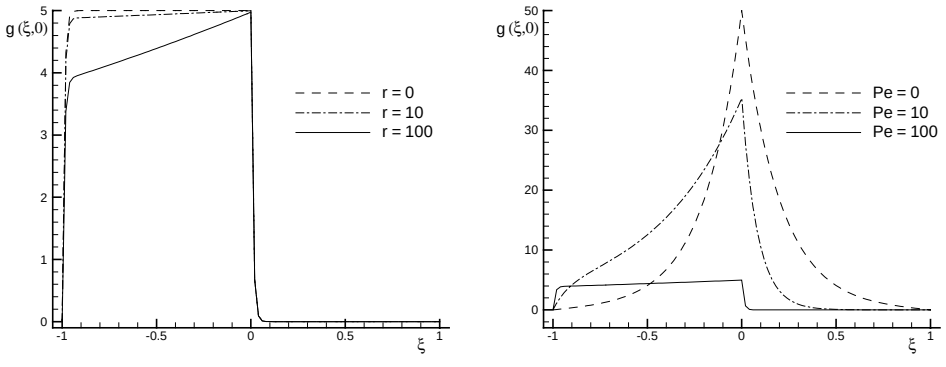

a) b)

Fig. 4.7. Element Green's function: a) *Pe =100*, varying *r*, b) *r=100*, varying Pe.

It is worth noting that $g_e(\xi, 0)$ modulates the element error distributor mechanism moving from advection dominated limit ($r \rightarrow 0$), where it behaves like an *upwind Heaviside* function, to reaction dominated condition where it approaches a symmetric impulsive-like shape (Corsini et al. (2005a)).

By expressing the integral time scale using the element Green's function, a fundamental feature of the proposed *V-SGS model* becomes evident:

$$\begin{aligned} \tau^{V-SGS}(y) &= \int_{\Omega_e} \tau^{V-SGS}(x)\delta(x,y)d\Omega_x = \\ &= \int_{\Omega_e} g_e(x,y)d\Omega_x = \int_{-1}^{+1} g_e(\xi,\zeta)(\det J)d\xi \end{aligned} \tag{4.96}$$

and in the above integral the Jacobian determinant is defined:

$$\det J = \left(\frac{h}{2}\right) \tag{4.97}$$

It could be thus inferred that the *V-SGS formulation* does not depend on the choice between quadratic or linear finite elements, thus being suitable for both these types of formulation. In this viewpoint, it must be recalled that one of the most remarkable criticisms on the use of a element-wise constant τ lays on its ability to control only element-wise constant residuals, that are obtained on advective-diffusive problems with linear elements (Hughes et al. (1998)). If reactive terms appear and/or high order elements are used, there is no agreement between a constant stabilizing parameter and a variable residual, thus addressing the need for a space dependent τ, as pursued by the designed τ^{V-SGS}.

Another important feature of the proposed formula τ^{V-SGS} is its *bubble behaviour*, that permits to eliminate the inter-element integrals related to the properties of the trial and test function spaces used, thus allowing integration by parts for the diffusive term in the residual based operator. In order to show these properties it is worthwhile considering Table 4.3, where the τ^{V-SGS} expression in master element coordinates for the different combinations of reactive and advective effects is shown.

r=0	$\tau^{V-SGS}(\xi)=\tau_{SC}^{avdf}\left[1+\left(\frac{u}{\|u\|}\xi-\frac{e^{\frac{u}{\|u\|}Pe\xi}}{sinh(Pe)}+\frac{1}{Pe}\right)\Big/\left(coth(Pe)-1/Pe\right)\right],$ $\tau_{SC}^{avdf}=\tau^{SUPG}=\frac{h}{2\|u\|}\left(coth(Pe)-1/Pe\right)$
Pe=0	$\tau^{V-SGS}(\xi)=\tau_{SC}^{dfrt}\cdot$ $\cdot\left[1+\frac{\left(-e^{-(\sqrt{r}/2)(1+\xi)}+e^{-\sqrt{r}-(\sqrt{r}/2)(1-\xi)}+e^{-\sqrt{r}-(\sqrt{r}/2)(1+\xi)}-e^{-(\sqrt{r}/2)(1-\xi)}+\frac{2}{\sqrt{r}}\left(1-e^{-\sqrt{r}}\right)^2\right)}{\left(1-e^{-2\sqrt{r}}-\frac{2}{\sqrt{r}}\left(1-e^{-\sqrt{r}}\right)^2\right)}\right],$ $\tau_{SC}^{dfrt}=\frac{1}{c}\left(1-\frac{2\left(1-e^{-\sqrt{r}}\right)^2}{\sqrt{r}\left(1-e^{-2\sqrt{r}}\right)}\right)$
r,Pe≠0	$\tau^{V-SGS}(\xi)=\tau_{SC}^{avdfrt}\cdot$ $\cdot\left[\begin{array}{l}1+A_1^{avdfrt}\Big/A_3^{avdfrt}\left(-e^{-\lambda_2(1+\xi)}+e^{-\lambda_1(1+\xi)-2(\lambda_2-\lambda_1)}+e^{\lambda_2(1-\xi)-2(\lambda_2-\lambda_1)}-e^{\lambda_1(1-\xi)}\right)+\\ +A_2^{avdfrt}\Big/A_3^{avdfrt}\left(e^{-\lambda_2(1+\xi)}-e^{-\lambda_1(1+\xi)-2(\lambda_2-\lambda_1)}-e^{\lambda_2(1-\xi)-2(\lambda_2-\lambda_1)}+e^{\lambda_1(1-\xi)}\right)+\\ -8(1+r/Pe^2)\Big/A_3^{avdfrt}(coth(\lambda_1)-coth(\lambda_2))r^2/Pe^3\end{array}\right]$ $\tau_{SC}^{avdfrt}=\frac{h}{\|u\|}2\frac{Pe}{r}\left[1+4\frac{Pe}{r}\frac{\sqrt{1+r/Pe^2}}{(coth(\lambda_1)-coth(\lambda_2))}\right],$ $A_1^{avdfrt}=\frac{1}{(-sgn(u)-\sqrt{1+r/Pe^2})(e^{-2(\lambda_2-\lambda_1)}-1)},$ $A_2^{avdfrt}=\frac{1}{(-sgn(u)+\sqrt{1+r/Pe^2})(e^{-2(\lambda_2-\lambda_1)}-1)},$ $A_3^{avdfrt}=2\frac{\sqrt{1+r/Pe^2}}{r/Pe^2}\left[1+4\frac{Pe}{r}\frac{\sqrt{1+r/Pe^2}}{(coth(\lambda_1)-coth(\lambda_2))}\right]$

Table 4.3. One-dimensional intrinsic time scale parameter τ^{V-SGS}.

It is remarkable that in each examined case, τ^{V-SGS} could be decomposed in the product between a scaling factor, namely τ_{SC}^{case}, which represents the average value of the parameter, and a function which gives the space dependence. Moreover in the advective-diffusive limit (*r=0*), the scaling factor τ_{SC}^{avdf} is exactly the τ^{SUPG} intrinsic time scale parameter, according to the general concept that the origin of classical stabilized

formulations is related to the general Variational MultiScale approach (i.e. see Hughes (1995)).

In order to clarify all these aspects, Fig. 4.8 shows the bubble-like behavior of τ^{V-SGS} for $h = 10^{-1}$, $k = 10^{-4}$, and various combinations of advection and reaction effects. It is noticeable that the proposed intrinsic time scale exploits a relevant space-dependence with respect to its average value, adding a sensitisation to the "*wind direction"*, extremely important in advection dominated situations.

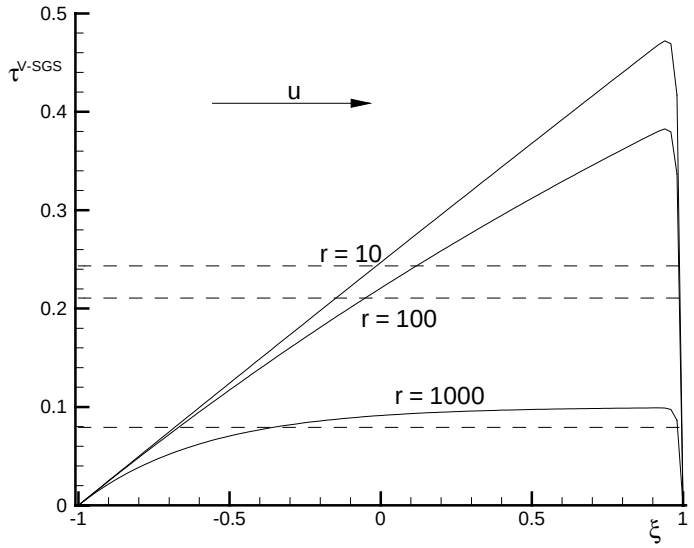

Fig. 4.8. $\tau^{V\text{-}SGS}$ for advection-diffusion-reaction with *Pe=100* . Dashed lines: τ_{SC}^{avdfrt} .

The multi-dimensional formulation of the proposed stabilized method must face the difficulties arising in the treatment of the multi-dimensional integral of element Green's functions in case of advective-diffusive-reactive problem (Kythe et al. (2003)). This forces the definition of the *V-SGS model* for *nsd > 1* on the basis of a multi-dimensional generalization of the time scale τ^{V-SGS}. The proposed method combines the 1D intrinsic time scale parameters computed from the element Green's functions associated to each parent domain coordinate direction. In the 2D case, we solve the Green's function problem for ξ and η directions, which differ due to the velocity components magnitudes that unbalance the advective phenomena on the parent domain. On the basis of the *directional Peclet numbers* the time scale is:

$$\tau_{\xi_i}^{V-SGS}(x,y)=\tau_{\xi_i}^{V-SGS}\left(\xi_i(x,y)\right)=\int_{-1}^{+1} g_e(\zeta,\xi_i)(\det J)d\zeta=$$
$$=\tau_{SC_{\xi_i}}^{V-SGS}\cdot\left(1+f_{\xi_i}\left(\xi_i,Pe_{\xi_i},r\right)\right) \tag{4.98}$$

The two directional intrinsic time scales, namely $\tau_{\xi}^{V-SGS},\tau_{\eta}^{V-SGS}$, computed in each element node must be composed in order to obtain the τ^{V-SGS} to be used for the sub-grid scales contribution. In this respect, the composing criterion, aimed to both a correct scale evaluation of the resulting stabilizing parameter and a simple extension to three-dimensional problems, consists in using the following combination between the directional τ_{ξ}^{V-SGS} and τ_{η}^{V-SGS}:

$$\tau^{V-SGS}(x,y)=\left(\frac{1}{(\tau_{SC}^{V-SGS})_{\xi}^{r_s}}+\frac{1}{(\tau_{SC}^{V-SGS})_{\eta}^{r_s}}\right)^{-\frac{1}{r_s}}\cdot\left(1+f_{\xi}\left(\xi,Pe_{\xi},r\right)\right)\cdot\left(1+f_{\eta}\left(\eta,Pe_{\eta},r\right)\right) \tag{4.99}$$

where an *r-switch combination*, with an integer exponent r_s of tuning (i.e. see Tezduyar (2003)) has been employed for controlling the multi-dimensional scaling factor.

The *V-SGS/PSPG stabilized formulation* of the RANS problem is formally very similar to the *SUPG/PSPG* and *SPG/PSPG* already proposed, because it includes only a new expression of the stabilization integral, reading as:

$$find\ \overline{\boldsymbol{U}}^h\in\boldsymbol{H}^{1h}\ \ \forall\boldsymbol{w}_p^h\in\boldsymbol{W}_p^h,\ \forall w_c^h\in W_c^h,\ such\ that$$

$$c\left(\overline{\boldsymbol{V}}^h,\tilde{\boldsymbol{U}}^h,\boldsymbol{w}^h\right)+s\left(\tilde{\boldsymbol{U}}^h,\boldsymbol{w}^h\right)+r\left(\tilde{\boldsymbol{U}}^h,\boldsymbol{w}^h\right)+\Pi\left((\tilde{\boldsymbol{U}}^h,\tilde{\boldsymbol{\mathcal{B}}}),\boldsymbol{\pi}\right)=\left(\tilde{\boldsymbol{\mathcal{B}}},\boldsymbol{w}^h\right)-\left(\boldsymbol{\theta}_N,\boldsymbol{w}^h_{|\Gamma_N}\right)_{\Gamma_N} \tag{4.100}$$

where the PSPG contribution remains the same (i.e. formula (4.40b)), while the components of the stabilization integral related to primary variables are now defined as:

$$\Pi\left((\tilde{\boldsymbol{U}}^h,\tilde{\boldsymbol{\mathcal{B}}}),\boldsymbol{\pi}\right)=\sum_{e=1}^{nel}\int_{\Omega_e}\left[\boldsymbol{\pi}\cdot\left(\boldsymbol{\mathcal{F}}_{a,j}^h+\boldsymbol{\mathcal{F}}_r^h-\tilde{\boldsymbol{\mathcal{B}}}\right)-\boldsymbol{\pi}_{,j}\cdot\boldsymbol{\mathcal{F}}_d^h\right]d\Omega \tag{4.101}$$

where the stabilizing diffusive contributions have been integrated by parts according to the bubble nature of intrinsic time scale parameters, and each of the components of the $\boldsymbol{\pi}$ vector is obtained, according to (4.87) and (4.91), as a product between the intrinsic time

scale for the considered primary variable and the adjoint operator acting on the weight, which reads as:

$$L^* w_p^h = -\mathcal{F}_a(w_p^h)_{,j} + \mathcal{F}_d(w_p^h)_{,j} + \mathcal{F}_r(w_p^h) \tag{4.102}$$

4.3.2 V-SGS + DRDJ and the influence of stabilization in turbulence modeling

The *VMS (Variational MultiScale)* method has opened new perspectives on the stabilization techniques nature or origin, revealing some fundamental relationships between subgrid scales formulations and turbulence modeling (i.e. see Hughes et al. (2000)). The most fascinating theme related to this new research issue is the fact that a model for the subgrid scales could be seen also as a sort of *non-linear turbulence model*, because it is a window opened on what happens into each element of the grid discretization.

On the stabilization point of view, the VMS approach introduces additional features with respect to classical tools, but as shown in Hauke (2002), there is still lack of stability in presence of high reaction associated with sharp solution layers, thus addressing a shock capturing mechanism for this kind of problems.

Starting from these considerations, the already introduced *DRDJ* method has been developed in Corsini et al. (2005c), based not only on the reaction rate but also on the solution gradient, turning to a *DRD-like Discontinuity Capturing* technique, able to improve the performance of existing stabilized formulations, both in a Petrov-Galerkin and in a Variational Multiscale finite elements context. The main scope of this research has been to demonstrate which is the influence of a stabilized formulation with a SGS contribution not only in *computing*, but also in *modeling* turbulence, with particular interest in the flow features appearing in turbomachinery CFD. To this end, the *DRDJ* has been employed within the *V-SGS/PSPG stabilized finite element method*, and after some tests on scalar model problems, the final *V-SGS+DRDJ* formulation has been applied for the study of a complex three-dimensional turbomachinery flow (i.e. a compressor cascade), that will be presented in the last Chapter of this work.

The idea of adopting a stabilized finite element formulation as a contribution to turbulence modeling could be found in the recent works by Tezduyar (2001, 2003) and Rispoli et al. (2005), where the *low-frequency pass filtering* properties of stabilization techniques are shown, and the role and importance of each of the parameters that define a stabilized formulation are emphasized, in the more general framework of *implicit numerical filters* to the Navier-Stokes equations. In the RANS context, these arguments lead to interpret the VMS approach (given its pure numerical effect of stabilizing tool) as a sensitization tool for the adopted turbulence closure, that enables it to be influenced by certain parameters that govern the more complex aspects of the flow behavior, such as *transition* and *separation*.

References

Akin J. E. and Tezduyar T. E., "Calculation of the Advective Limit of the SUPG Stabilization Parameter for Linear and Higher-Order Elements", *Computer Methods in Applied Mechanics and Engineering*, v. 193, pp. 1909-1922, (2004).

Babuska I., "Error bounds for finite element method", *Numer. Math.*, v. 16, pp. 322-333, (1971).

Borello D., Corsini A. and Rispoli F., "A finite element overlapping scheme for turbomachinery flows on parallel platforms", *Computers and Fluids*, v. 32/7, pp. 1017-1047, (2003).

Brezzi F., "On the existence, uniqueness and approximation of saddle point problems arising from Lagrange multipliers", *RAIRO, Ser. Rouge Anal. Numer.*, v. 8 R-2, (1976).

Brezzi F., Franca L. P., Hughes T. J. R., Russo A., "b=$\int g$", *Computer Methods in Applied Mechanics and Engineering*, v. 145 pp. 329-339, (1997).

Brezzi F., Marini D., Russo A., "Applications of the pseudo residual-free bubbles to the stabilization of convection-diffusion problems", *Computer Methods in Applied Mechanics and Engineering*, v. 166, pp. 51-63, (1998).

Codina, R., "A stabilized finite element method for generalized stationary incompressible flows", *Computer Methods in Applied Mechanics and Engineering*, v. 190, pp. 2681-2706, (2001).

Codina R. and Soto O., "Finite element solution of the Stokes problem with dominating Coriolis force", *Computer Methods in Applied Mechanics and Engineering*, v. 142, pp. 215-234, (1997).

Codina R., Oñate, E., Cervera, M., "The intrinsic time for the streamline upwind/Petrov-Galerkin formulation using quadratic elements", *Computer Methods in Applied Mechanics and Engineering*, v. 94, pp. 239-262, (1992).

Corsini A., Rispoli F., Santoriello A., "A new stabilized finite element method for advection-diffusion-reaction equations using quadratic elements", *in: T. Lajos, J. Vad, ed., CMFF'03 Conference Proceedings Vol.2 (Department of Fluid Mechanics, Budapest University of Technology and Economics),* pp. 791-799, (2003).

Corsini A., Rispoli F., Santoriello A., "A New Stabilized Finite Element Method for Advection-Diffusion-Reaction Equations using Quadratic Elements", in: *Modelling Fluid Flow. The state of the art*, Ed.s J. Vad, T. Lajos and R. Schilling, *Springer*, pp. 247-266, (2004a).

Corsini A., Rispoli F., Santoriello A., "A quadratic Petrov-Galerkin formulation for advection-diffusion-reaction problems in turbulence modeling", *Journal of Computational and Applied Mechanics*, v. 5-2, pp. 237-249, (2004b).

Corsini A., Rispoli F., Santoriello A., "A VMS/Stabilized formulation for the k-ε-v^2-f turbulence closure: application to turbomachinery CFD", *ECCOMAS 2004*, paper 1872, (2004c).

Corsini A., Rispoli F., Santoriello A., "A variational multiscale higher-order finite element formulation for turbomachinery flow computations", *Computer Methods in Applied Mechanics and Engineering*, v. 194, pp. 4797-4823, (2005a).

Corsini A., Rispoli F., Santoriello A.,"Quadratic Petrov-Galerkin finite elements for advective-reactive features in turbomachinery CFD", *International Journal of Numerical Methods for Heat and Fluid Flow*, v. 15-8, pp. 894-925, (2005b).

Corsini A., Rispoli F., Santoriello A., Tezduyar T. E., "Improved Discontinuity-Capturing finite element techniques for reaction effects in turbulence computation", submitted to *Computational Mechanics*, (2005c).

Franca L. P., Farhat C., "Bubble functions prompt unusual stabilized finite element methods", *Computer Methods in Applied Mechanics and Engineering,* v. 123 ,pp. 299-308, (1995).

Franca L. P., Valentin F., "On an improved unusual stabilized finite element method for the advective-reactive-diffusive equation", *Computer Methods in Applied Mechanics and Engineering,* v. 190, pp. 1785-1800, (2001).

Gresho P. M., Lee R. L., "Don't suppress wiggles – they're telling you something", in: T.J.R. Hughes ed., *Finite Element Methods for Convection-Dominated Flow*, AMD v. 34, *ASME, New York*, (1979).

Harari I., Hughes T. J. R., "Stabilized finite element methods for steady advection-diffusion with production", *Computer Methods in Applied Mechanics and Engineering,* v. 115, pp. 165-191, (1994).

Hauke G., "A simple subgrid scale stabilized method for the advection-diffusion-reaction equation", *Computer Methods in Applied Mechanics and Engineering,* v. 191, pp. 2925-2947, (2002).
Hauke G., Garcia-Olivares A., "Variational subgrid scale formulations for the advection-diffusion-reaction equation", *Computer Methods in Applied Mechanics and Engineering,* v. 190, pp. 6847-6865, (2001).

Hughes T. J. R., "Multiscale phenomena: Green's functions, the Dirichlet-to-Neumann formulation, subgrid scale models, bubbles and the origin of stabilized methods", *Computer Methods in Applied Mechanics and Engineering*, v. 127, pp. 387-401, (1995).

Hughes T. J. R., "The Finite Element Method – Linear Static and Dynamic Finite Element Analysis", *Dover*, (2000).

Hughes T.J.R. and Brooks A. N., "Streamline Upwind/Petrov-Galerkin formulations for convection dominated flows with particular emphasis on the incompressible Navier-Stokes equations", *Computer Methods in Applied Mechanics and Engineering*, v. 32, pp. 199-259, (1982a).

Hughes T.J.R. and Brooks A. N., "A theoretical framework for Petrov-Galerkin methods with discontinuous weighting functions: application to the Streamline-Upwind procedure", *Finite Elements in Fluids,* v. 4, pp. 47-65, (1982b).

Hughes T. J. R., Mallet M., "A new finite element method for CFD: IV. A discontinuity-capturing operator for multidimensional advective-diffusive systems", *Computer Methods in Applied Mechanics and Engineering*, v. 58, pp. 329-336, (1986).

Hughes T. J. R., Mallet M., Mizukami A., "A new finite element formulation for computational fluid dynamics: II. Beyond SUPG", *Computer Methods in Applied Mechanics and Engineering*, v. 54, pp. 341-355, (1986).

Hughes T. J. R., Mazzei L., Jansen K. E., "Large eddy simulation and the variational multiscale method", *Computing and Visualization in Science*, v. 3, pp. 47-59, (2000).

Hughes T. J. R., Feijòo G. R., Mazzei L., Quincy J.-B., "The variational multiscale method-a paradigm for computational mechanics", *Computer Methods in Applied Mechanics and Engineering*, v. 166, pp. 3-24, (1998).

Idelsohn S., Nigro N., Storti M., Buscaglia G., "A Petrov-Galerkin formulation for advection-reaction-diffusion problems", *Computer Methods in Applied Mechanics and Engineering*, v. 136, pp. 27-46, (1996).

Kythe P. K., Puri P., Schaferkotter M. R., "Partial differential equations and boundary value problems with Mathematica", *CRC press*, (2003).

Leonard B. P., "A survey of finite differences of opinion on numerical muddling of the incomprehensible defective confusion equation", in: T.J.R. Hughes ed., *Finite Element Methods for Convection-Dominated Flow*, AMD v. 34, ASME, New York, (1979).

Oberai A. A:, Pinski P. M., "A multiscale finite element method for the Helmoltz equation", *Computer Methods in Applied Mechanics and Engineering*, v. 154, pp. 281-297, (1998).

Rispoli F., Corsini A., Tezduyar T. E., "Finite element computation of turbulent flows with the Discontinuity-Capturing Directional Dissipation (DCDD)", in press on *Computers and Fluids*, (2005).

Roach G. F., "Green's functions – introductory theory with applications", *VNR, London*, (1970).

Saavedra Garcia Zabaleta R., "Una metodologia di calcolo per flussi comprimibili in turbomacchine assiali", *Ph D thesis (in italian), University of Rome "La Sapienza"*, (2004).

Sani R. L., Gresho P. M., Lee R. L., Griffiths D. F., "The cause and cure (?) of spurious pressures generated by certain FEM solutions of the incompressible Navier-Stokes equations: part 1", *Int. J. Num. Meth. Fluids*, v. 1, pp. 17-43, (1981).

Tezduyar T. E., "Adaptive determination of the finite element stabilization parameters", *Proceedings of the ECCOMAS Computational Fluid Dynamics Conference 2001 (CD-ROM)*, (2001).

Tezduyar T. E., "Computation of moving boundaries and interfaces and stabilization parameters", *International Journal For Numerical Methods in Fluids*, v. 43, pp. 555-575, (2003).

Tezduyar T. E., Park Y. J., "Discontinuity capturing finite element formulations for nonlinear convection-diffusion-reaction problems", *Computer Methods in Applied Mechanics and Engineering*, v. 59, pp. 307-325, (1986).

Tezduyar T. E., Osawa Y., "Finite element stabilization parameters computed from element matrices and vectors", *Computer Methods in Applied Mechanics and Engineering*, v. 190, pp. 411-430, (2000).

Tezduyar T. E., Park Y. J., Deans H. A., "Finite element procedures for time-dependent convection-diffusion-reaction systems", *International Journal For Numerical Methods in Fluids*, v. 7, pp. 1013-1033, (1987).

Tezduyar T. E., Mittal S., Ray S. E., Shih R., "Incompressible flow computations with stabilized bilinear and linear equal-order-interpolation velocity-pressure elements", *Computer Methods in Applied Mechanics and Engineering*, v. 95, pp. 221-242, (1992).

Chapter 5

SCALAR TEST CASES

5.1 Introduction

It is a common procedure in the CFD stabilized finite element framework to test the numerical performance of the formulations on some scalar model problems before addressing the more complicated situation of real turbulent flows, where several parameters could influence the results, such as the geometry of the domain, and it is more difficult to distinguish in detail which are the properties of a specified numerical technique. In this respect, a fundamental question is the evaluation of the numerical dissipation introduced by the stabilization scheme (Tezduyar (2001) and (2003)), that could be easier quantified considering a scalar unknown on a simple geometry, and then generalized to more complex situations.

It is worth noting that consistent stabilized formulations, which are the main subject of this work, are generally designed in order to fulfil the super-convergence feature for one-dimensional problems (Idelsohn et al. (1996), Corsini et al. (2003)). In this viewpoint, preliminary one-dimensional tests on linear model problems are useful to demonstrate the correctness and the main characteristics of a certain formulation (i.e. see Corsini et al. (2005a)), and to highlight the similarities and differences with other formulations proposed in the open literature (i.e. see Hauke (2002)). Nonetheless, historically the most used test cases to assess the performance of stabilized finite elements are two-dimensional scalar problems on simple square domains (i.e. see Hughes and Brooks (1982)). that permit to better address the question of the stability parameters design (Franca et al. (1992)). For these reasons, in this short Chapter that acts as an introduction to the last Chapter, which is the "experimental" Section of this work, some important two-dimensional test cases will be addressed, in order to investigate on the performance of the stabilized finite elements presented in the preceding Chapter.

Following the already discussed criterion of dividing numerical instabilities in *advection* and *reaction* induced ones, the following Sections deal separately on these problems, presenting results on classical model problems, that could be found in the most popular papers on stabilized finite elements. A particular emphasis is also given to the order of interpolation spaces, showing results on both *Q1* and *Q2* elements. In this respect it must be recalled that the formulations presented in Chapter 4 cover the whole range of instability sources (including also *shocks* and *div-stab* condition), and are classified with respect to the finite elements order too.

The numerical performance will be investigated using *SUPG* results as benchmark solution, with the main objective of assessing the new developed *SPG* (for Q2 elements and reactive features) and *V-SGS* (for both Q1 and Q2 elements and both advective and reactive features) formulations, and to show the improvement introduced by the adoption of *DRDJ* to capture reaction induced sharp layers .

Each of the proposed model problems could be obtained as a particular expression of the general *advection-diffusion-reaction* problem statement with respect to the scalar unknown *U*, that reads as follows:

$$\begin{aligned} F_a(U)_{,j} + F_d(U)_{,j} + F_r(U) &= B \qquad \text{in } \Omega \in \mathbb{R}^2, j = 1, 2 \\ U &= U_D \qquad \text{on } \Gamma \end{aligned} \tag{5.1}$$

where for the sake of simplicity only Dirichlet boundary conditions have been considered, and the structure of the operators reads as:

$$\begin{aligned} F_a(U) &= u_j U \\ F_d(U) &= -kU_{,j} \\ F_r(U) &= cU \end{aligned} \tag{5.2}$$

In (5.1) and (5.2), *2* is the number of space dimensions, $k > 0$ is a constant diffusivity, u_j are solenoidal velocity components, $c \geq 0$ is a reaction coefficient, and *B* the source term.

5.2 Advection instabilities

For advection induced instabilities, it is possible to find a number of publications addressing scalar problems on linear finite elements, since the work on SUPG by Hughes and Brooks (1982). Such a kind of problems originate by a one-dimensional difference equation that with linear interpolation functions gives rise to a *constant residual* (i.e. of the same order of the *test function derivative*), as underlined in the work by Hughes et al. (1998), and could be successfully tackled by classical stabilized tools. In order to introduce a more severe problem for the new proposed VMS stabilized formulation, namely the *V-SGS*, at least linear residuals have to be considered, and this led to the decision of considering an advection test case on Q2 elements.

5.2.1 Advection skew to the mesh on Q2 elements

As a first model problem, the classical *advection skew to the mesh* of a scalar unknown (i.e. a temperature field) will be considered, that could be described analytically by imposing $c=0$, $B=0$ and $k=10^{-5}$ in (5.1). The *Pe* number is $6 \cdot 10^3$, due to a velocity

field with intensity equal to *1,* and based on h_{UGN} (Tezduyar and Park (1986), Tezduyar and Osawa (2000)) as element characteristic length. The problem statement is shown in Fig. 5.1, where the direction of the advection velocity field $\boldsymbol{u}$ is evident, so as the boundary conditions. The calculations have been performed on a 2D unit square domain with a uniform grid of *100 quadratic elements*, thus consisting of *441 nodes.*

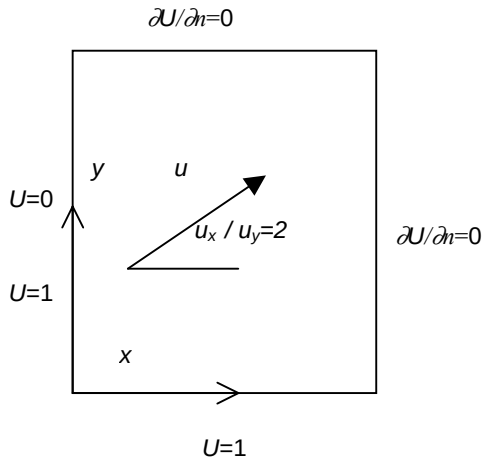

Fig. 5.1. Advection skew to the mesh problem statement.

The solutions predicted by Galerkin (labelled GQ2), SPG improved with the addition of Discontinuity Capturing (labelled SPG+DC) and V-SGS are compared in Fig. 5.2. It is worth noting that Galerkin method gives rise to an oscillating solution, due to the relevant *Pe* number considered and that the SPG method here behaves like the *SUPG* for quadratic elements developed in Codina et al. (1992), that represents its limit in absence of reaction. Considering thus the SPG+DC solution as a benchmark, the superior behaviour of V-SGS in predicting strongly advective fields is evident, due to its capability of managing with non-constant residuals.

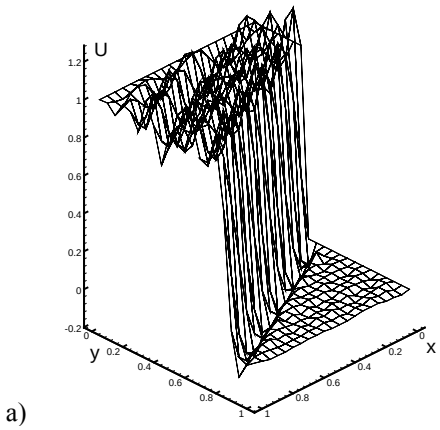

a)

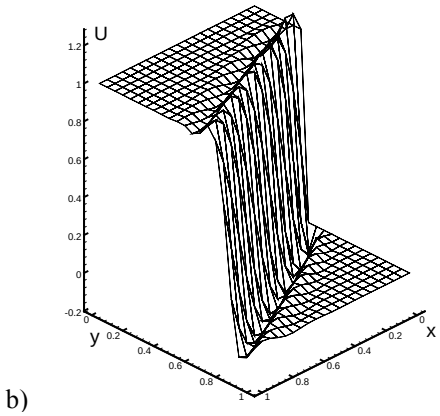

b)

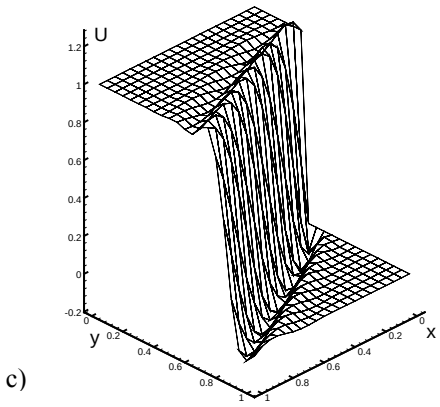

c)

Fig. 5.2. Comparison of solution fields for advection skew to the mesh: a) Galerkin GQ2, b) SPG+DC and c) V-SGS.

This tendency is confirmed in Fig.5.3 with the *x-constant* profiles of the solutions for *x=0.1* and *x=0.9*.

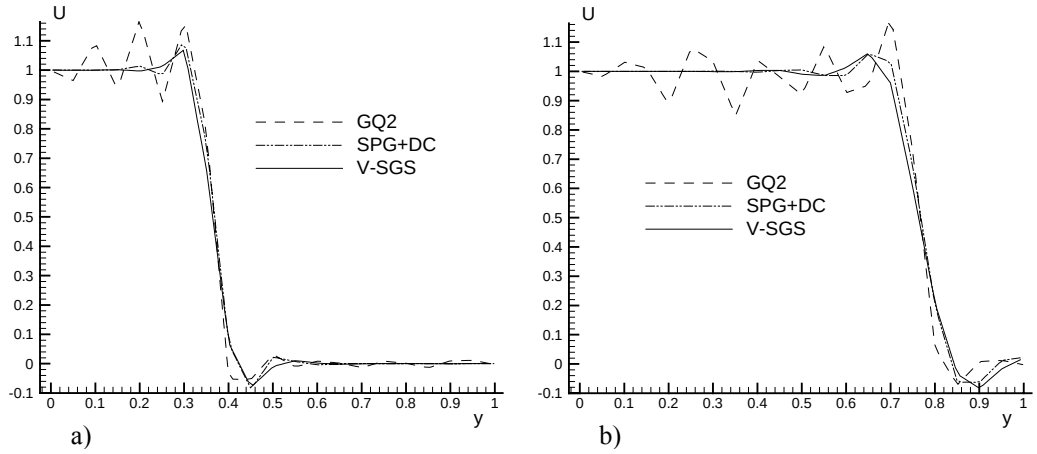

Fig. 5.3. Comparison of solution profiles: a) *x=0.1* and b) *x=0.9*.

5.3 Reaction instabilities

Reaction effects stabilization has been originally ignored, because of an excessive trust in *Mass Lumping* techniques and also for the lack of real problems modeled with reaction terms. This situation changed with the development of simulation techniques for chemical reactions and with the growing number of turbulence closures. In the author's opinion the work that started the "reaction effects stabilization" literature could be considered the one by Tezduyar and Park (1986) and Tezduyar et al. (1987), where the *DRD* technique was developed for chemical reactions simulation.

With respect to advection instabilities, reaction effects are less treated in literature, thus it is worth considering model problems for both linear and quadratic elements, with some additional considerations on the effect of non-uniform grids and source terms, that could thus be considered as some further steps towards the *applied simulation* of turbulent flows pertinent to turbomachinery.

5.3.1 Advection-diffusion-reaction on Q1 elements

This model problem was first proposed in Tezduyar and Park (1986) as a test for the original DRD formulation, and its analytical expression could be obtained by imposing *c=5*, *B=0* and *k=0* in (5.1). The domain is again the unit square, and the advection velocity profile is not constant, reading as:

$$u(y) = u_{max}(1 - y^2)$$
$$u_{max} = 1 \tag{5.3}$$

The main objective of this choice is to have different situations along the solution field, with advection dominated zones and pure reaction layers. The geometry has been discretized by means of a non-uniform grid of 41x21 linear finite elements, and the problem statement is shown in Fig. 5.4.

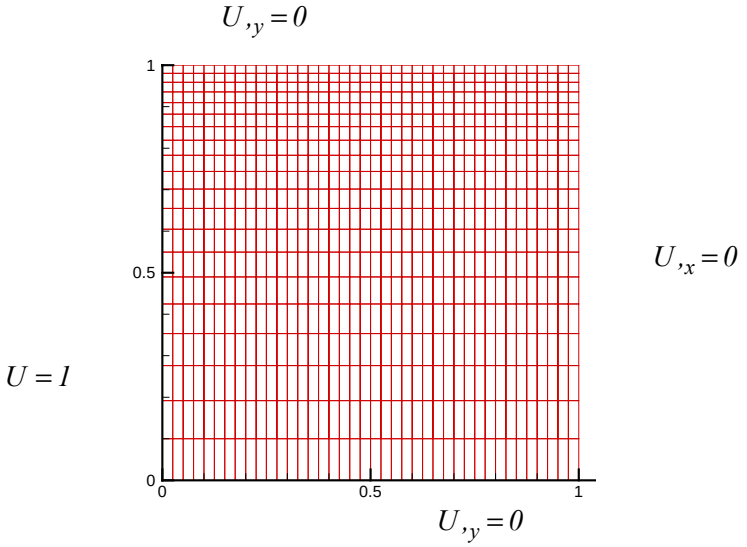

Fig. 5.4. Problem statement, grid and boundary conditions.

This problem has been reconsidered in Corsini et al. (2005b), in order to test the performance of *DRDJ* and to assess its reliability for both *Petrov-Galerkin* and *Variational Multiscale* context.

It must be remarked that this second test case introduces three additional difficulties with respect to the first one:

1. The presence of reaction combined with advection, given a negligible diffusivity;
2. The advection velocity field is not constant, thus the numerical difficulties changes within the domain;
3. The grid is non-uniform.

In Fig.5.5 the solution fields obtained with *SUPG, SUPG + Mass Lumping, SUPG + DRD, SUPG + DRDJ, V-SGS, V-SGS + DRD* and *V-SGS + DRDJ* are presented with respect to the exact solution field. We note that the stabilization parameters have been obtained with h_{UGN} (Tezduyar and Park (1986), Tezduyar and Osawa (2000)) for all the formulations, except for the DRD and DRDJ contributions, that makes use of h_{RGN} (Tezduyar (2003)) in proximity of the null advection layer.

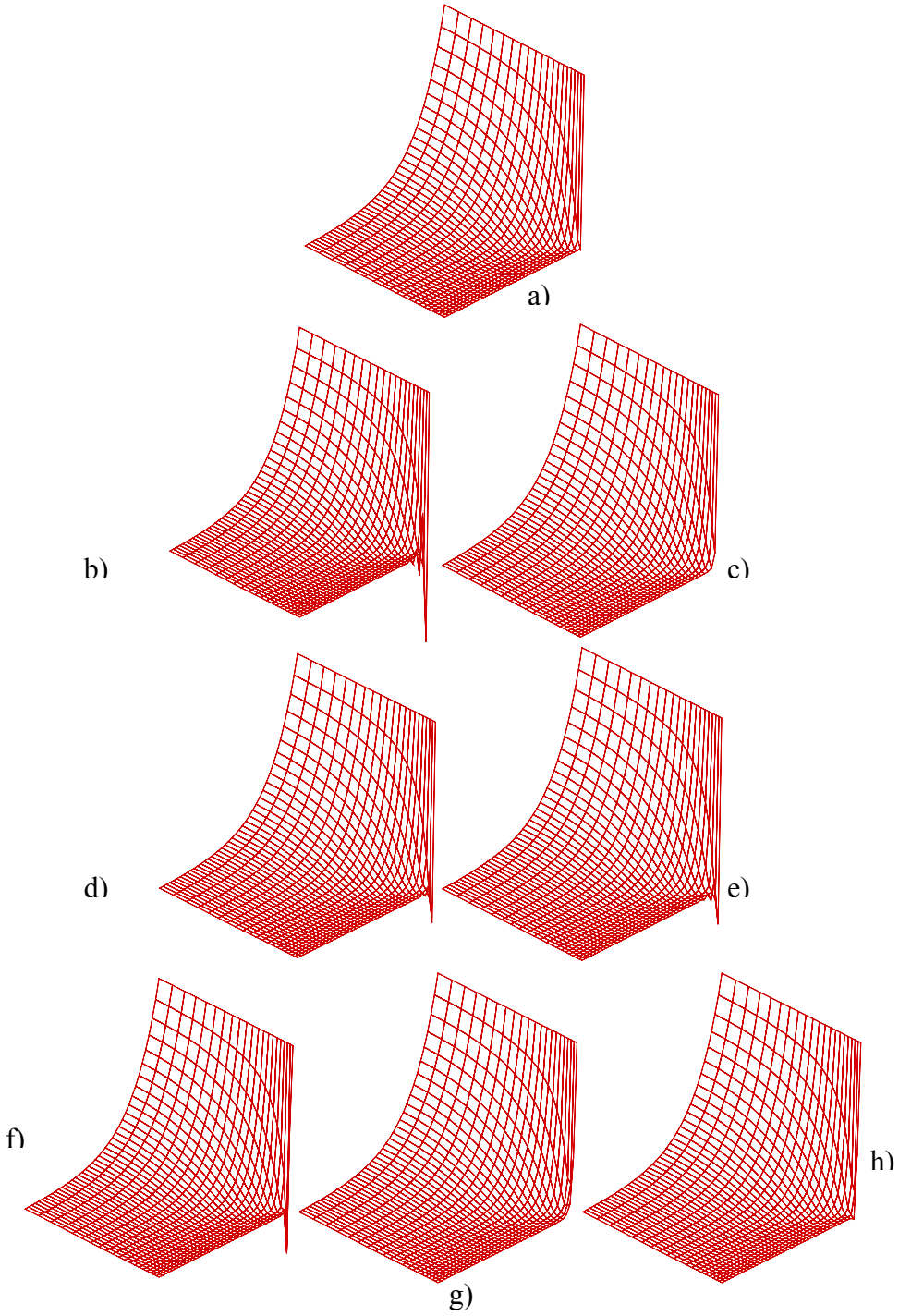

Fig. 5.5. Scalar test problem: a) exact solution, b) SUPG, c) SUPG + Mass Lumping, d) SUPG + DRD, e) SUPG + DRDJ, f) V-SGS, g) V-SGS + DRD, h) V-SGS + DRDJ.

Fig. 5.5 shows that SUPG (b) solution generates the largest oscillations, while V-SGS (g) is able to reduce them due to its control mechanism on reaction effects. Moreover the option of Mass Lumping seems to add too much diffusion while the DRD treatments are both efficient in reducing oscillations and maintaining accuracy of the solution. These considerations could be further developed with the observation of some extracted solution profiles near the boundaries where reaction dominates on convection, as shown in Figs. 5.6, 5.7 and 5.8.

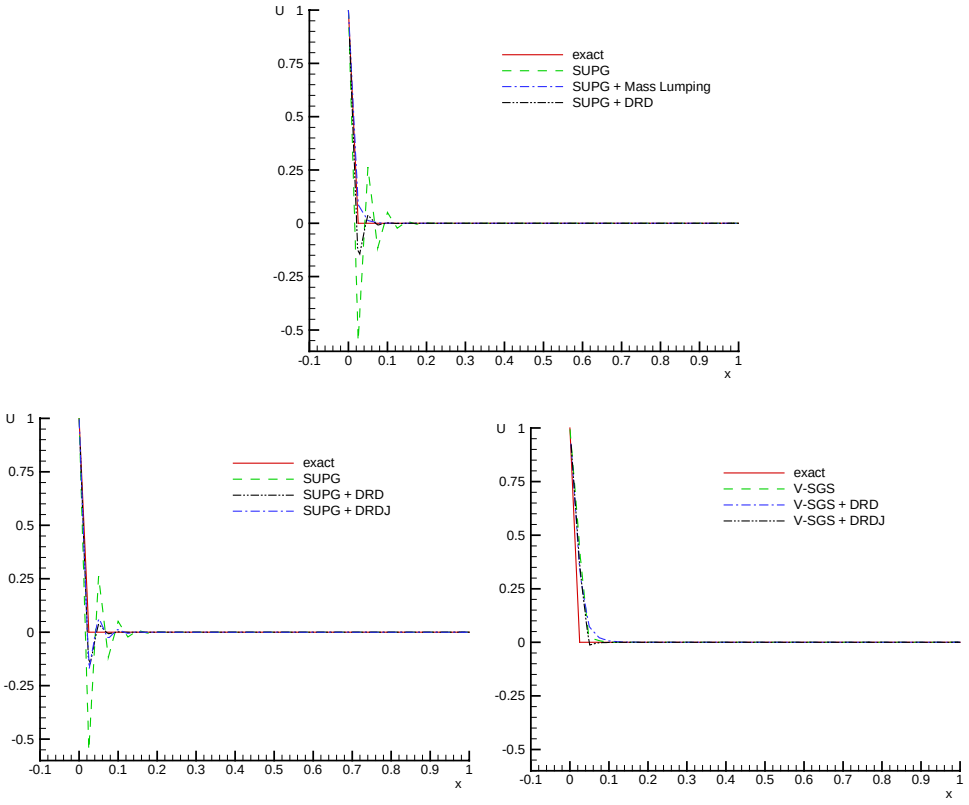

Fig. 5.6. Profiles extracted @ y=1 (first row of nodes).

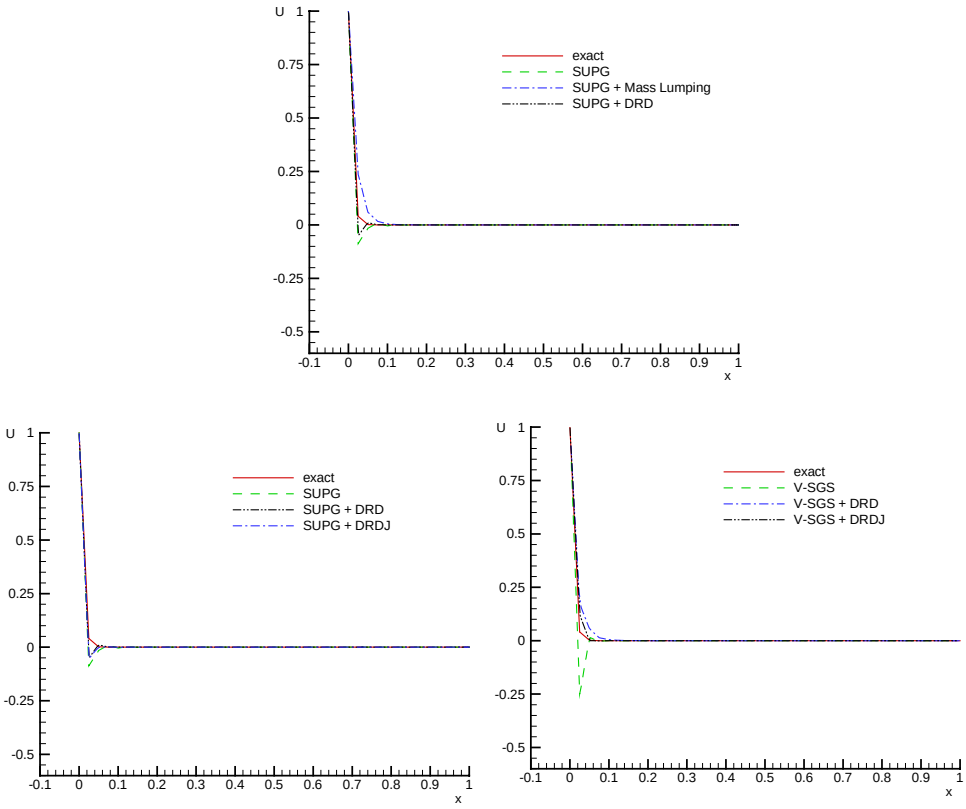

Fig. 5.7. Profiles extracted @ second row of nodes.

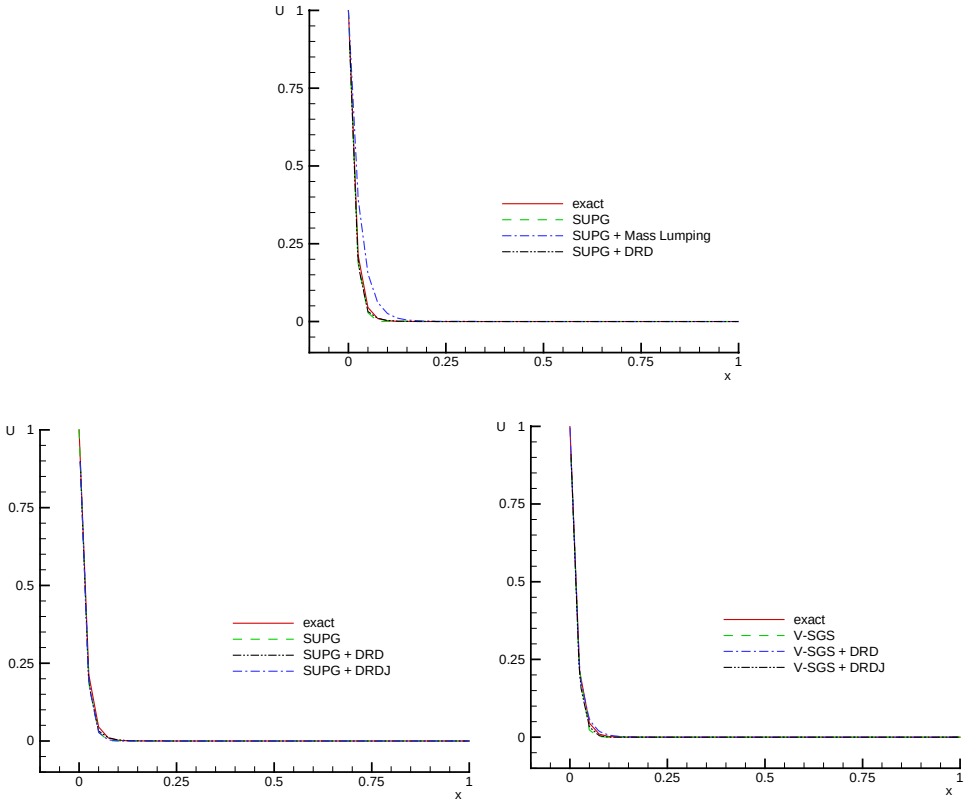

Fig. 5.8.Profiles extracted @ third row of nodes.

The SUPG solution exhibits a 57% undershoot in the first row of nodes (Fig. 5.6), that is reduced to less than 20% by DRD and DRDJ, while Mass Lumping adds too much diffusion. In the same row the V-SGS solution is good and also the addition of DRD and DRDJ permits to obtain good results, the latter being sharper.

Turning to the second row of nodes, SUPG continues to have some undershooting that can be minimized by DRD and DRDJ, while Mass Lumping still adds too much diffusion. The V-SGS shows here a 25% undershoot, that is completely eliminated by DRD and DRDJ, the latter being closer to the exact solution.

Finally in Fig. 5.8 all the formulations recover a sharp solution except that SUPG + Mass Lumping which is too diffusive and too far from the exact solution behaviour.

From these considerations it is possible to draw some conclusions:

- *SUPG* is not capable of controlling reaction induced instabilities and needs some additional numerical technique, that should not be the addition of *Mass Lumping* which creates an unacceptable loss of accuracy, that could be amplified in presence of certain sets of boundary conditions;

- *V-SGS* formulation is able on its own to control reaction effects even if it needs an additional tool to deal with sharp solution gradients.

It is possible to give the same answer to these two problems by means of the *DRD tools*. These additional diffusions are able to control reaction effects with a little reduction in accuracy of the solution, and the optimization introduced with the *DRDJ* concept guarantees a minimization of this accuracy reduction without affecting the efficiency of the method.

As a conclusive remark on V-SGS performance, it demonstrated to be reliable for tackling both advection and reaction induced instabilities, and possesses the distinctive feature of being applicable for both linear and quadratic finite elements, thus representing a promising tool to be used for the simulation of turbomachinery flows.

5.3.2 Advection-diffusion-reaction on Q2 elements

The test case concerns the numerical solution of the linear scalar advective-diffusive-reactive model problem (5.1), in the already introduced unit square domain. The mesh is uniform with 10×10 quadratic elements, 441 nodes. The complete problem statements is shown in Fig. 5.9. The known velocity field u is assumed to have a parabolic profile (e.g. $u(x,y) = 2y - y^2$, $v(x,y) = 0$), with maximum value equal to 1. The coefficients are: $k = 10^{-5}$, $c = 5 \times 10^2$, and the related maxima for dimensionless numbers are: $Pe = o(10^3)$ and $r = o(10^5)$, obtained with the pure geometrical element characteristic length h (i.e. see Section 4.2).

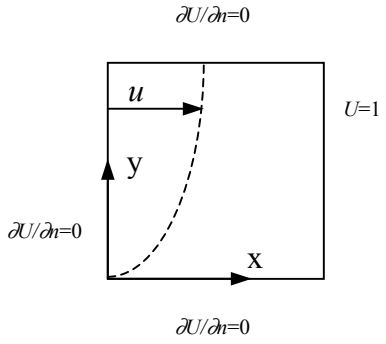

Fig. 5.9. Scalar advective-diffusive-reactive problem statement.

This test case, that has been extensively discussed in Corsini et al. (2005c), is considered here for investigating the performance of the SPG formulation, with respect to quadratic Galerkin (labelled G Q2), Streamline Upwind (labelled SU Q2) and SUPG Q2 ones. Fig. 5.10 shows the solution fields, and demonstrates that the SU Q2 is unable to remarkably improve Galerkin solution, suffering from the combination of its inconsistency and its inability to control reactive effects. With respect to the PG schemes,

both feature stable fields, being able of controlling completely the instability origins in the near- and far-wall regions, but it is evident the sharper behaviour of SPG solution, more correct than the benchmark one, obtained with SUPG Q2.

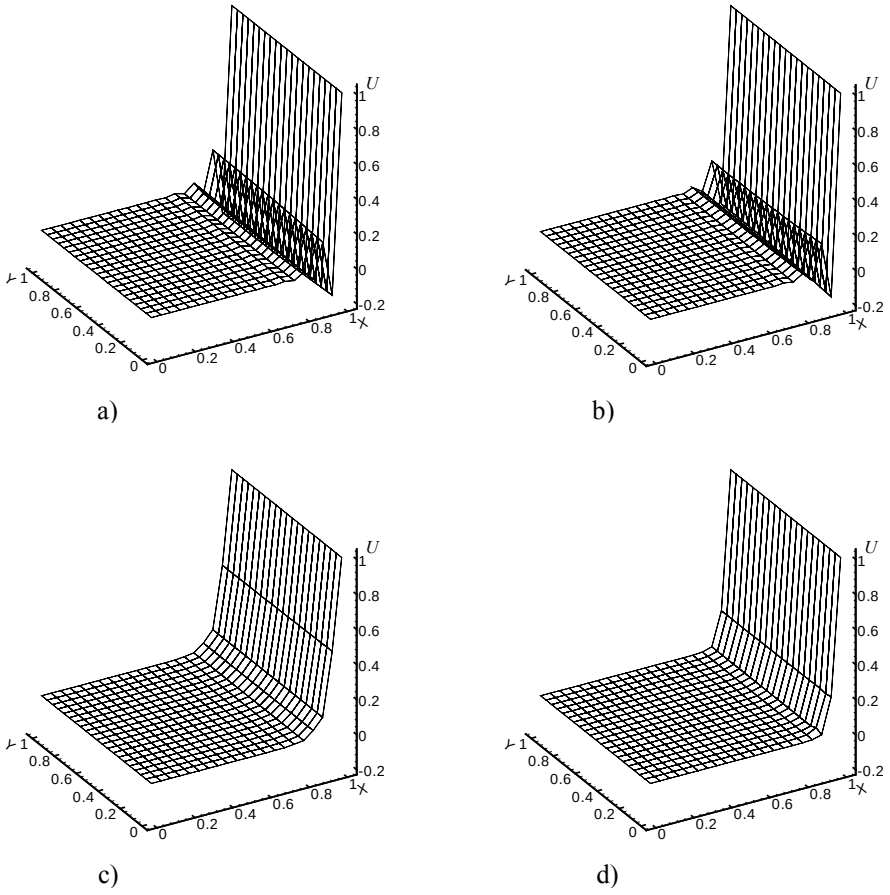

Fig. 5.10. Solution fields: a) G Q2; b) SU Q2; c) SUPG Q2; d) SPG.

Fig. 5.11 shows the *U* streamwise profiles predicted by G Q2, SUPG Q2 and SPG schemes at $y = 0.05$ and $y = 0.1$, close to the null advection boundary line, with a list of the last nodal values. The comparison between the PG-like solutions confirms that the

SUPG Q2 returns an over-diffused layer close to the Dirichlet conditions, thus confirming its inability to control the reactive effects, with respect to SPG solution that returns a sharp but continuous solution layer.

a)

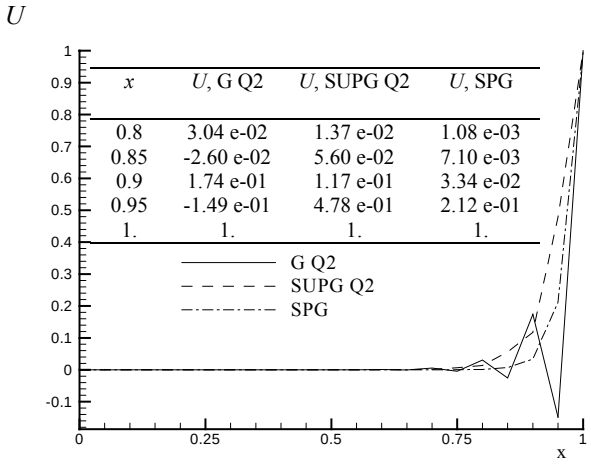

b)

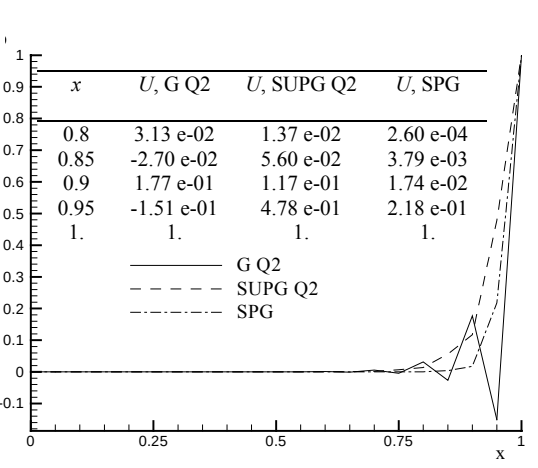

Fig. 5.11. Comparison of streamwise *U* profiles: a) at y=*0.05* and b) at y=*0.1*.

5.3.3 Advection-diffusion-reaction on Q2 elements: effect of a source term

The preceding test cases confirmed that the SPG is a reliable Petrov-Galerkin quadratic formulation for both advection dominated (with a limit behavior equal to SUPG

Q2) and reaction dominated problems. A final assessment of the method could has been obtained in Corsini et al. (2005c) by investigating its behavior in presence of relevant source terms. The last test case proposed in this Chapter reconsider the previous advection-diffusion-reaction problem (i.e. $k = 10^{-5}$, $c = 5 \times 10^2$, $u(x,y) = 2y - y^2$, $v(x,y) = 0$), and introduce a relevant source term B, with a linear-like behaviour, as shown in Fig. 5.12, that presents the problem statement.

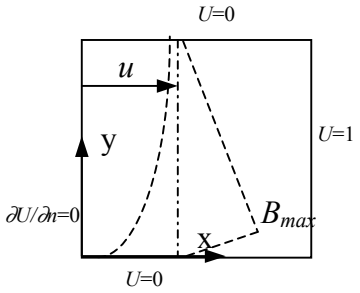

Fig. 5.12. Advective-diffusive-reactive problem statement with B_{max} ($y = 0.1$) = 50.

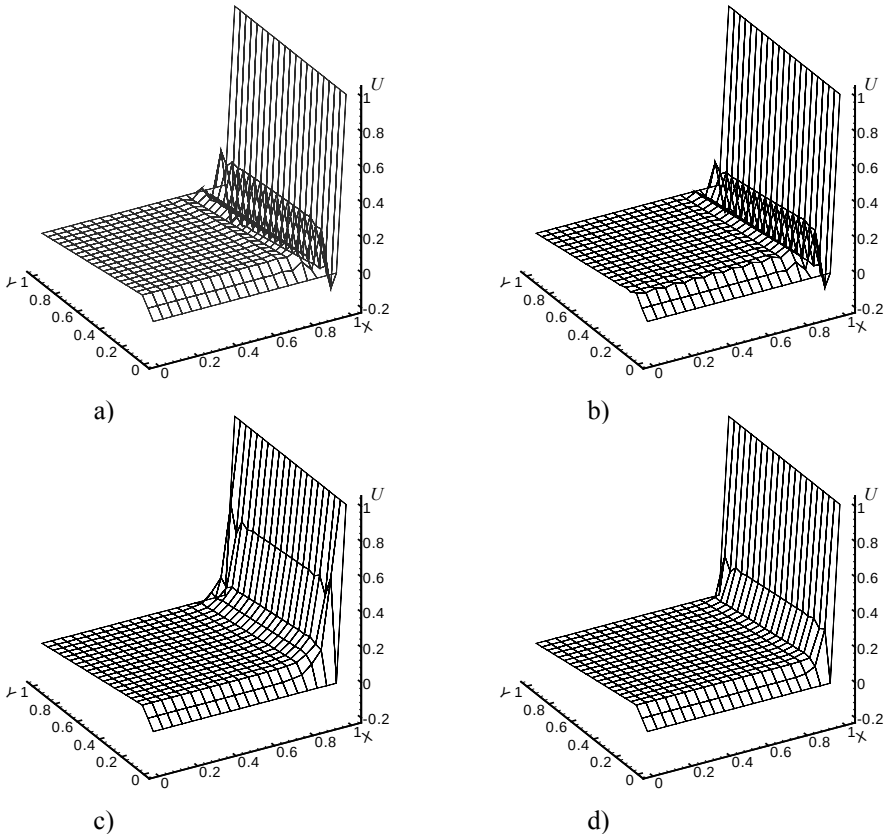

Fig. 5.13. Solution fields: a) G Q2; b) SU Q2; c) SUPG Q2; d) SPG.

Fig. 5.13 demonstrates that even in this case the SU Q2 solution suffers from the same oscillations arising in the Galerkin one, while PG-like solutions are fairly better. Nonetheless SPG outperforms SUPG Q2, as shown in Fig. 5.14, with a comparison of the *U* streamwise profiles predicted by G Q2, SUPG Q2 and SPG schemes at $y = 0.05$ and $y=0.1$, where a reactive effect is combined with a relevant derivative of the source term.

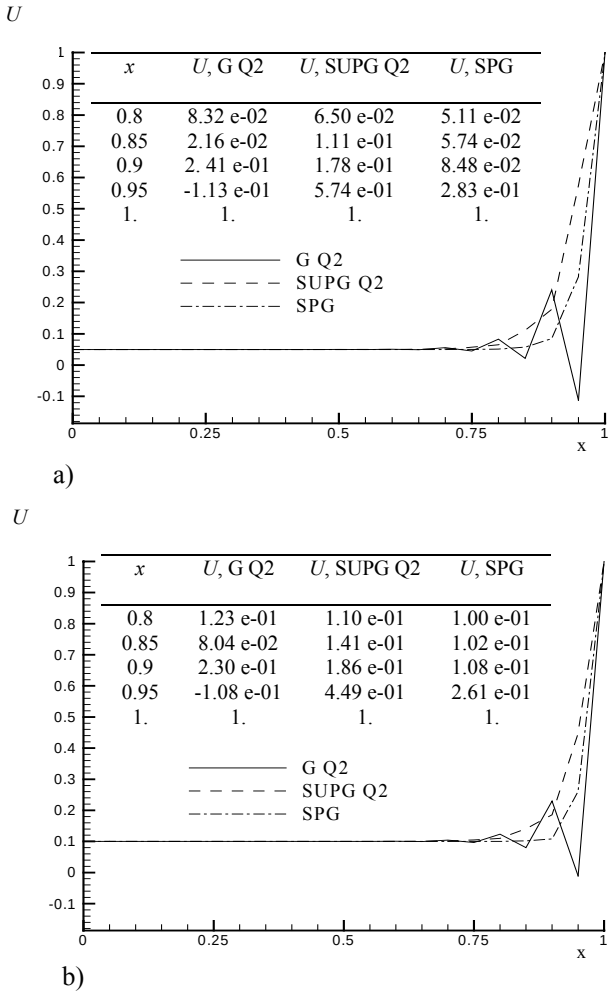

Fig. 5.14. Comparison of streamwise *U* profiles: a) at $y = 0.05$ and b) at $y = 0.1$.

The comparison between the shown nodal values confirms that the SPG is able to recover a non-oscillatory solution, also where the sharp streamwise solution layer develops under the effect of a non uniform source. In addition to the higher diffusivity of

the SUPG solution, a further analysis of Fig. 5.13c shows some numerical pathologies due to the presence of the relevant source term.

It is thus possible to conclude that SPG formulation could be used to tackle all the instability origins appearing in turbulence closure equations, being able to capture reaction effects, as well as recovering a SUPG Q2 behavior for advection dominated equations.

References

Codina R., Oñate, E., Cervera, M., "The intrinsic time for the streamline upwind/Petrov-Galerkin formulation using quadratic elements", *Computer Methods in Applied Mechanics and Engineering*, v. 94, pp. 239-262, (1992).

Corsini A., Rispoli F., Santoriello A., "A new stabilized finite element method for advection-diffusion-reaction equations using quadratic elements", *in: T. Lajos, J. Vad, ed., CMFF'03 Conference Proceedings Vol.2 (Department of Fluid Mechanics, Budapest University of Technology and Economics),* pp. 791-799, (2003).

Corsini A., Rispoli F., Santoriello A., "A variational multiscale higher-order finite element formulation for turbomachinery flow computations", *Computer Methods in Applied Mechanics and Engineering*, v. 194, pp. 4797-4823, (2005a).

Corsini A., Rispoli F., Santoriello A., Tezduyar T. E., "Improved Discontinuity-Capturing finite element techniques for reaction effects in turbulence computation", submitted to *Computational Mechanics*, (2005b).

Corsini A., Rispoli F., Santoriello A.,"Quadratic Petrov-Galerkin finite elements for advective-reactive features in turbomachinery CFD", *International Journal of Numerical Methods for Heat and Fluid Flow*, v. 15-8, pp. 894-925, (2005c).

Franca L. P., Frey S. L., Hughes T. J. R., "Stabilized finite element methods: I. Application to the advective-diffusive model", *Computer Methods in Applied Mechanics and Engineering,* v. 95, pp. 253-276, (1992).

Hauke G., "A simple subgrid scale stabilized method for the advection-diffusion-reaction equation", *Computer Methods in Applied Mechanics and Engineering,* v. 191, pp. 2925-2947, (2002).

Hughes T.J.R. and Brooks A. N., "Streamline Upwind/Petrov-Galerkin formulations for convection dominated flows with particular emphasis on the incompressible Navier-Stokes equations", *Computer Methods in Applied Mechanics and Engineering*, v. 32, pp. 199-259, (1982).

Hughes T. J. R., Feijòo G. R., Mazzei L., Quincy J.-B., "The variational multiscale method-a paradigm for computational mechanics", *Computer Methods in Applied Mechanics and Engineering*, v. 166, pp. 3-24, (1998).

Idelsohn S., Nigro N., Storti M., Buscaglia G., "A Petrov-Galerkin formulation for advection-reaction-diffusion problems", *Computer Methods in Applied Mechanics and Engineering*, v. 136, pp. 27-46, (1996).

Tezduyar T. E., "Adaptive determination of the finite element stabilization parameters", *Proceedings of the ECCOMAS Computational Fluid Dynamics Conference 2001 (CD-ROM)*, (2001).

Tezduyar T. E., "Computation of moving boundaries and interfaces and stabilization parameters", *International Journal For Numerical Methods in Fluids*, v. 43, pp. 555-575, (2003).

Tezduyar T. E., Park Y. J., "Discontinuity capturing finite element formulations for nonlinear convection-diffusion-reaction problems", *Computer Methods in Applied Mechanics and Engineering*, v. 59, pp. 307-325, (1986).

Tezduyar T. E., Osawa Y., "Finite element stabilization parameters computed from element matrices and vectors", *Computer Methods in Applied Mechanics and Engineering*, v. 190, pp. 411-430, (2000).

Tezduyar T. E., Park Y. J., Deans H. A., "Finite element procedures for time-dependent convection-diffusion-reaction systems", *International Journal For Numerical Methods in Fluids*, v. 7, pp. 1013-1033, (1987).

Chapter 6

TURBOMACHINERY FLOW SIMULATIONS

6.1 Introduction

In the first Chapters of this work, after an introduction to the Finite Element Method, an extensive discussion of turbulence and its modeling has been performed, showing an overview of the most adopted solutions in *CFD*. After that stabilized finite element methods have been investigated, with particular emphasis on the new formulations developed both in a *Petrov-Galerkin* and in a *Variational MultiScale* framework, whose numerical performance have been preliminary tested on some scalar model problems. The conclusive step of this path is the application of all these studies for the simulation of real turbulent flows.

Probably the most complex framework, and in the author's opinion the most important one, for turbulent flows simulation, is *turbomachinery CFD*. On the industrial point of view this concept has been already depicted in the Preface, while on the computational point of view it is useful to recall now that turbomachinery flow phenomena prediction must account for a number of challenging features, such as impingement, separation, transition, complex geometries, rotation, tip and passage vortex, to mention but a few (Borello et al. (2003)). In this respect, computational fluid dynamics is playing and will play a fundamental role in reducing development times and costs, indicating the guiding lines to improve machines performance.

This final Chapter represents both the main scope of this work and the most severe test for the developed numerical techniques. It is in fact focused on the application of *SPG*, *V-SGS* and *DRDJ* formulations for incompressible turbomachinery flows simulation, in order to demonstrate their extreme reliability for this kind of studies. While doing this, it addresses, as requested by the deep analysis performed in Chapter 3, also the question of turbulence modelling on a computational point of view, showing the main characteristics of the proposed closures in predicting turbomachinery flows. In this respect, it is worth noting that all the turbulence models used in this work have been considered in their *Low-Reynolds* extension, as discussed in Chapter 3.

The differences in the behaviour of turbulence models are well treated in Section 6.2, where a pair of two-dimensional flow configurations, widely used as benchmark studies by the CFD community, will be addressed, namely the *ERCOFTAC T3L* test case and the *Controlled Diffusion Compressor Cascade***.**

After that, as a final evidence of the numerical formulation impact on the prediction of flow patterns and aerodynamic properties of blade rows, Section 6.3 will focus on a three-dimensional *Compressor Cascade*, characterized by *NACA 65-1810* blades with flat ends.

As established in Chapter 5, the numerical performance will be investigated using *SUPG* results as benchmark solution, with the main objective of assessing the new developed *SPG* and *V-SGS* formulations, and to show the improvement introduced by the adoption of *DRDJ* to capture reaction induced sharp layers .

6.2 Two-dimensional flow configurations

In this Section, a couple of turbomachinery flows will be considered. The first one, namely the *ERCOFTAC T3L* test case, includes a preliminary comparison between the performance of *LS74* (Launder and Sharma (1974)) standard two equations closure and *CLS96* (Craft et al. (1996)) non-linear model. After that the investigation focuses on the numerical formulations, comparing *SPG* and *SUPG* on *Q2* elements, in order to demonstrate the outperforming behavior of the first on the latter one.

The second test case, namely the *Controlled Diffusion Compressor Cascade*, is considered firstly for investigating the improvement introduced in turbulence computation by the k-ε-v^2-f turbulence model (Durbin (1995)), with respect to the classical *LS74* one. With this discussion, a complete assessment of the turbulence closures introduced in Chapter 3 is given, and the investigation could focus on the numerical formulations, with a comparison between *V-SGS* and *SUPG* performance on *Q1* elements.

6.2.1 Flow over a semi-circular leading edge (ERCOFTAC T3L test case)

The test case concerns the prediction of the boundary layer development on a flat plate with a *semi-circular leading edge*. The leading edge configuration, labelled *T3L*, was proposed in 1991 by the *ERCOFTAC Special Interest Group on Transition* (i.e. see Savill (1992)). The main issue of this computation is the correct resolution of some flow features, with particular emphasis on *transition*, that is one of the most challenging aspects of turbomachinery CFD (i.e. see Savill (2002) for an extensive discussion on the question). In particular, the present study refers to the experiments carried out by Palikaras et al. (2002) for the zero pressure gradient configuration. The *Reynolds number*, based on the *inlet velocity* and the *leading edge radius* ($l_r = 5\ mm$), is equal to *1660*. The flow is assumed two-dimensional with constant temperature and incompressible, with an experimental inlet free stream turbulence intensity (*TI*) set to 7%, and a dissipation length l_ε of *18 mm*.

The computations have been performed first with the classical *LS74 standard* k-ε model, and then with the *non-linear CLS96* model, to show its capability of better

resolving stagnation and curvature effects with respect to the first one (i.e. see the analysis performed for this test case in Corsini et al. (2005a)).

The computational domain, that extends *15* l_r upstream the leading edge and *60* l_r downstream of it, has been modelled with a *12681* nodes block-structured (*H-O*) grid, and mixed *Q2-Q1 elements*. In the vicinity of the flat plate (i.e. O-connected region) the first node row has a dimensionless distance from the solid wall $y^+ = 1.0$. A grid detail in the vicinity of the leading edge is shown in Fig. 6.1.

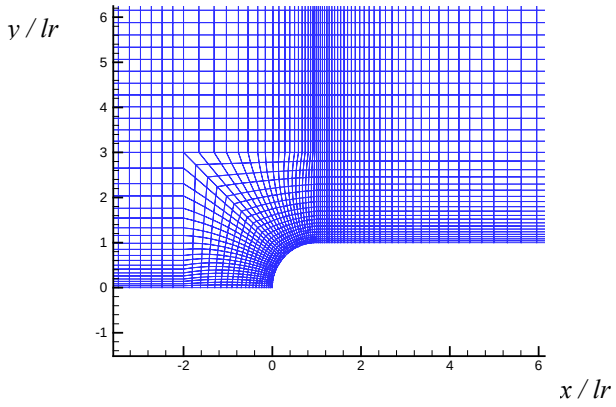

Fig. 6.1. T3L grid detail.

On the inlet section of the computational domain, the experimental free-stream uniform profile is used for the velocity ($\overline{u}$ = 5 m/s), and uniform distributions are also used for the turbulent unknowns (i.e. k and $\tilde{\varepsilon}$) which are computed on the basis of the measured *TI* and l_ε. No-slip conditions are used on the plate wall, and homogeneous *Neumann conditions* are imposed on the outlet section.

The numerical campaigns for the SPG scheme assessment were carried out using the *FGMRES*(20) solver (Saad (1993)) with convergence thresholds for error R_{res} and solution R_{sol} residuals set to 10^{-6}. Uniform initial fields were used for velocity components and turbulent variables, setting $\overline{u}$, k and $\tilde{\varepsilon}$ respectively to the free stream values and $\overline{v} = \overline{u}$ *0.01*. The stabilization parameters have been computed by means of the streamwise characteristic element length h_{UGN} (i.e. see Tezduyar and Park (1986) or Tezduyar and Osawa (2000)), and the quadratic *SUPG* formulation proposed in Codina et al. (1992) was used to produce the benchmark solution. According to the concepts discussed in the *PSPG* presentation (i.e. Section 4.2.1.1), though not necessary for the stability of the formulation, computations have been performed with *PSPG* method (following the formulation proposed in Tezduyar et al. (1992)) for its beneficial effect on the matrix of coefficients.

The first analysis takes into account the numerical robustness by comparing, in Fig. 6.2, the convergence histories in terms of the R_{sol} and R_{res}. The plotted data refer to the use of *SPG* and *SUPG* stabilized formulations on RANS equations with the standard eddy viscosity closure, e.g. the k-ε model proposed by Launder and Sharma (1974). The

shown R_{sol} and R_{res} behaviours provide the evidence that the SPG produces a slight speed-up into the convergence.

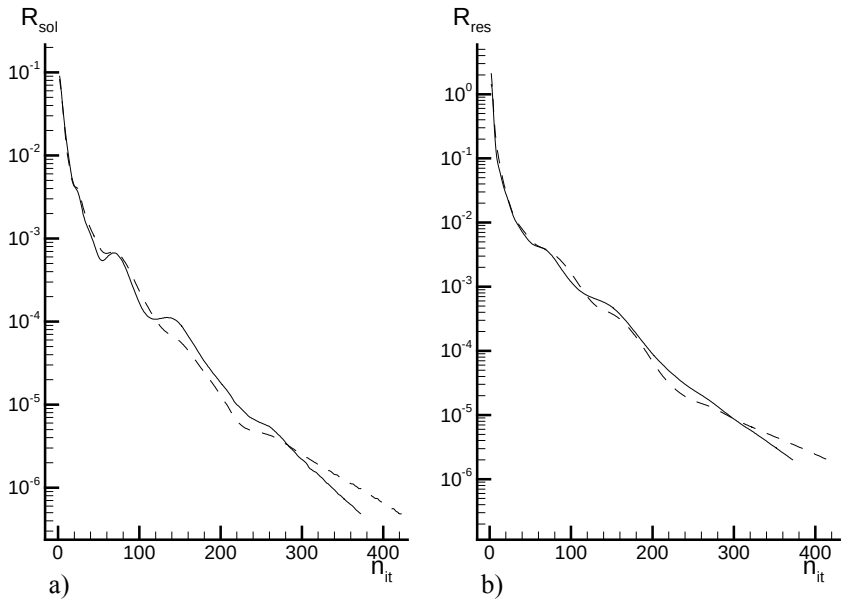

Fig. 6.2. T3L convergence histories for PG formulations: a) R_{sol} and b) R_{res} (solid line: SPG; dashed line: SUPG).

The analysis then extended to a RANS closure based on an anisotropic turbulence model, e.g. the cubic k-ε CLS96 (Craft et al. (1996)), considered as a fair baseline in turbomachinery simulation, as it includes provisions to account for curvature and non-equilibrium effects, and to attenuate stagnation-point inconsistency (Corsini and Rispoli (2002)). In this viewpoint, a first assessment concerned the comparison between the performance of *LS74* and *CLS96*. Fig. 6.3 shows the profiles obtained for streamwise velocity and turbulence intensity components in the first station downwind the leading edge, namely at $x/l_r = 1.2$, where experimental data are available.

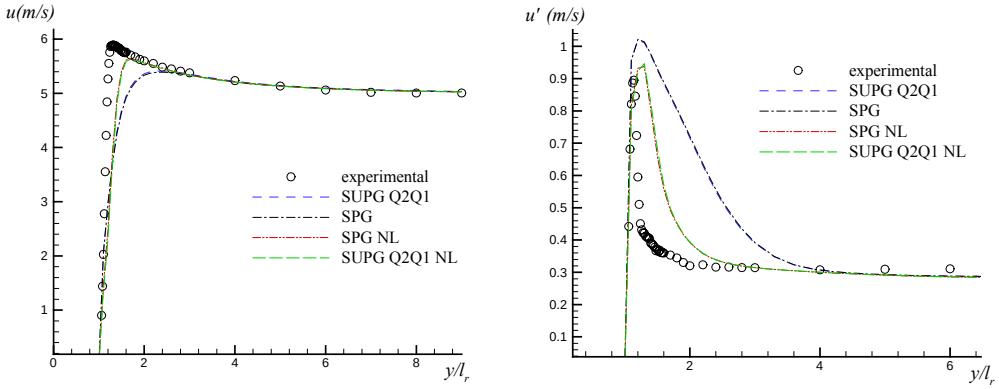

Fig. 6.3. S**treamwise velocity and turbulence intensity profiles @ x/l_r = *1.2.***

Fig. 6.3 confirms the relevant improvement introduced by the non-linear CLS96 model (NL labelled results), with respect to the standard one, affected by the well-known stagnation point anomaly (Durbin (1996)), that contributes to an over-production of turbulence when a stagnating flow core is approached, with several drawbacks in the prediction of the boundary layer development (Corsini et al. (2004a)). For this reason, in the following only results obtained with the CLS96 turbulence model will be shown.

After the comparison between turbulence closures performance, the study focused on the T3L flow regions typically affected by non-equilibrium phenomena, in order to figure out the magnitude of the resolved advective-reactive values. Figure 6.4 shows the contours of the ratio r_k/Pe_k (i.e. see Corsini et al. (2005a) or eq. (4.46)) about the leading edge profile in the case of the SPG solution. The isolines show that the reactivity of the turbulence equations manifests itself in the vicinity of the stagnation point, and downstream the leading edge starting from the axial location where the onset of the by-pass laminar-to-turbulence transition falls. It is worth noting that within the reactivity cores the reaction number r_k has a magnitude comparable to that of the local advection, while moving downstream its value grows up to $o(10^3)$.

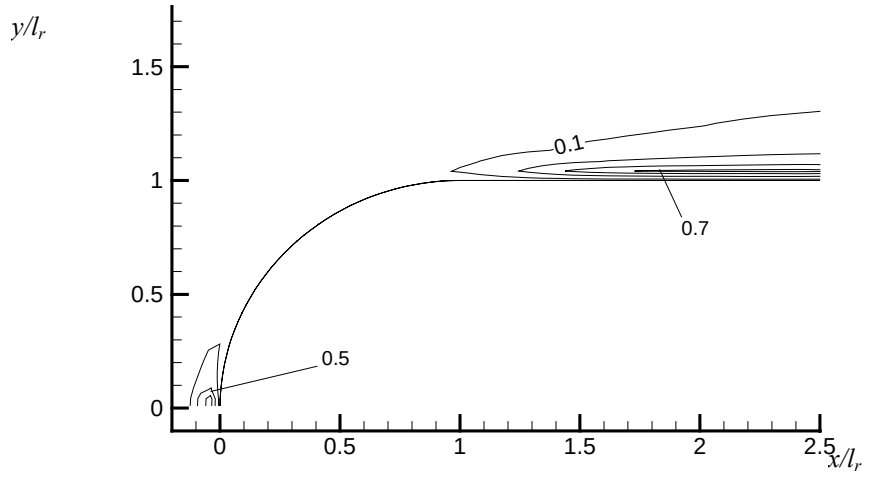

Fig. 6.4. Reaction-to-advection ratio r_k/Pe_k contours.

Fig. 6.4 shows the importance of taking into account the reaction intensity in designing the stabilization parameter, as done with SPG. Thus, it would be expected some difference in the results obtained in the simulation of the boundary layer development. This issue is first addressed in terms of streamwise velocity profiles and integral boundary layer parameters. Figure 6.5 shows the streamwise velocity evolution along the flat plate for different stations that cover the boundary layer development, comparing SPG results with SUPG one, with respect to the available experimental data.

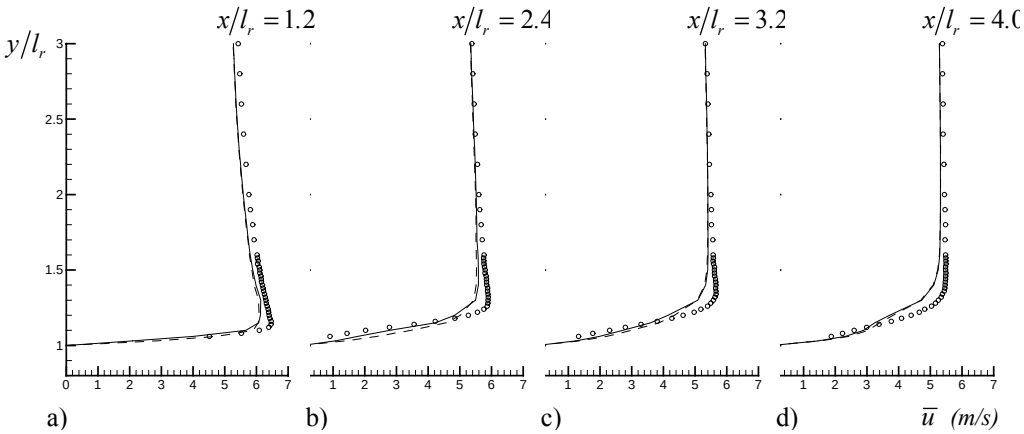

Fig. 6.5. **Streamwise velocity profiles**
(symbols: experiments; dashed line: SUPG; solid line: SPG).

Fig. 6.5 shows no remarkable differences between the computed profiles, both (SUPG and SPG) in fair agreement with the experimental data. Instead, Figure 6.6 compares the axial evolution of the integral properties of the flat plate boundary layer. The following quantities have been plotted against the available measurements: the displacement δ^* and momentum θ^* thicknesses, and the shape factor H.

Contrarily to the velocity profiles, the axial evolutions of the displacement thickness, in Fig. 6.6a, provide the evidence of differences between the PG formulations under exam. Though the computational data under-predict the measured one, the SPG δ^* distribution shows an improved capability of mimicking the velocity layer thickness evolution up to a fully-turbulent state, featuring higher δ^* values and similar axial profile shape. This circumstance is further confirmed by the momentum thickness distributions, Fig. 6.6b. Here the SPG is shown to return qualitatively the variation of the boundary layer momentum content reproducing also the profile gradient discontinuity at the transition onset (e.g. $x = 0.008$, $x/l_r = 1.6$). Figure 6.6c, finally, compares the shape factor evolutions. It is remarkable that, though under-predicting the experiments, the SPG solution is able of recovering a profile shape similar to the measured one and mainly characterized by the abrupt slope variation in the transition region where, as shown in Fig. 6.4, r and Pe assume a comparable magnitude.

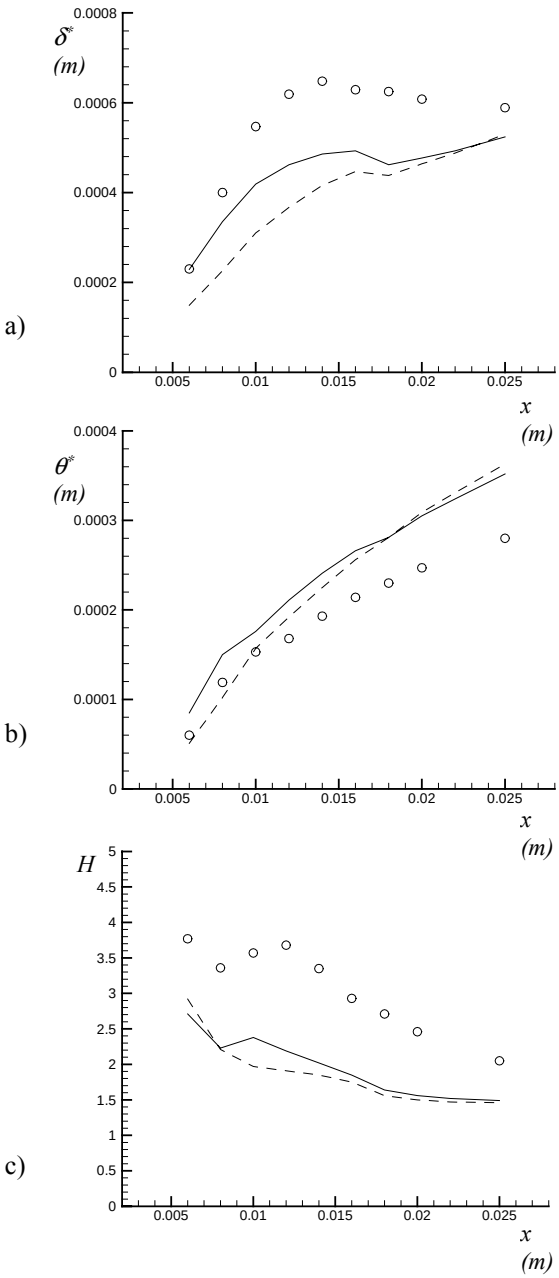

Fig. 6.6. Integral boundary layer parameters: a) displacement thickness, b) momentum thickness and c) shape factor. (symbols: experiments; dashed line: SUPG; solid line: SPG).

Figure 6.7, finally, investigates the streamwise evolution of the boundary layer in terms of the turbulence intensity profile normal to the wall.

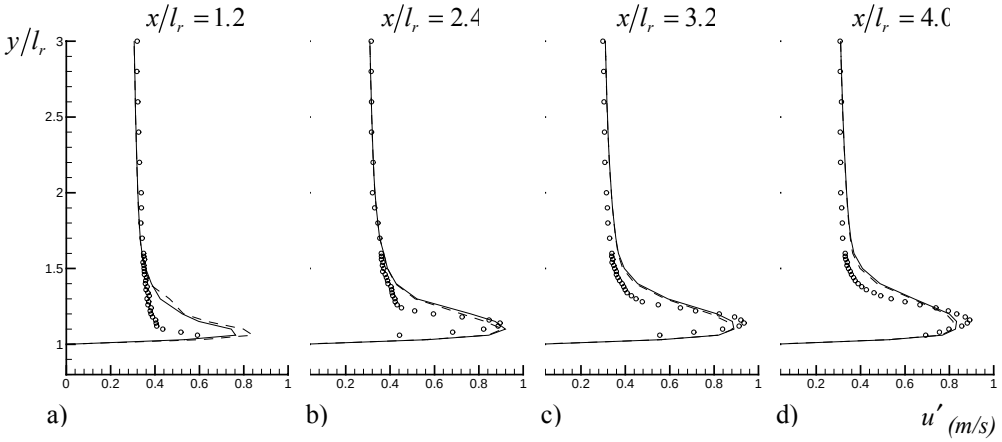

Fig. 6.7. Streamwise turbulence intensity profiles
(symbols: experiments; dashed line: SUPG; solid line: SPG).

The turbulence intensity field, explicitly affected by the reactivity of the implemented turbulence equations, shows that the SPG solution outperforms the SUPG one in predicting the re-arrangement of the boundary layer. In detail, the *u'* profiles at $x/l_r = 1.2$ clearly show that in the buffer-layer region, where the local reaction number is of $o(10^0)$, the SPG is able of reducing the over-prediction of the local turbulence level related to the well known EVM failure of correctly detecting the by-pass transition.

The application of the SPG residual scheme to the RANS equations with an anisotropic eddy-viscosity closure had enabled the turbulence phemonena to be realistically captured in flow configuration pertinent to turbomachinery. Moreover, the proposed advective-diffusive-reactive Petrov-Galerkin formulation improves the solution accuracy with respect to a standard streamline driven stabilization schemes, e.g. the SUPG, in that it properly accounts for the boundary layer region flow phenomena in presence of non-equilibrium effects. The SPG solution outperforms the purely advective scheme resolving adequately the axial and chord-wise evolution of the velocity layer thickness, as well as the turbulent energy contents. In this respect the insufficient cross-wise turbulent mixing shown by the SUPG solutions, that typically affects the non-linear EVM owing to the cubic stress-strain relationship (Chen et al., 1998) (Corsini and Rispoli, 2002), appears to be attenuated. This feature origins from the dependence of the residual distributor mechanism from the reaction magnitude, through the numbers r_k and r_ε. The weight additive structure proposed with SPG is able to correct, on an element scale, the spatial shape of the projection operator balancing the purely anisotropic streamwise deformation with an elliptic diffusive-reactive effect.

6.2.2 Controlled Diffusion Compressor Cascade

This test case concerns a 2D *compressor cascade* with controlled-diffusion (*CD*) blade profile, designed by Sanger (1983) and experimentally studied by Elazar and Shreeve (1990) using two-component *LDV* system. The blade profile has a *14.4°* stagger angle, a solidity $\sigma = 1.67$, and a chord length $l_c = 127.3$ mm. Three inlet flow angles were measured (quasi-design, weak off-design, off-design) and only the off-design condition with incidence angle β equal to 46° is here considered. In this condition the suction side is subjected to a strong adverse pressure gradient, that promotes a challenging transitional flow, with a boundary layer becoming thicker and thicker as the trailing edge is approached (Chen et al., (1998)). The chord Reynolds number, based on the inlet flow velocity U_{in} (*=85 m/s*), is set to 7×10^5. The flow is 2D with constant temperature, and could be considered virtually incompressible.

This flow configuration is used to assess the k-ε-v^2-f model with respect to the classical *LS74* one, and to focus on the *V-SGS* method performance on *Q1* elements (i.e. see Corsini et al. (2005b) for a complete assessment of the method on both Q2 and Q1 elements).

A H topology consisting of 27324 nodes on Q1 elements was used to model the flow region, as sketched in Fig. 6.8, with two details near the *leading* and *trailing edge* of the blade. The refinement is such that the highest dimensionless distance for the nearest node to the wall along the boundary is $y^+ = 1.0$.

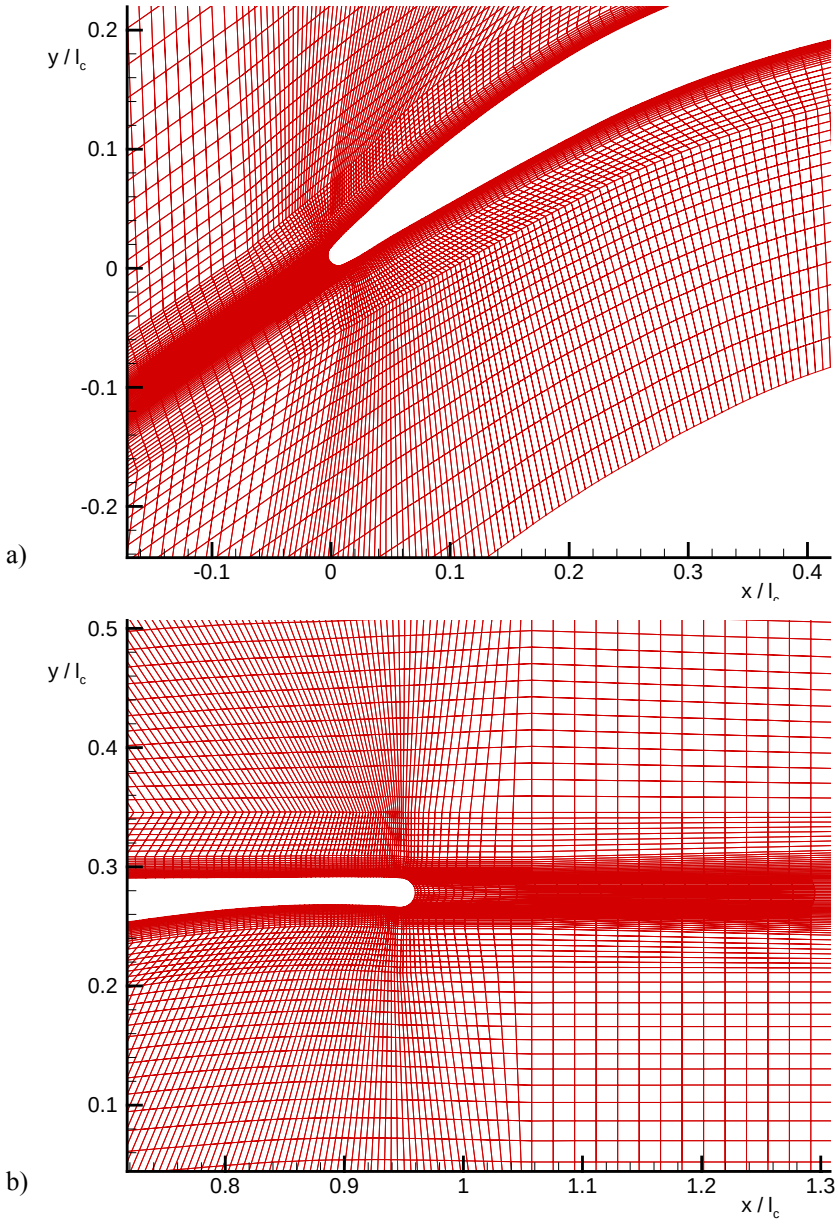

Fig. 6.8. Controlled Diffusion grid details: a) leading and b) trailing edge.

The numerical campaigns were carried out using the FGMRES(15) solver with convergence thresholds for error R_{res} and solution R_{sol} residuals set to 10^{-5} and PSPG treatment (as proposed in Tezduyar et al. (1992)) for tackling incompressibility constraint. The k-ε-v^2-f model, in its code-friendly version (Lien et al. (1998)) has been used in order to test the V-SGS formulation on the convection-diffusion-reaction

equations that model k, ε and v^2, and on the diffusion-reaction equation that model f, for which SUPG is not applicable. It is worth noting that the chosen element characteristic length used to compute the stabilization parameters has been h_{UGN} (i.e. see Tezduyar and Park (1986), Tezduyar and Osawa (2000)) for all the equations except for f, in which case h_{RGN} (Tezduyar (2003)) has been employed.

At the inlet section of the computational domain uniform profiles are used for the velocity components and the turbulent quantities. The experimental free-stream distribution is used for the mean velocity profile. The turbulence intensity and the characteristic length scale are $TI = 1.5\%$ and $l_e/l_c = 5.6\%$. These return the physical turbulence level at the blade leading edge, located half a chord downstream the inlet plane. Homogeneous Neumann conditions are used at the outlet section, one chord downstream the trailing edge, and the flow periodicity is strictly imposed at the permeable boundaries in the middle of adjacent blade passages.

Before going into the V-SGS related details, let consider the performance of the advanced turbulence closure adopted, due to the complex structure of this flow, with a leading edge separation bubble that could not be resolved with a standard k-ε model and a strong adverse pressure gradient characterizing all the boundary layer development.

Fig. 6.9 shows a comparison of the streamwise velocity and turbulence intensity solutions obtained, using a SUPG stabilization, by k-ε-v^2-f model and LS74 one, at the first experimental station in the suction side, downwind the leading edge, namely x/l_c = 5.2%. It is worth noting that the profiles are normalized as in Chen et al. (1998).

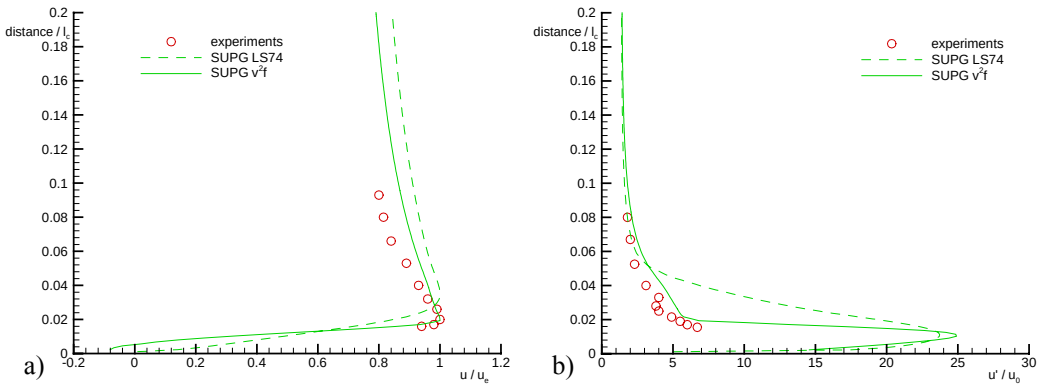

Fig. 6.9. Streamwise velocity a) and turbulence intensity b) profiles on blade suction side @ 5.2 % of the chord: comparison between turbulence models.

As in the T3L test case computations, the standard LS74 model is outperformed: the Durbin's turbulence closure is capable of better controlling the stagnating region prediction, and this feature is propagated downwind, where a reduced mixing permits to obtain profiles that agree quite better with the experimental data concerning both the peak zone and the recovering of the free stream value (see Corsini et al. (2004b) for further

details on the comparison between k-ε-v^2-f model and LS74 one). Therefore in the following, only results obtained with k-ε-v^2-f turbulence closure will be considered.

It is now possible to focus on the assessment of V-SGS finite element method on this real flow configuration, with respect to the benchmark solution given by SUPG, using an advanced turbulence closure, namely the k-ε-v^2-f. The experimental static pressure coefficient C_p distribution (i.e. $C_p = \left(p - p_{ref}\right)/(1/2)\rho U_{ref}{}^2$),shown in Fig. 6.10, suggests the existence of a substantial uniform adverse pressure gradient governing the boundary layer evolution on the suction side downwind the leading edge. The PG formulations appear to be, quite generally, in fairly sensitive matching with the measured pressure distribution, and both approximate the pressure profile flattening about 15% of the chord that traces the leading-edge separation.

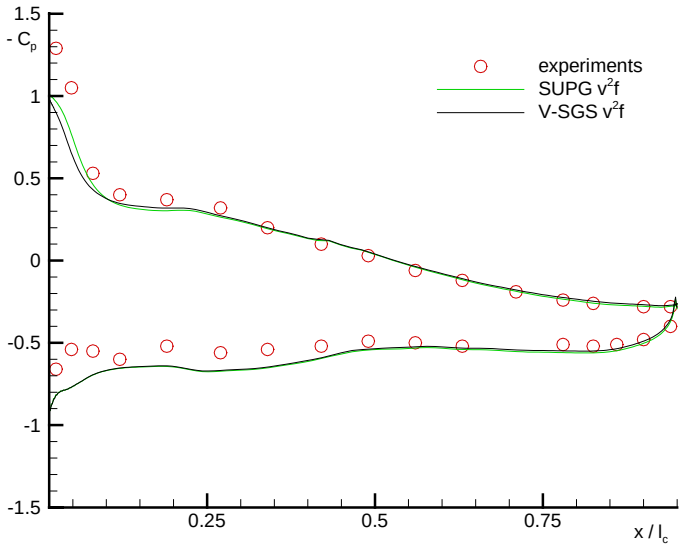

Fig. 6.10. Static Pressure Coefficient for Controlled Diffusion.

As a first difference in the V-SGS and SUPG solution behaviors, the experimentally predicted suction side leading edge separation is computed by both the numerical formulations, but Fig. 6.11 shows, by means of the streamlines plots, that SUPG over-estimates its thickness, due to an excessive numerical dissipation introduced in cross-wise direction. On the contrary, V-SGS is able to better resolve this crucial flow feature, that influences the evolution of the boundary layer in all the suction side.

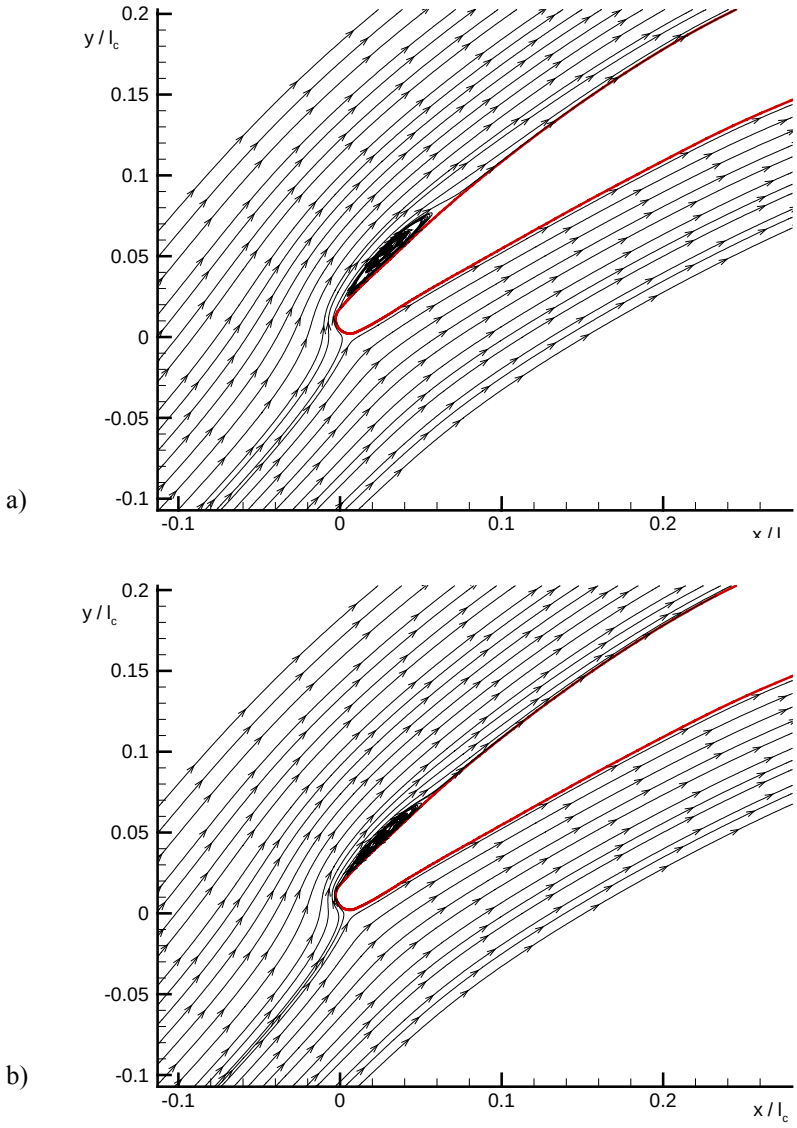

Fig. 6.11. Suction side leading edge separation bubble: a) SUPG, b) V-SGS.

The streamwise-velocity and turbulence intensity distributions on the blade suction-side are plotted, respectively, in Fig. 6.12 and Fig. 6.13 for the chordwise location x/l_c = *5.2%,* in Fig. 6.14 and Fig. 6.15 for the chordwise location x/l_c = *64%,* and in Fig. 6.16 and 6.17 for the chordwise location x/l_c = *95%,* against the distance normalized with l_c.

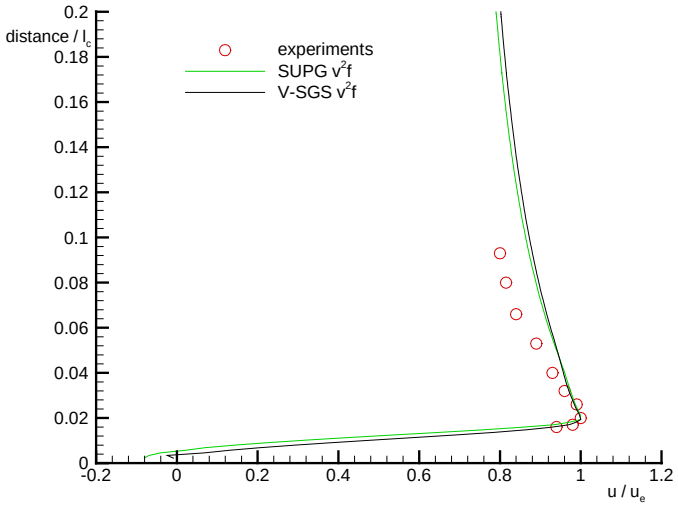

Fig. 6.12. Streamwise velocity profiles on blade suction side @ 5.2 % of the chord.

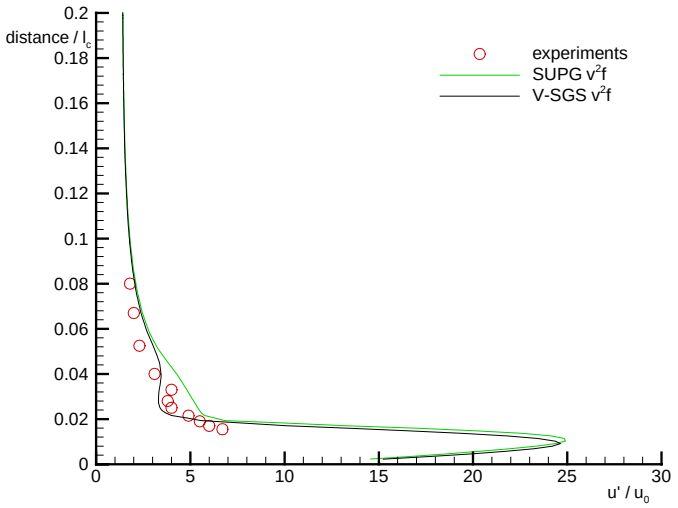

Fig. 6.13. Streamwise turbulence intensity profiles on suction side @ 5.2 % of chord.

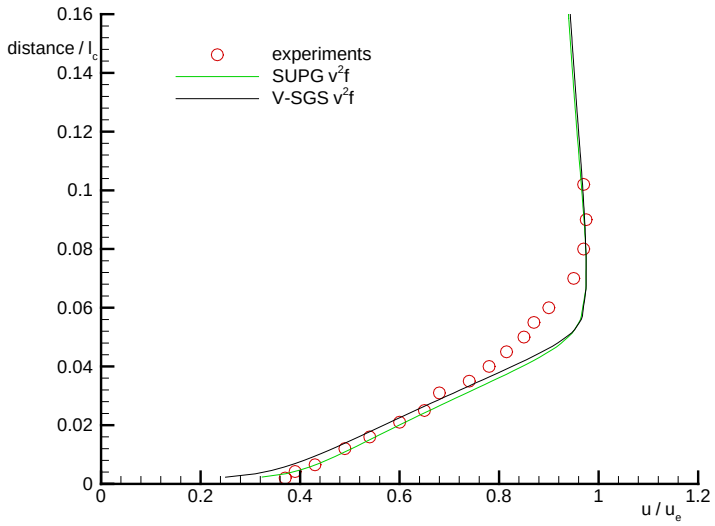

Fig. 6.14. Streamwise velocity profiles on blade suction side @ 64 % of the chord.

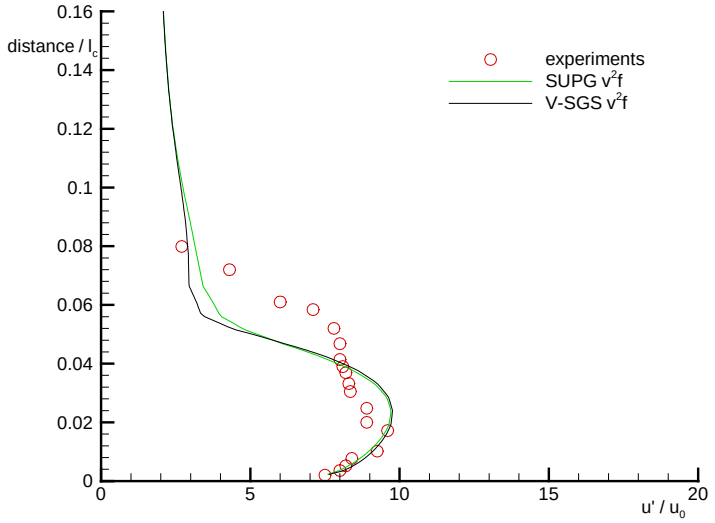

Fig. 6.15. Streamwise turbulence intensity profiles on suction side @ 64 % of chord.

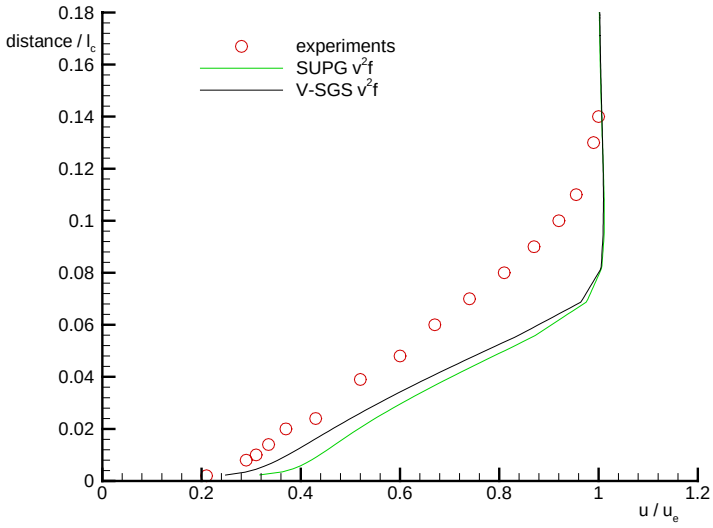

Fig. 6.16. Streamwise velocity profiles on blade suction side @ 95 % of the chord.

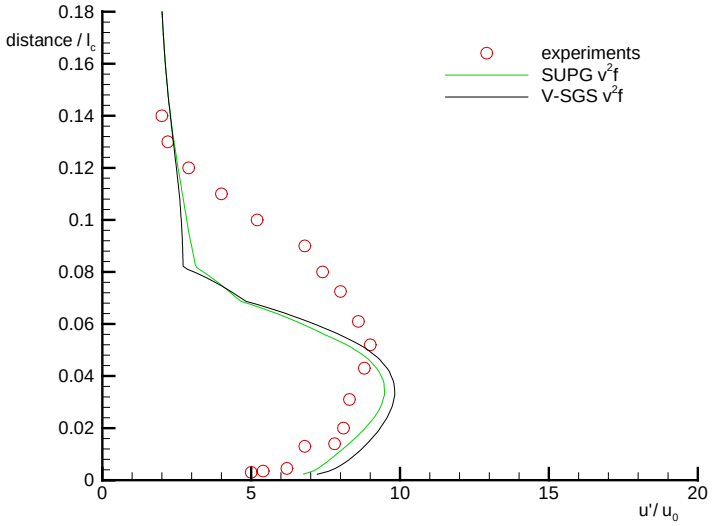

Fig. 6.17. Streamwise turbulence intensity profiles on suction side @ 95 % of chord.

The velocity and turbulence intensity profiles show a good agreement between experiments and numerical results, in the limit of a too high turbulence intensity predicted near the stagnation point at the leading edge. This numerical drawback of the turbulence closure adopted (it must be recalled that the k-ε-v^2-f model is still a linear EVM) is however recovered before reaching 64% of the chord, where the turbulence intensity peak is computed with good accuracy (i.e. see Fig. 6.15).

Both the computed boundary layer developments appear to return the physical issues shown by the experiments, within the inner and the outer layers. It is important to note that the presence of an adverse pressure gradient, causing the reactivity to be more relevant compared to the T3L configuration, gives rise to noticeable differences in the streamwise velocity and turbulence intensity profiles. In detail, the V-SGS appears to resolve the boundary layer thickening and the turbulence energy contents in a far better agreement than the SUPG scheme. In fact it is possible to note in Fig. 6.13 a verification of the fact that V-SGS outperforms SUPG in predicting the turbulence intensity profile within the bubble, as stated when commenting Fig. 6.11. Moreover Figs. 6.12, 6.14 and 6.16 show that the boundary layer thickness prediction obtained with V-SGS is in better agreement with experiments, while SUPG over-estimates it in the separation region, due to its larger separation bubble (i.e. see Fig. 6.11), and under-estimates it downwind, going towards the trailing edge.

6.3 Three-dimensional flow configurations

The two-dimensional test cases showed some important aspects related to the quality of the turbulence closures adopted for the calculations. In this respect it must be recalled that in turbomachinery flows non-equilibrium phenomena can not be resolved adequately with the *Boussinesq* effective viscosity concept. The overview of recent open literature on computational studies for *compressors*, indicates that the turbulence models in use range from simple algebraic eddy viscosity models (EVMs) (e.g. Furukawa et al. (1999), Gallimore et al. (2002)), to one-equation *Spalart-Almaras* (Eulitz (2001)) or isotropic two-equation models with low-Reynolds number extensions (Hah et al. (1999)). More advanced models, such as non-equilibrium eddy-viscosity variants (Borello et al. (1997)), are occasionally adopted. Only recently, second moment closure applications to two- and three-dimensional (3D) compressor cascade flows started to be applied, (i.e. see Borello et al. (2005)).

This state of the art is mainly related to the need to work with so-called *engineering turbulence approaches*, which give ease of coding and numerical robustness, thus constraining industrial research to simpler models. As a result remains an unsatisfactory level of accuracy in demanding flow problems, and the reliability of numerical simulations can not be guaranteed.

On the modeling point of view, the preceding test cases demonstrated that the two-equation non-isotropic closure CLS96 possesses some distinctive features that make it preferable with respect to the other two proposed, i.e. the standard LS74 and the k-ε-v^2-f.

In fact the performed systematical assessment showed outperforming results with respect to LS74 model (i.e. in the T3L test case), without including additional equations, as done instead by k-ε-v^2-f, that still remains a *linear* eddy viscosity model, affected by turbulence over-production near stagnating points. The *CLS96* closure thus represents an alternative simpler route for approximating the Reynolds stresses, with respect to second-moment closure, widely seen as the optimum level for complex flows.

The addressed non-linear turbulence closure, still undergoing validation efforts in several flow problems (such as: external aerodynamics, environmental problems, etc.), has not yet been extensively applied in the context of real turbomachinery configurations. In Corsini and Rispoli (2005) the predictive capabilities of the presented cubic two-equation model in simulating complex high-pressure axial ventilation fan have been tested with encouraging results. In this work the CLS96 closure is applied for the simulation of a challenging test case for turbomachinery CFD, namely a *Linear Compressor Cascade with tip clearance*.

On the numerical point of view, this last test case is used to show the performance of the recently proposed *V-SGS + DRDJ* formulation (Corsini et al. (2005c)), with respect to the benchmark *SUPG* solution.

6.3.1 Linear Compressor Cascade with tip clearance (NACA 65-1810)

This conclusive test case concerns the three-dimensional flow in a *Compressor Cascade* with stationary endwall at design conditions, with tip clearance, and an adopted blade that reproduces the *NACA 65-1810* profile with flat ends. Experimental investigations on this machine were carried out in the Vrije Universiteit Brussel (VUB), and a detailed description and analysis of the measured data can be found in Kang and Hirsch (1993a and b). Details of the linear cascade are given in Tab. 6.1.

Profile Type	NACA 65-1810
Aspect Ratio	1.0
Chord	200 mm
Pitch	180 mm
Solidity	1.111
Stagger angle	10°
Inlet angle	32.°
Outlet angle	-12.5°
Mach Number	< 0.1

Tab. 6.1. Geometry of the Linear VUB Compressor Cascade.

The cascade flow is simulated by imposing a small incidence angle (about *-2.5°*). The flow is regarded as incompressible and steady. In accord with the experimental findings, the flow at the inlet was considered as fully turbulent, (the measured *shape factor* at the inlet, *40%* chord upstream of the leading edge, is about *1.22*). The *Reynolds number*, based on the chord length and the inlet bulk velocity is $3x10^5$. The experimental free stream turbulence intensity is *3.4%*. The dissipation length scale l_ε has been set equal to *5 %* of chord length.

On the grid point of view, the tip clearance is *4 mm* (*2%* of the blade chord) and theoretically appears near both end walls; however experimental measurements were only done until *midspan*, so that a *tip clearance* only appears near a wall, and this choice was also used for the calculations. The resulting mesh height in span direction is thus equal to *104 mm*. A Stretched *H*-grid with zero values of flow variables inside the blade has been adopted to avoid distortion in the discretisation of the leading and trailing edge regions.

The inlet and outlet sections are placed in the first measurement section (*40 %* chord upstream from the leading edge) and one chord downstream from the blade passage respectively. Experimental data have been imposed as inflow-velocity Dirichlet boundary conditions. Inlet distribution for turbulent kinetic energy *k* has been imposed by scaling a turbulence intensity profile experimentally derived for a fan rotor of similar performance (Corsini and Rispoli (2004)). The scalar dissipation ($\tilde{\varepsilon}$) distribution at the inlet has been derived by imposing $\tilde{\varepsilon}_{in} = \left((k)^{3/2} / l_\varepsilon \right) + 2\nu \left(\partial \sqrt{k} / \partial x_j \right)^2$. Neumann conditions are set on the outflow boundaries. On the walls, no slip conditions have been used, Flow *periodicity* has been strictly imposed at the permeable boundaries, thus permitting to simulate only one *pitch* distance, while symmetry has been imposed in the mid-span section.

In order to achieve grid independent solutions, the grid was progressively refined up to *141x73x81* points (*IxJxK*), thus obtaining *833733* nodes on *Q1* elements, to which the following results refer. The maximum y^+ values in the first nodes row close to the solid boundary have been maintained under a threshold value of 2. Fig.6.18 shows a detail of the blade discretization.

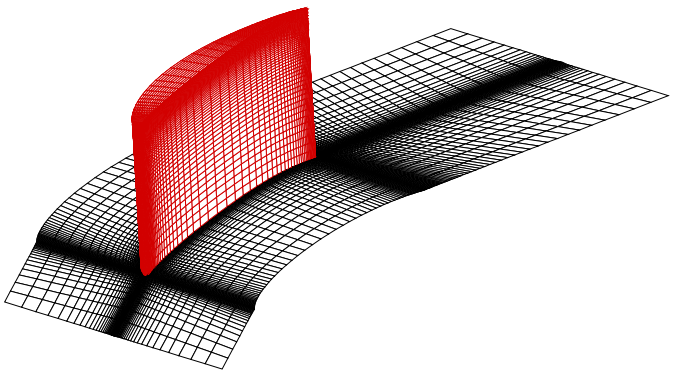

Fig. 6.18. Blade grid.

Computations have been performed with equal-order linear Q1-Q1 elements, and *PSPG* stabilization (i.e. see Tezduyar et al. (1992)) to eliminate the undesirable pressure-checkerboarding effects related to the combination of interpolation spaces. Both *V-SGS* + *DRDJ* and *SUPG* stabilization parameters have been obtained using the h_{UGN} element length (Tezduyar and Park (1986), Tezduyar and Osawa (2000)). The solutions have been obtained using an in-house overlapping parallel solver (Borello et al. (2003)), with an original block structured domain decomposer managed by the *MPI* libraries and running on a *XEON* Cluster with *14* processors and *7* Gb RAM. The numerical campaigns were carried out using the *FGMRES(8)* solver with convergence thresholds for error R_{res} and solution R_{sol} residuals set to 10^{-4}.

The first parameter considered for analysing numerical results is the Static pressure coefficient C_p, shown in Figs. 6.19 and 6.20 for two different spanwise locations, respectively at *midspan* and *30 mm* far from the tip, where experimental data are available.

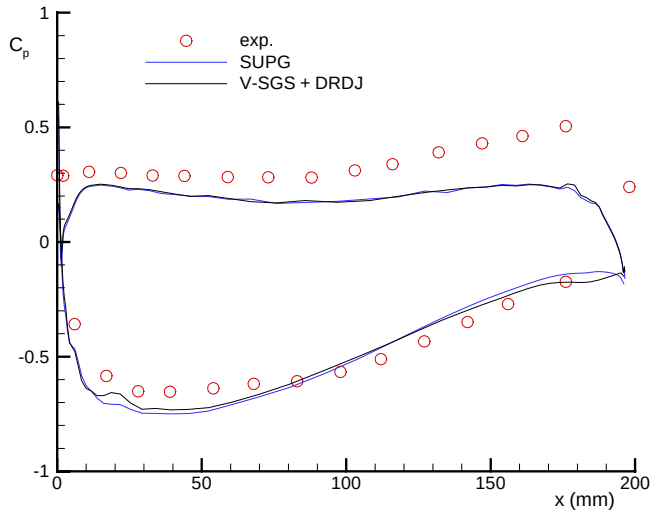

Fig. 6.19. Static Pressure Coefficient @ midspan.

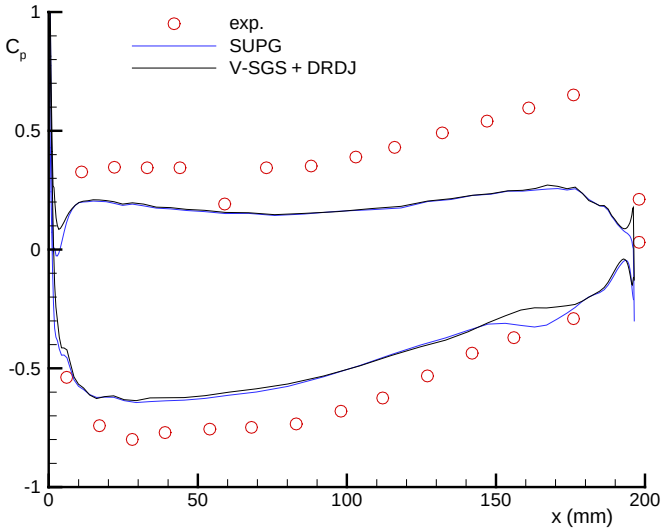

Fig. 6.20. Static Pressure Coefficient @ 30 mm from the tip.

Fig. 6.19 and 6.20 show a similar behavior of the two numerical solutions, able both of being in fair agreement with experimental results at midspan, while going towards the tip, some turbulence modelling drawbacks limit the pressure increase on pressure side, while suction side phenomena are well represented.

It is a matter of fact that the *endwall zone* of the field contains the most interesting feature, i.e. the *tip leakage vortex*, thus being worthwhile showing in Fig. 6.21 the streamlines evolution on a plane located at half of the tip clearance region, using the contour plots of static pressure as background.

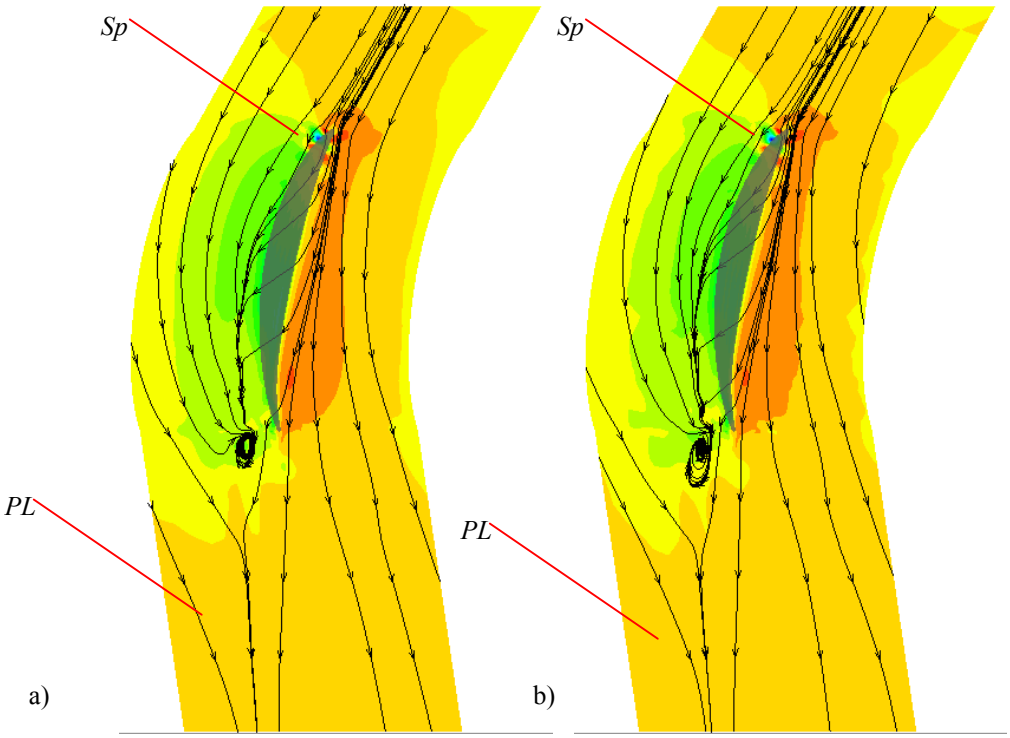

Fig. 6.21. Flow patterns in the tip clearance: a) SUPG, b) V-SGS + DRDJ.

Following the argumentations presented in Kang and Hirsch (1993a), experimental results show that approaching the leading edge it could be found a *Saddle Point*, also seen in the computations and labelled *Sp* in Fig. 6.21. From this point the flow patterns split into two lines, creating a leading edge *horseshoe vortex*, well resolved by both the numerical formulations. The pressure side branch stretches downstream a short distance, and then tends to join the suction side one, giving rise to the *tip leakage vortex*, that could be seen in both the solutions. Finally, another experimental feature of the flow in the *tip gap* is well resolved by the numerical simulations, namely the tendency of the reattachment line of the tip leakage vortex to go near the reattachment line of the *passage vortex*, labelled *PL* in Fig. 6.21.

In order to better understand the complex structure of the flow, Fig. 6.22 shows the velocity vectors at the tip, considering two adjacent blades.

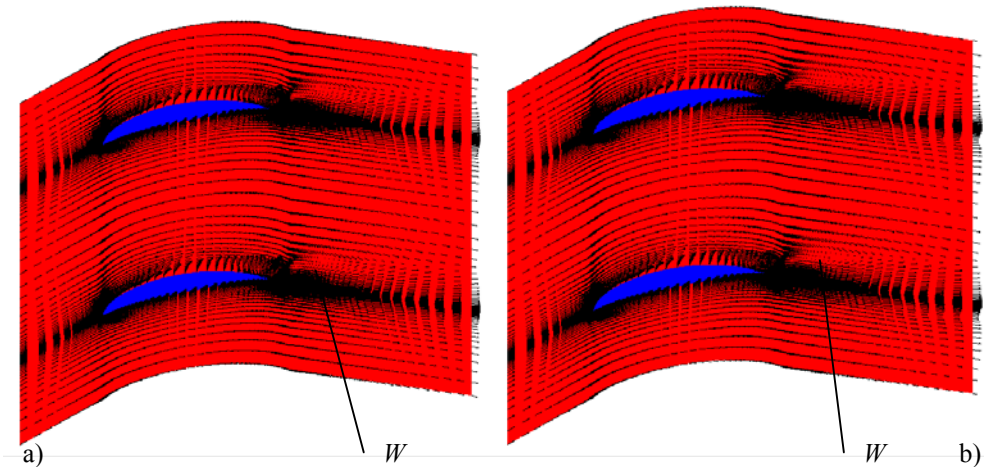

Fig. 6.22. Velocity vectors @ tip: a) SUPG, b) V-SGS + DRDJ.

From the vector plots shown in Fig. 6.22, it is possible to see some first differences between the two numerical formulations in resolving the wake zone after the trailing edge, labelled with *W*. *SUPG* wake is in fact more limited with respect to *V-SGS + DRDJ* one, and this aspect will be confirmed in the following.

Considering now the whole velocity field, some appreciable differences in the numerical solutions could be highlighted by the streamlines patterns. In this viewpoint, Fig. 6.23 shows the streamlines patterns along the pressure side, Fig. 6.24 considers the suction side, and Fig. 6.25 shows a detail of the streamlines patterns that define the *tip leakage vortex*.

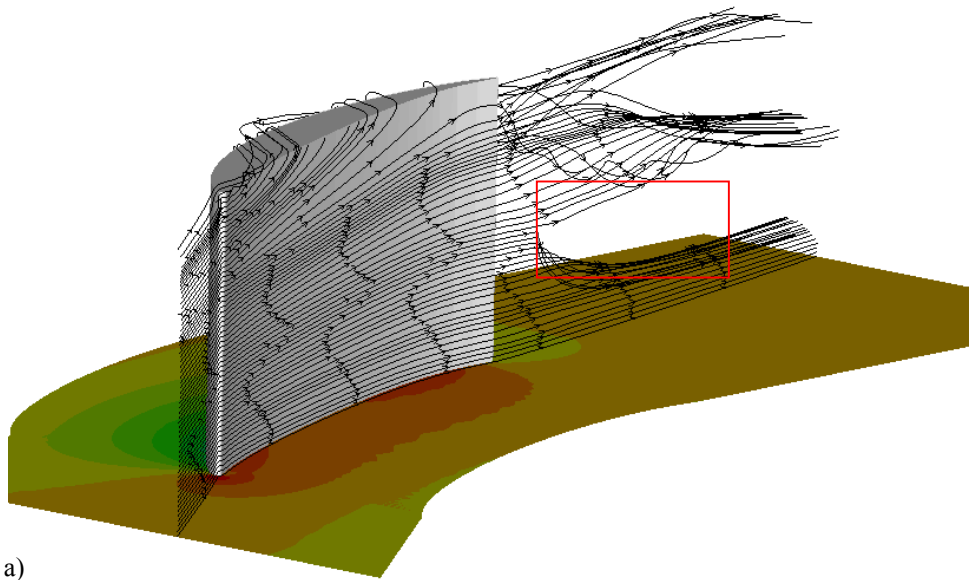

a)

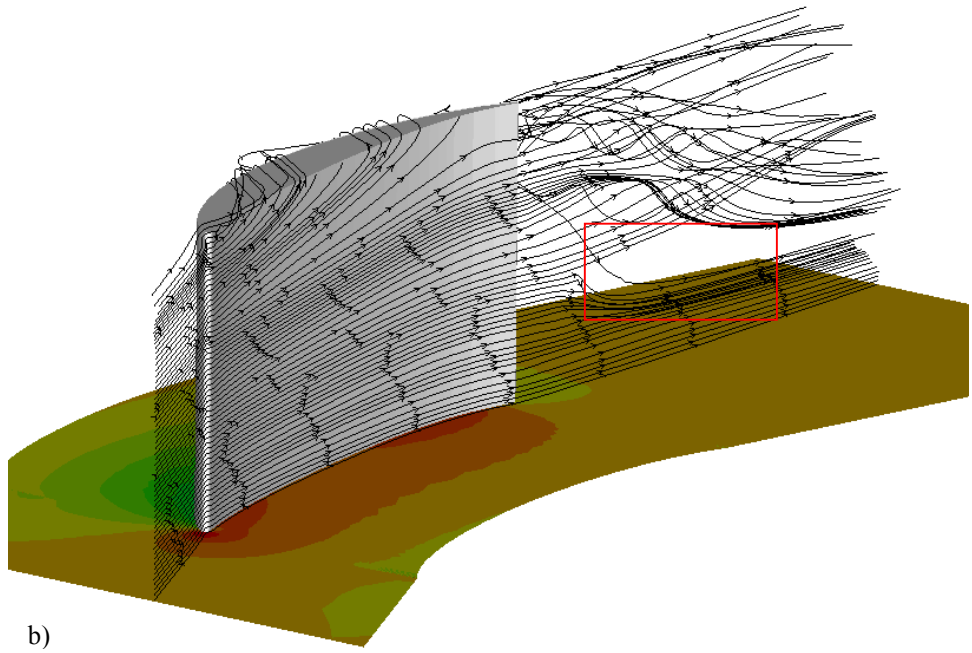

b)

Fig. 6.23. Streamlines along pressure side: a) SUPG, b) V-SGS + DRDJ.

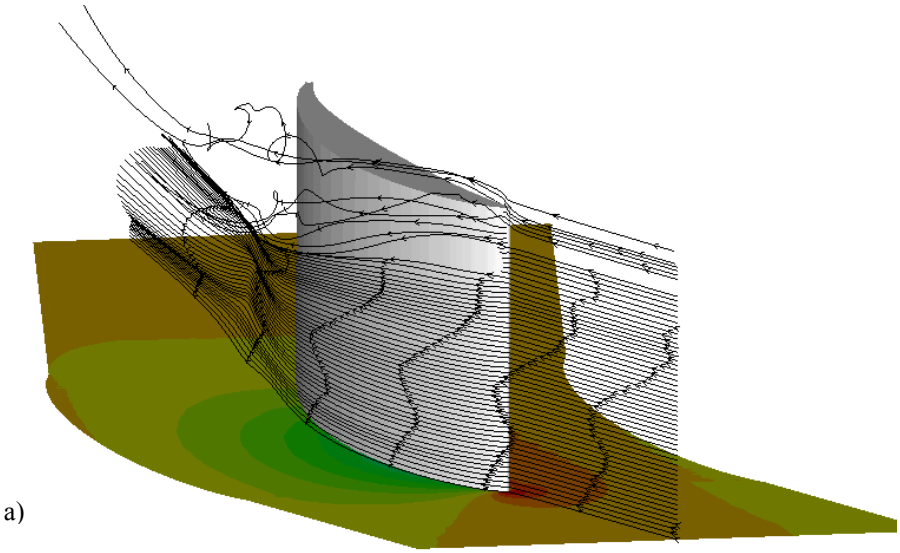

a)

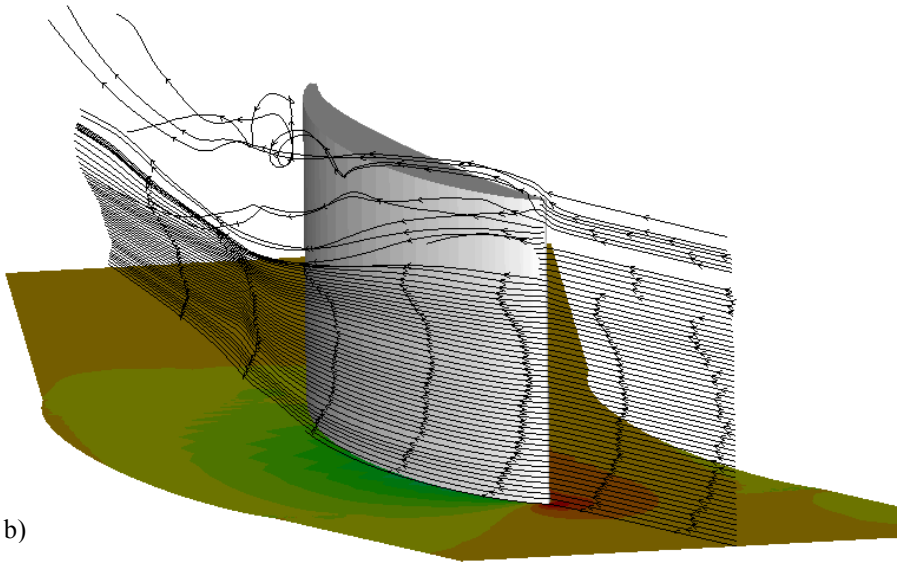

b)

Fig. 6.24. Streamlines along suction side: a) SUPG, b) V-SGS + DRDJ.

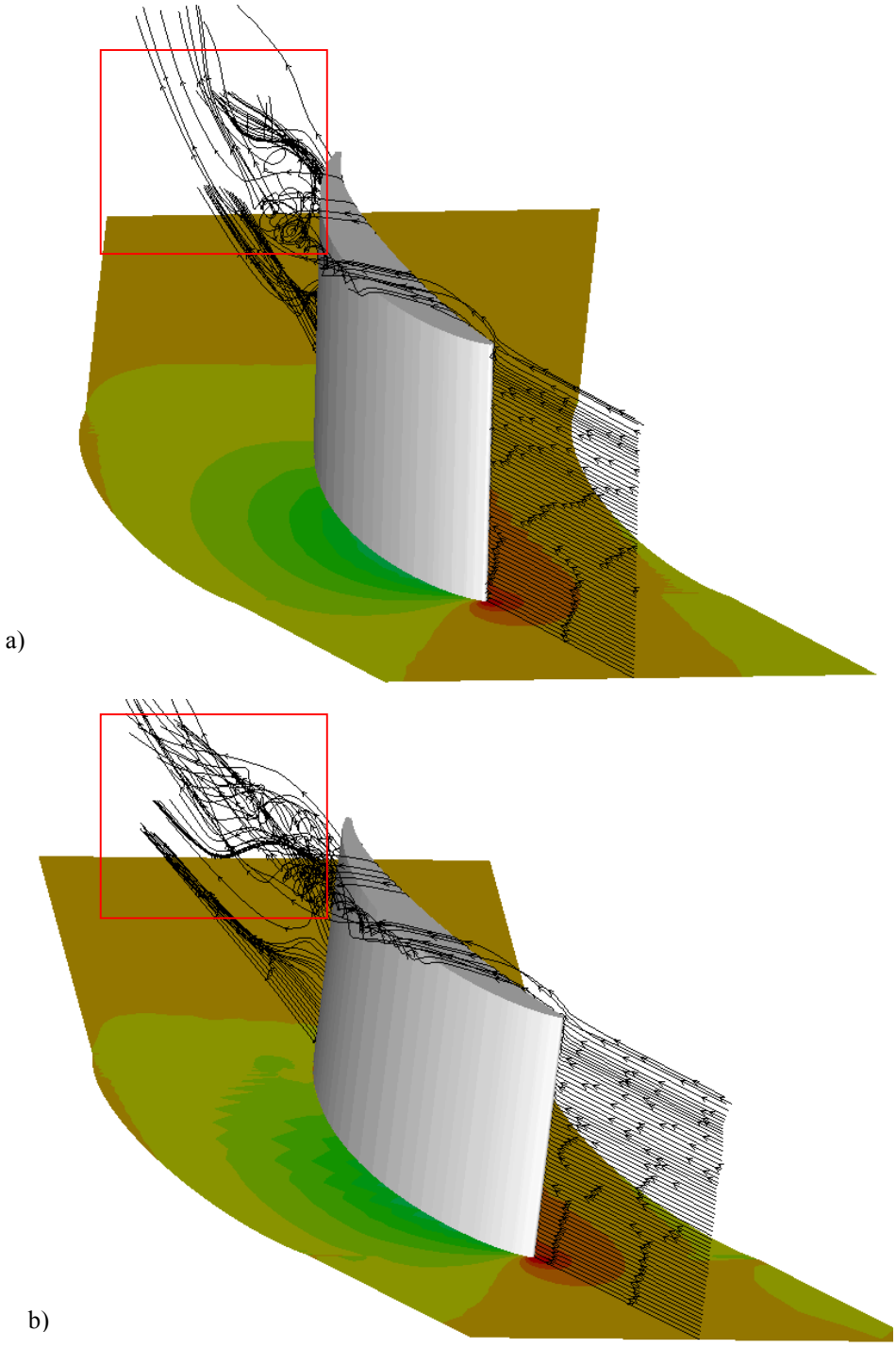

Fig. 6.25. Streamlines along tip leakage vortex: a) SUPG, b) V-SGS + DRDJ.

The observation of the red boxed areas in Fig. 6.23 demonstrates that SUPG solution contains two separate zones in the wake, while V-SGS + DRDJ tends to make them closer. This aspect could be fully understood considering the red boxed areas of Fig. 6.25, where it is possible to realize that the tip leakage vortex created by SUPG solution is weaker than the one obtained with V-SGS + DRDJ, capable of promoting much more mixing. These aspects find their counterpart in the *vortex core analysis* performed in Fig. 6.26.

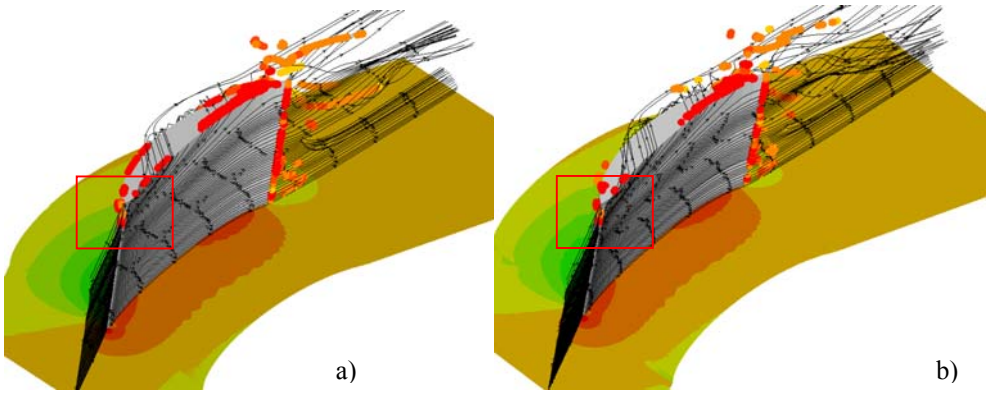

Fig. 6.26. Vortex core analysis: a) SUPG, b) V-SGS + DRDJ.

The red boxed areas of Fig. 6.26 trace the presence of the *horseshoe vortex* at leading edge in proximity of the tip, with a big difference in the two computed solutions, namely a too extended horseshoe for SUPG solution, that reduces the energy available for the tip leakage vortex, which remains too attached to the blade near the trailing edge. On the contrary, V-SGS + DRDJ is able of controlling the leading edge separation (due too a less *pitchwise* numerical dissipation), and gives rise to a larger tip leakage flow, capable of uniformly involving much of the span, as already shown in Fig. 6.25.

The *vorticity vectors* in a crosswise plane, corresponding to station *n. 15* (i.e. *50 mm* after trailing edge) of the experimental results reported in Kang and Hirsch (1993b), are shown in Fig. 6.27.

a)

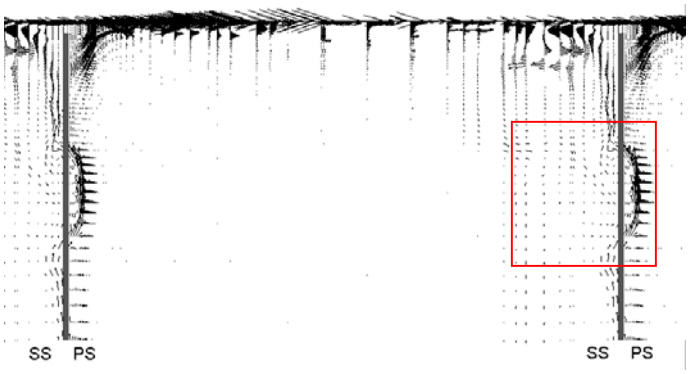

b)

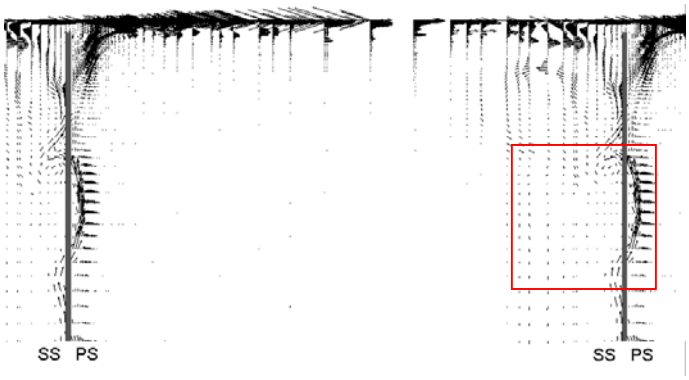

Fig. 6.27. Vorticity vectors : a) SUPG, b) V-SGS + DRDJ.

The comparison between Fig. 6.27a and b with the experimental data plots in Kang and Hirsch (1993b) shows a good agreement, with some differences between the numerical computations in the red boxed areas, where SUPG solution is not so capable as V-SGS + DRDJ solution of maintaining a correct span direction of the vorticity vectors.

The last aspect to be examined is the evolution of the turbulent variables, and in particular the streamwise turbulence intensity. The more interesting zone of the field is the wake, thus the analysis has been performed on a section corresponding to station n. 14 of the experimental results, i.e. just downstream the trailing edge. Fig. 6.28 shows the turbulence contour plots of streamwise turbulence intensity in station n. 14.

a)

b)

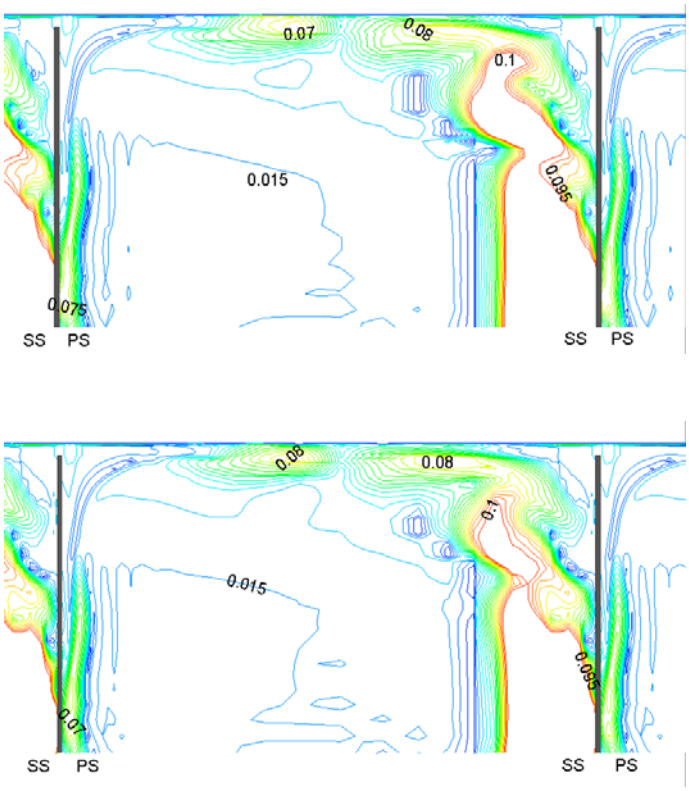

Fig. 6.28. Streamwise turbulence intensity @ station 14: a) SUPG, b) V-SGS + DRDJ.

The comparison of the contour plots demonstrates that V-SGS + DRDJ is capable of reducing the spurious high turbulence intensity core (red zone) more than SUPG, especially near the tip, where a better prediction of the tip leakage vortex is obtained, with a subsequent better resolution of the wake features.

All these considerations permit thus to conclude that the *V-SGS + DRDJ* method is able of giving accurate predictions of complex three-dimensional flows pertinent to turbomachinery CFD. Therefore its reliability for RANS turbulence modelling is demonstrated, so as its capability of introducing certain particular features in the numerical solution that could not be obtained with a classical SUPG stabilization.

References

Borello D., Corsini A., Rispoli F., "Prediction of Francis turbine runner performance using a 3D finite element technique with unassembled stiffness matrix treatment", in *2nd European Conf. on Turbomachinery, Antwerp, Belgium*, (1997).

Borello D., Corsini A. and Rispoli F., "A finite element overlapping scheme for turbomachinery flows on parallel platforms", *Computers and Fluids*, v. 32/7, pp. 1017-1047, (2003).

Borello D., Rispoli F., Hanjalic K., "Numerical simulation of turbulent flows in 3d decelerating cascade using second moment closure modeling", *ETC6 Conference*, (2005).

Chen W. L., Lien F. S., Leschziner M. A., "Computational prediction of flow around higly loaded compressor cascade blades with non-linear eddy-viscosity models", *International Journal of Heat and Fluid Flow*, v. 19, pp. 307-319, (1998).

Codina R., Oñate, E., Cervera, M., "The intrinsic time for the streamline upwind/Petrov-Galerkin formulation using quadratic elements", *Computer Methods in Applied Mechanics and Engineering*, v. 94, pp. 239-262, (1992).

Corsini A., Rispoli F., "Anisotropic turbulence modelling of near wall effects pertinent to turbomachinery flows", *FEDSM'02 Proceedings*, paper FEDSM2002-31206, pp. 1-10, (2002).

Corsini A., Rispoli F. ,"Using sweep to extend stall-free operational range in sub-sonic axial fan rotors", *Proc. Instn Mech. Engrs. v. 218 Part A, J. of Power and Energy*, pp. 129-139, (2004).

Corsini A., Rispoli F., "Flow analyses in a high-pressure axial ventilation fan with a non-linear eddy viscosity closure", *Int. J. Heat and Fluid Flow* , v. 26-3, pp. 349-361, (2005).

Corsini A., Rispoli F., Santoriello A., "A quadratic Petrov-Galerkin formulation for advection-diffusion-reaction problems in turbulence modeling", *Journal of Computational and Applied Mechanics*, v. 5-2, pp. 237-249, (2004a).

Corsini A., Rispoli F., Santoriello A., "A VMS/Stabilized formulation for the k-ε-v^2-f turbulence closure: application to turbomachinery CFD", *ECCOMAS 2004*, paper 1872, (2004b).

Corsini A., Rispoli F., Santoriello A.,"Quadratic Petrov-Galerkin finite elements for advective-reactive features in turbomachinery CFD", *International Journal of Numerical Methods for Heat and Fluid Flow*, v. 15-8, pp. 894-925, (2005a).

Corsini A., Rispoli F., Santoriello A., "A variational multiscale higher-order finite element formulation for turbomachinery flow computations", *Computer Methods in Applied Mechanics and Engineering*, v. 194, pp. 4797-4823, (2005b).

Corsini A., Rispoli F., Santoriello A., Tezduyar T. E., "Improved Discontinuity-Capturing finite element techniques for reaction effects in turbulence computation", submitted to *Computational Mechanics*, (2005c).

Craft T. J., Launder B. E., Suga K., "Development and application of a cubic eddy-viscosity model of turbulence", *Int. J. Heat and Fluid Flow*, v. 17, pp. 108-115 (1996).

Durbin P. A., "Separated flow computations with the k-ε-v^2 model", *AIAA J.*, v. 33, pp. 659-664, (1995).

Durbin P.A., "On the k-ε stagnation point anomaly", *International Journal of Heat and Fluid Flow*, v. 17, pp.89-90, (1996).

Elazar Y. and Shreeve R. P., "Viscous Flow in a Controlled Diffusion Compressor Cascade With Increasing Incidence", *Transactions of the ASME,* v. 112, pp.256-266, (1990).

Eulitz F., "Numerical simulation and modeling of unsteady turbomachinery flows", in *Recent developments in numerical methods for turbomachinery flows*, *VKI LS 2002-2001*, (2001).

Furukawa M., Inoue M., Saiki K., Yamada K., "The role of tip leakage vortex breakdown in compressor rotor aerodynamics", *J. of Turbomachinery*, v. 121, pp. 469-480, (1999).

Gallimore S. J., Bolger J. J., Cumpsty N. A., Taylor M. J., Wright P. I., Place J. M. M., "The use of sweep and dihedral in multistage axial flow compressor blading – Part I: University research and methods development", *J. of Turbomachinery*, v. 124, pp. 521-532, (2002).

Hah C., Loellbach J., "Development of hub corner stall and its influence on the performance of axial compressor blade rows", *J. of Turbomachinery*, v. 121, pp. 67-77, (1999).

Kang S., Hirsch C., "Experimental Study on the Three-Dimensional Flow within a Compressor Cascade with Tip Clearance: Part I -- Velocity and Pressure Fields", *J. of Turbomachinery*, v. 115, pp. 435-443, (1993a).

Kang S., Hirsch C., "Experimental Study on the Three-Dimensional Flow within a Compressor Cascade with Tip Clearance: Part II – The Tip Leakage Vortex", *J. of Turbomachinery*, v. 115, pp. 444-452, (1993b).

Launder B. E. and Sharma B. I., "Application of the energy dissipation model of turbulence to the calculation of flow near a spinning disc", *Lett. In Heat and Mass Transfer*, v. 1, pp. 131-138 (1974).

Lien F. S., Kalitzin G., Durbin P. A., "RANS modeling for compressible and transitional flows", *Proceedings of the Summer Program 1998*, *Center for Turbulence Research - Stanford University*, pp. 267-286, (1998).

Palikaras A., Yakinthos K., Goulas A., "Transition on a flat plate with a semi-circular leading edge under uniform and positive shear free-stream flow", *International Journal of Heat and Fluid Flow*, v. 23, pp. 455-470, (2002).

Saad Y., "A Flexible inner-outer Preconditioned GMRes algorithm", *SIAM J. Sci. Statistical Comput*., v. 14, pp. 461-469, (1993).

Sanger N. L., "The use of optimisation techniques to design Controlled-Diffusion Compressor blading", ASME *Journal of Engineering for Power,* v. 105, pp. 256-264, (1983).

Savill A. M., "Evaluating turbulence model predictions of transition – an ERCOFTAC Special Interest Group project", *Appl. Scientific Research*, v. 51, p. 555, (1992).

Savill A. M., "By-pass transition using conventional closures", in *Closure Strategies for Turbulent and Transitional Flows*, ed. Launder B. and Sandham N. D., pp. 464-492, *Cambridge University Press*, (2002).

Tezduyar T. E., "Computation of moving boundaries and interfaces and stabilization parameters", *International Journal For Numerical Methods in Fluids*, v. 43, pp. 555-575, (2003).

Tezduyar T. E., Park Y. J., "Discontinuity capturing finite element formulations for nonlinear convection-diffusion-reaction problems", *Computer Methods in Applied Mechanics and Engineering*, v. 59, pp. 307-325, (1986).

Tezduyar T. E., Mittal S., Ray S. E., Shih R., "Incompressible flow computations with stabilized bilinear and linear equal-order-interpolation velocity-pressure elements", *Computer Methods in Applied Mechanics and Engineering*, v. 95, pp. 221-242, (1992).

Tezduyar T. E., Osawa Y., "Finite element stabilization parameters computed from element matrices and vectors", *Computer Methods in Applied Mechanics and Engineering*, v. 190, pp. 411-430, (2000).

Conclusions

This work deals with two of the most important aspects in turbomachinery flow simulation, namely turbulence modelling and stabilization of finite element method.

For the first subject, the discussion develops considering the state of the art of turbulence models used for computations presented in publications and conferences, and addresses some new solutions to the closure problem in the RANS framework, showing the physical and numerical characteristics of some recent turbulence models. All the aspects of these formulations are commented with respect to well established standard closures, in order to show similarities, differences and innovative features.

Concerning the stabilization, this work contains some novel contributions developed by the research team which the author belongs to. The argument of stabilized finite elements is in fact considered as a crucial aspect for the correct computation of complex turbulent flows, such as turbomachinery ones. To this end, both the Petrov-Galerkin and the more recent Variational MultiScale approach to computational mechanics are addressed, focusing on the most important formulations available in the open literature, and commenting on their reliance for tackling all the typical instability origins arising in turbomachinery flows computation with finite element method. More in particular, advection, reaction and shocks induced instabilities are considered, highlighting some deficiencies of well established finite element formulations in dealing with them, focusing on the interpolation functions order too.

After a clarification of all the numerical problems still affecting the computation of turbomachinery flows, the work presents the new developed SPG, V-SGS and DRDJ finite element formulations, showing their characteristic features and ease of implementation in CFD codes.

Numerical tests are performed with both quadratic and linear finite elements in two and three dimensions for both model problems and real turbulent flow configurations pertinent to turbomachinery.

From the performed theoretical analysis and the results of the computations here presented, it is possible to draw some conclusions, as follows:

- Complete stabilized formulations are obtained for the RANS approach to incompressible turbulent flows with advanced turbulence closure models, with particular emphasis on the parameters governing advection and reaction induced instabilities;

- The proposed SPG, V-SGS and DRDJ stabilization techniques improve the stability with respect to the state-of-art stabilization methods designed for turbulent problems, on linear and quadratic finite elements;

- The interpretation of stabilization methods as non conventional tools for recasting the fine scales effect in the coarse ones, permits to conclude that the new developed finite element formulations exert an influence on turbulence modeling itself, introducing some non-linear aspects that naturally arise from the subgrid structures.

Appendix

Author's publications

As a conclusive item of this Ph D thesis, the author would like to express once again his gratitude to the "room 21" team, by including the complete list of the publications done in this three years fellowship:

Corsini A., Rispoli F., Santoriello A., "A new stabilized finite element method for advection-diffusion-reaction equations using quadratic elements", *in: T. Lajos, J. Vad, ed., CMFF'03 Conference Proceedings Vol.2 (Department of Fluid Mechanics, Budapest University of Technology and Economics),* pp. 791-799, (2003).

Corsini A., Rispoli F., Santoriello A., "A quadratic Petrov-Galerkin formulation for advection-diffusion-reaction problems in turbulence modeling", *Journal of Computational and Applied Mechanics*, v. 5-2, pp. 237-249, (2004).

Corsini A., Rispoli F., Santoriello A., "A New Stabilized Finite Element Method for Advection-Diffusion-Reaction Equations using Quadratic Elements", in: *Modelling Fluid Flow. The state of the art*, Ed.s J. Vad, T. Lajos and R. Schilling, *Springer*, pp. 247-266, (2004).

Corsini A., Rispoli F., Santoriello A., "A VMS/Stabilized formulation for the k-ε-v^2-f turbulence closure: application to turbomachinery CFD", *ECCOMAS 2004*, paper 1872, (2004).

Corsini A., Rispoli F., Santoriello A.,"Quadratic Petrov-Galerkin finite elements for advective-reactive features in turbomachinery CFD", *International Journal of Numerical Methods for Heat and Fluid Flow*, v. 15-8, pp. 894-925, (2005).

Corsini A., Rispoli F., Santoriello A., "A variational multiscale higher-order finite element formulation for turbomachinery flow computations", *Computer Methods in Applied Mechanics and Engineering*, v. 194, pp. 4797-4823, (2005).

Corsini A., Rispoli F., Santoriello A., Tezduyar T. E., "Improved Discontinuity-Capturing finite element techniques for reaction effects in turbulence computation", submitted to *Computational Mechanics*, (2005).